

**Live cell imaging of meiosis in anthers
of *Arabidopsis thaliana***

Dissertation with the aim of achieving a doctoral degree at
the Faculty of Mathematics, Informatics and Natural Sciences

Department of Biology
of Universität Hamburg

Submitted by
Maria Ada Prusicki

2018 in Hamburg

Supervisor: Prof. Dr. Arp Schnittger

1st Examiner: Prof. Dr. Arp Schnittger

2nd Examiner: Jun. Prof. Dr. Wim Walter

Date of oral defense: 22.02.2019

Index

ABSTRACT	V
ZUSAMMENFASSUNG	VI
NOMENCLATURE	IX
1 INTRODUCTION	1
1.1 MEIOSIS IN PLANTS AND ITS REGULATION	1
1.1.1 <i>Meiosis, a brief introduction</i>	1
1.1.2 <i>Cytology of meiotic progression</i>	3
1.1.3 <i>Chromosome dynamics and the role of cohesion in meiosis</i>	8
1.1.4 <i>Meiosis in polyploids</i>	11
1.2 TIME COURSES OF PLANT MEIOSIS.....	14
1.2.1 <i>Temperature and genotype effects on meiotic duration</i>	15
1.2.2 <i>Meiotic duration in polyploids</i>	16
1.2.3 <i>Experimental procedures of time courses</i>	17
1.3 IMAGING OF MEIOSIS.....	21
1.3.1 <i>Live cell imaging setups</i>	21
1.3.2 <i>Live cell imaging of plant meiosis</i>	22
2 OBJECTIVES	25
3 RESULTS	27
3.1 TECHNIQUE ESTABLISHMENT	27
3.1.1 <i>Sample isolation and mounting</i>	27
3.1.2 <i>Microscope set up</i>	29
3.2 SELECTION OF REPORTER LINES.....	31
3.2.1 <i>Functionality of the $PRO_{REC8}:REC8:mEGFP$ and the $PRO_{RPS5A}:TagRFP:TUB4$ reporter</i>	33
3.2.2 <i>The KINGBIRD line</i>	34
3.3 A LANDMARK SYSTEM FOR MALE MEIOSIS OF ARABIDOPSIS THALIANA	36
3.3.1 <i>Cell features description and co-occurrence</i>	36
3.3.2 <i>Assessment of cellular states and definition of neighboring score</i>	39
3.3.3 <i>A Landmark system</i>	41
3.3.4 <i>The case of the Nuclear Envelope breakdown</i>	44

3.4	TETRAPLOID GENERATION.....	45
3.4.1	<i>VIGS treatment and KINGBIRD tetraploids.....</i>	45
3.4.2	<i>Meiosis of the F2 tetraploid KINGBIRD line progresses through the same landmarks as diploid plants.....</i>	48
3.5	TIME COURSE OF MEIOSIS IN DIPLOID AND TETRAPLOID KINGBIRD LINES	49
3.5.1	<i>Diploid time course.....</i>	49
3.5.2	<i>Tetraploid time course and comparison.....</i>	53
3.6	TOWARDS NEW APPLICATIONS	55
3.6.1	<i>Screen of reporters and generation of new crossed lines.....</i>	55
3.6.2	<i>KINGBIRD2 and its introgression in mutant backgrounds.....</i>	55
3.6.3	<i>Generation of PRO_{REC8}:REC8:mNG.....</i>	58
3.6.4	<i>Performance of PRO_{REC8}:REC8:mNG.....</i>	58
4	DISCUSSION	63
4.1	STRENGTHS AND LIMITATIONS OF THE MICROSCOPE SET UP	63
4.2	LIVE CELL IMAGING APPLICATION TO STUDY MEIOSIS IN CROPS	65
4.3	THE LANDMARK SYSTEM.....	66
4.4	TOWARDS AN ATLAS OF MEIOSIS.....	67
4.5	SINGLE CELL IMAGING REVEALS NEW INSIGHTS INTO MEIOTIC TIMING AND TISSUES SYNCHRONIZATION	69
4.6	TIME COURSE IN 2X AND 4X.....	71
4.7	FUTURE PERSPECTIVES	72
5	MATERIAL AND METHODS	75
5.1	PLANT MATERIAL AND GROWTH CONDITIONS.....	75
5.2	GENOTYPING	75
5.3	CLONING OF PROREC8:REC8:MNG.....	76
5.4	PLANT TRANSFORMATION AND CROSSING	77
5.5	VIGS.....	77
5.5.1	<i>VIGS treatment.....</i>	77
5.5.2	<i>Selection of VIGS treated plants.....</i>	78
5.6	PHENOTYPE EVALUATION	79
5.6.1	<i>Evaluation of seed abortion.....</i>	79
5.6.2	<i>Pollen viability test.....</i>	79
5.6.3	<i>Cell spreads.....</i>	79
5.7	CONFOCAL MICROSCOPY	80

5.7.1 Still pictures	80
5.7.2 Live cell imaging	80
5.8 TIME LAPSES PROCESSING AND ANALYSIS.....	81
5.9 QUANTITATIVE ANALYSIS OF LIVE CELL IMAGING DATA	81
5.9.1 Landmark extraction	81
5.9.2 Meiotic time course calculation.....	83
REFERENCES.....	85
ANNEXES.....	102
APPENDIX	XI
INDEX OF FIGURES	XI
INDEX OF TABLES	XI
INDEX OF ANNEXES.....	XII
INDEX OF ABBREVIATIONS.....	XIII
PUBLICATIONS AND PRESENTATIONS.....	XV
EIDESSTATTLICHE VESRICHERUNG /DECLARATION ON OATH	XVI
CONFIRMATION OF CORRECT ENGLISH	XVII
ACKNOWLEDGMENTS	XVIII

Abstract

Meiosis is a crucial event for sexual reproduction; during its course the chromosome number is halved, and recombination between homologs takes place. Understanding how meiosis is regulated in plants has a direct impact on breeding applications and, therefore, researchers invest constant effort in studying its fundamental aspects. Extensive knowledge about the meiotic progression results from the cytological analysis of fixed material. Although highly informative, this approach is not sufficient to understand the dynamics of meiosis; numerous works have demonstrated that key meiotic events as homologs pairing and segregation are heavily dependent on chromosome movements and cytoskeleton rearrangements, underpinning the need of a spatiotemporal description of the cell division.

This dissertation introduces a live cell imaging technique, based on confocal microscopy, which allows the observation of the entire meiotic division of pollen mother cells of *Arabidopsis thaliana*. In this study, the behavior of single meiocytes is monitored throughout the progression of meiosis by the simultaneous visualization of the meiotic subunit of cohesin, RECOMBINATION 8 (REC8), and microtubules. The double reporter line, named *KINGBIRD* (*Kleisin IN Green, tuBulin In Red*), allows the description of five cellular features: cell shape, nucleus position, nucleolus position, chromosome conformation, and microtubule array. These features combine in a non-random manner to form cellular states; the analysis here performed led to the identification of 11 principal states, referred to as landmarks, which are convergent points of the meiotic progression. Using the landmark system as a reference, it was possible to describe a precise time course of meiosis, which included the duration of short and asynchronous phases, such as metaphases and anaphases. Taken together, the here established microscopy technique and landmark system constitute a novel approach, which opens new ways to the study of plant meiosis.

Zusammenfassung

Die Meiose ist ein essentieller Schritt der sexuellen Fortpflanzung; während ihres Verlaufs wird die Chromosomenzahl halbiert und eine Rekombination zwischen homologen Chromosomen ermöglicht. Unser Verständnis der Regulation der Meiose in Pflanzen ist für die Pflanzenzüchtung von direktem Interesse, weshalb große Anstrengungen unternommen werden, die grundlegenden Abläufe zu verstehen.

Aus der zytologischen Analyse von fixiertem Material wurde bereits umfangreiches Wissen über den grundsätzlichen Ablauf der Meiose gewonnen. Obwohl sehr informativ, reicht dieser Ansatz aber nicht aus, um die Dynamik der Meiose im Detail zu verstehen. Zahlreiche Arbeiten haben gezeigt, dass meiotische Schlüsselereignisse wie Paarung der Homologen und deren Segregation stark von Chromosomenbewegungen und Zytoskelettlagerungen abhängen, was die Notwendigkeit einer genauen räumlich-zeitlichen Beschreibung der meiotischen Zellteilung untermauert. Mit dieser Dissertation wird eine Technik zur Lebendzellbeobachtung während der Meiose eingeführt, die auf konfokaler Lasermikroskopie basiert und die Beobachtung des gesamten Ablaufs der meiotischen Teilung der Pollenmutterzellen von *Arabidopsis thaliana* ermöglicht

Durch eine gleichzeitige Visualisierung der Mikrotubuli und der meiotischen Untereinheit von Kohäsin, RECOMBINATION 8 (REC8), kann die Entwicklung einzelner Meiozyten während des Verlaufs der Meiose genau mitverfolgt werden. Die hierfür konstruierte zweifache Reporterlinie namens *KINGBIRD* (*Kleisin IN Green, tuBulin In Red*) ermöglicht die Beschreibung von fünf Zellmerkmalen: Zellform, Position des Zellkerns, Position des Nucleolus im Zellkern, Chromosomenkonformation und die Anordnung der Mikrotubuli. Die spezifische Kombination dieser Merkmale charakterisiert jeweils bestimmte meiotische Stadien. Die hier durchgeführte Analyse führte zur Identifizierung von 11 Hauptzuständen, sogenannten Referenzpunkten, die konvergente Punkte des meiotischen Ablaufs darstellen. Mit Hilfe des Referenzpunkt-Systems konnte ein genauer zeitlicher Verlauf der Meiose beschrieben werden, der es nun ermöglicht, auch die Dauer kurzer und asynchroner Phasen, wie Metaphase und Anaphase, präzise zu erfassen.

Die hier etablierte mikroskopische Technik zur Lebendbeobachtung und das Referenzpunkt-System stellen einen innovativen Ansatz dar, der es ermöglicht, neue Wege in der Erforschung der Meiose in Pflanzen zu gehen.

.

Nomenclature

The Nomenclature style used in this dissertation follows the nomenclature guidelines of TAIR and refers to Meinke and Koornneef, 1997 (Meinke and Koornneef, 1997). Plant genes are abbreviated with a three-letter symbol, written in uppercase italic letters (e.g. *REC8*), the respective protein is named by the same abbreviation written in uppercase roman letters (e.g. REC8); mutant genes are referred in lowercase italic letters (e.g. *rec8*), specific mutant alleles are specified by numbers after a slash sign (e.g. *tam1-2*), when it is relevant the mutant name is followed by +/- for heterozygous, and by -/- for homozygous plants.

Transgenic lines are named after the construct and written in uppercase italic (e.g. *PRO_{REC8}:REC8:mEGFP*), with the exception of the *KINGBIRD1* and *KINGBIRD2* lines, which are double constructs and therefore have been renamed for practical reasons. *KINGBIRD1* could be followed by 2X or 4X to inform about its ploidy state. The reporter gene is as well indicated by the name of the construct in uppercase italics (e.g. *PRO_{REC8}:REC8:mEGFP*), while the fusion protein is indicated by the same name written in uppercase roman letters (e.g. REC8:mEGFP). Plasmid names are written in uppercase roman letters preceded by lowercase p (pGWB501) eventually followed by the T-DNA inserted (e.g. pGWB501-REC8-mNG).

Organisms are indicated using the Linnean name written in italics (e.g. *Arabidopsis thaliana*, *Zea mays* or *Saccharomyces cerevisiae*) or using the short version of it (e.g. *C. elegans*, *S.pombe*). Alternatively, the commonly used name can be found in the text (e.g. maize).

1 Introduction

1.1 Meiosis in plants and its regulation

1.1.1 Meiosis, a brief introduction

Meiosis is a specialized eukaryotic cell division, which takes place in the reproductive tissues. In animals, meiosis gives rise to gametes whereas in plants spores are generated that eventually form the actual gametes. Meiosis consists of only one cycle of DNA replication followed by two consecutive chromosome segregation events. Thus, meiosis allows the formation of haploid gametes in a diploid organism. This is crucial for sexual reproduction as it prevents the doubling of a genome in every new generation. Moreover, meiosis drives genetic diversity as crossovers (CO) between homologous chromosomes (homologs) result in new assortments of genetic alleles. In addition, homologous chromosomes are randomly segregated to complete new chromosome sets, further contributing to genetic variation.

Given its importance in the rearrangement of genetic information, understanding meiosis is of crucial interest for breeding that largely relies on the combination of favorable alleles (Crismani *et al.*, 2013; Lambing and Heckmann, 2018; Hand and Koltunow, 2014). Thus, the molecular mechanisms underlying recombination and chromosome segregation, as well as entry and progression of meiosis, have been a hot topic for plant investigation over the last decades. More than 80 meiotic genes have up to now been identified in *Arabidopsis thaliana*, *Zea mays* and *Oryza sativa* (Mercier *et al.*, 2015; Wijnker and Schnittger, 2013; Ma, 2006; Zhou and Pawlowski, 2014; Lambing *et al.*, 2017). Manipulation of these genes is also a cornerstone of new molecular tools that are being developed for crop breeding (Barakate *et al.*, 2014; Calvo-Baltanas *et al.*, 2018; Dirks *et al.*, 2009).

Meiosis is highly conserved among taxa, and its core factors such as elements involved in double strand break (DSB) initiation and recombination (SPO11, RAD51, DMC1, etc.), COs formation (MHS4, MHS5, MLH1, etc.) (Figure 1.1), and structural proteins of the synaptonemal complex (ZYP1) have been found encoded in genomes from protists to land plants and animals (Mercier *et al.*, 2015; Loidl, 2016).

Nonetheless, major differences exist among and within taxa, in processes such as homolog pairing, recombination control or in the presence of developmental hold and checkpoints (Loidl, 2016). For example in yeast and plants DSB formation and repair are necessary for pairing and synapsis (Henderson and Keeney, 2004; Grelon, 2001), while in *C. elegans* and drosophila the two process are independent (Dernburg *et al.*, 1998; McKim *et al.*, 1998).

In the course of this thesis, the flowering plant *Arabidopsis thaliana* was chosen as a model system, and therefore the description of meiosis that follows is referred to the progression in this organism; an explicit reference will be made when comparison or knowledge derived from other organisms are presented.

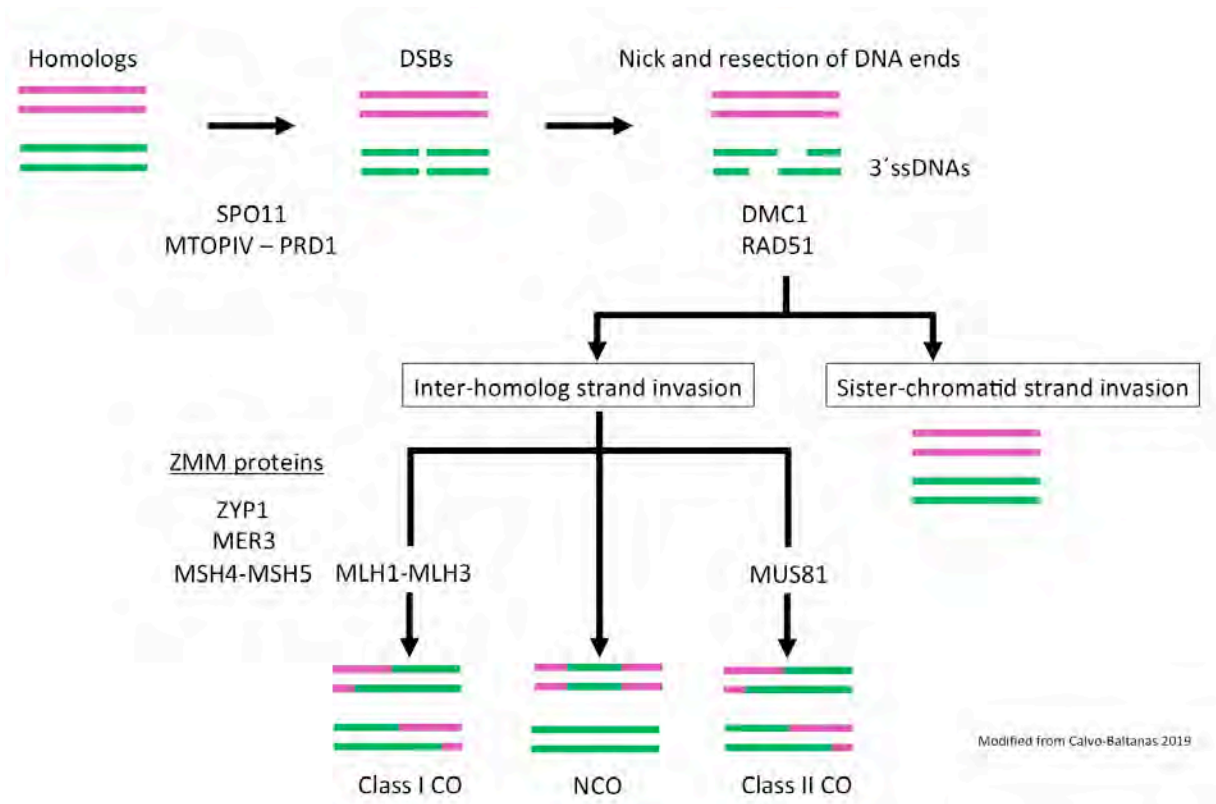


Figure 1.1 Recombination pathways of *Arabidopsis thaliana*

The scheme illustrates the different molecular pathways of recombination and crossover formation during meiosis of *Arabidopsis thaliana*. At first DSBs are formed by SPO11 and MTOPIV. DSB ends are processed to obtain single strand DNA. DMC1 and RAD51 bind the single strand DNA and mediate the strand invasion. The single strand DNA can invade the intact sister chromatid or one of the homologous chromatids. The inter-homologous intermediate can be resolved into Class I CO, mediated by ZMM proteins and MLH1- MLH3, into Class II CO, mediated by MUS81, or can result in a Non Cross Over (NCO) event.

1.1.2 Cytology of meiotic progression

In flowering plants, the establishment of the germline occurs in late stages of development, after the transition from a vegetative to a floral meristem (Schmidt *et al.*, 2015) and it consists in a fine reprogramming of somatic cell fate into a meiocyte through genetic pathways. This involves the activity of factors known to regulate plant development and cell proliferation as *RETINOBLASTOMA RELATED 1 (RBR1)* the *WUSCHEL (WUS)*, *CYCLIN-DEPENDENT KINESSES A;1 (CDKA;1)* and its inhibitor *KIP-RELATED PROTEINS (KRPs)* (Zhao *et al.*, 2012, 2017; Wijnker and Schnittger, 2013).

The newly designated meiocytes adopt a characteristic shape that radically changes while undergoing meiosis, ultimately resulting in the formation of spores. These changes have been classified into a set of phases, which became the frame of reference when analyzing meiotic progression. These consecutive phases are called S-phase/G2, prophase I, metaphase I, anaphase I, telophase I/interkinesis, prophase II, metaphase II, anaphase II, telophase II and cytokinesis. Prophase I is traditionally subdivided into several sub-phases: leptotene, zygotene, pachytene, diplotene and diakinesis (Figure 1.2). Each of these meiotic stages is characterized by phase-specific events, e.g., DSB are formed in early leptotene, COs are resolved at metaphase I and only at anaphase II the sister chromatid segregate. The molecular network that tightly regulates these events has been deeply explored in the past (for plant meiosis, summarized in the following reviews: Hamant *et al.*, 2006; Luo *et al.*, 2014; Mercier *et al.*, 2015; Wang and Copenhaver, 2018) and is currently being expanded, as for the characterization of *ASYNAPTIC 4 (ASY4)*, involved in chromosome synapsis (Chambon *et al.*, 2018), or for the new evidenced of the role of *TOPOISOMERASE II (TOPII)*, in the resolution of chromosome entanglements (Martinez-Garcia *et al.*, 2018).

A cytological description of each phase is of key importance in the context of this thesis, which investigates meiosis by microscopy. A graphical representation and cell spreads of each meiotic phase are illustrated in Figure 1.2.

- *S-Phase/G2*

During S-phase the DNA is duplicated; it is likely that the commitment to meiosis is settled in this phase and the first steps for the subsequent events of meiosis are prepared. Cells have a homogeneous interphase outlook, except for the bigger size

of nuclei and nucleoli comparing to somatic interphases (Armstrong *et al.*, 2003; Ross *et al.*, 1996). Its duration is estimated to last longer than a mitotic S-phase, between 5 and 9 hours in *Arabidopsis thaliana* (Armstrong *et al.*, 2003), and it coincides with the expression of meiotic-specific proteins such as the cohesin subunit RECOMBINATION DEFICIENT 8 (REC8) (Cai *et al.*, 2003). During G2 phase, the first stretches of chromosome axes appear, revealing a gradual transition between the meiotic interphase and the first phase of the division (Armstrong *et al.*, 2003; Armstrong and Jones, 2003).

• *Leptotene (Prophase I)*

Leptotene meiocytes are characterized by the presence of distinguishable thin, unpaired chromosome threads, which, towards the end of the phase, become unevenly distributed within the nuclear area (Armstrong and Jones, 2003; Ross *et al.*, 1996). At the same time, the nucleolus moves on the opposite corner of the nucleus (Stronghill *et al.*, 2014; Ross *et al.*, 1996).

• *Zygotene (Prophase I)*

Zygotene is the phase in which synapsis between homologs starts. DAPI-stained cell spreads show areas of thin (unsynapsed) and thick (synapsed) chromosomes in the same nucleus, revealing that synapsis progresses (Ross *et al.*, 1996). MTs and organelles polarize toward a side of the cell, while the nucleus moves from a central position to the side of the cell (Ross *et al.*, 1996; Peirson *et al.*, 1997; Armstrong and Jones, 2003; Stronghill *et al.*, 2014) In zygotene, telomeres cluster at the nuclear envelope (NE) and form a characteristic shape, called telomere bouquet. The telomere bouquet has been observed in many species including maize, barley, as well as fission, budding yeast, and mice (among many observations: Golubovskaya *et al.*, 2002; Higgins *et al.*, 2012; Yu *et al.*, 2010; Tomita and Cooper, 2007; Lee *et al.*, 2012, 2015). In *Arabidopsis thaliana*, telomeres also cluster but only very transiently (Hurel *et al.*, 2018). In addition, telomeres were reported to aggregate at the nucleolus during G2, and to loose this association at the early leptotene (Armstrong *et al.*, 2001).

• *Pachytene (Prophase I)*

Pachytene is defined as the stage of full synapsis, the two paired arms of the homologs are visible by cell spread as a double thread along the complete

chromosome length. Nucleus and organelles can be either unevenly or evenly distributed (Ross *et al.*, 1996; Armstrong *et al.*, 2003; Armstrong and Jones, 2003).

- *Diplotene (Prophase I)*

Also called diffused stage, diplotene is characterized by the gradual loss of synapsis. Bivalents extend and become a mixture of paired and unpaired areas, resembling the zygotene chromosome structure. Zygotene and diplotene cells can be distinguished from each other by the nucleus position: in diplotene, the nucleus has returned to the center of the cell; therefore organelles are homogenously distributed (Ross *et al.*, 1996; Armstrong *et al.*, 2003; Armstrong and Jones, 2003).

- *Diakinesis (Prophase I)*

Diakinesis is the last stage considered part of prophase; chromosome re-condense and the five bivalents of *Arabidopsis thaliana* can be detected as separate entities in a characteristic x-shape (Ross *et al.*, 1996; Armstrong *et al.*, 2003).

- *Metaphase I*

At metaphase I the five bivalents reach the maximum level of condensation. They align at the metaphase plate and chiasmata along the chromosome arms can be counted (Armstrong and Jones, 2003). The spindle is formed (Peirson *et al.*, 1997).

- *Anaphase I*

Homologs are segregated in two balanced pools and pulled towards the two opposite poles of the cell. Chromosomes are still highly condensed, and univalents can be distinguished (Ross *et al.*, 1996)

- *Telophase I/ Interkinesis*

After anaphase I, meiocytes present two distinct nuclear areas, containing five condensed univalents. The nuclear envelope (NE) is re-formed. *Arabidopsis thaliana* does not undergo cytokinesis at this stage of meiosis, differently from other plants such as maize and rice (Zhang *et al.*, 2018). Instead, an organellar band appears in the middle of the cell, which is maintained until the end of meiosis II (Ross *et al.*, 1996; Armstrong and Jones, 2003). Most of the MTs are located between the segregated chromosomes with a few radiating from each pole into the cortical cytoplasm (Peirson *et al.*, 1997).

• *Meiosis II*

The second meiotic division is thought to largely resemble a mitotic division. Its primary outcome is the segregation of sister chromatids and the formation of four spores. It can be divided into the sub-phases prophase II, metaphase II, anaphase II and finally telophase II, which is followed by cytokinesis and cell wall formation. Since meiosis II proceeds much faster than the first division, it is more complicated to obtain cell spreads of meiosis II, and hence, less detailed cytological descriptions have been published. Nonetheless, a few specific characteristics have been noted. Prophase II cells can be recognized by the presence of two distinct nuclei and diffused chromosomes. Five dense chromocenters are visible in each nucleus (Ross *et al.*, 1996). At the onset of metaphase II, two spindles are formed. They are smaller than the metaphase I spindle and composed by a lower number of MTs. They are parallel to the equatorial plane, but their reciprocal orientation can vary from parallel to perpendicular to each other. Chromosomes align in the metaphase plane as they would do in mitotic metaphase (Peirson *et al.*, 1997). At anaphase II individual chromatids are segregated, forming four groups of chromosomes. At telophase II, the phragmoplast is formed, and the cytoplasm is finally partitioned (Peirson *et al.*, 1997; Ross *et al.*, 1996; Armstrong and Jones, 2003).

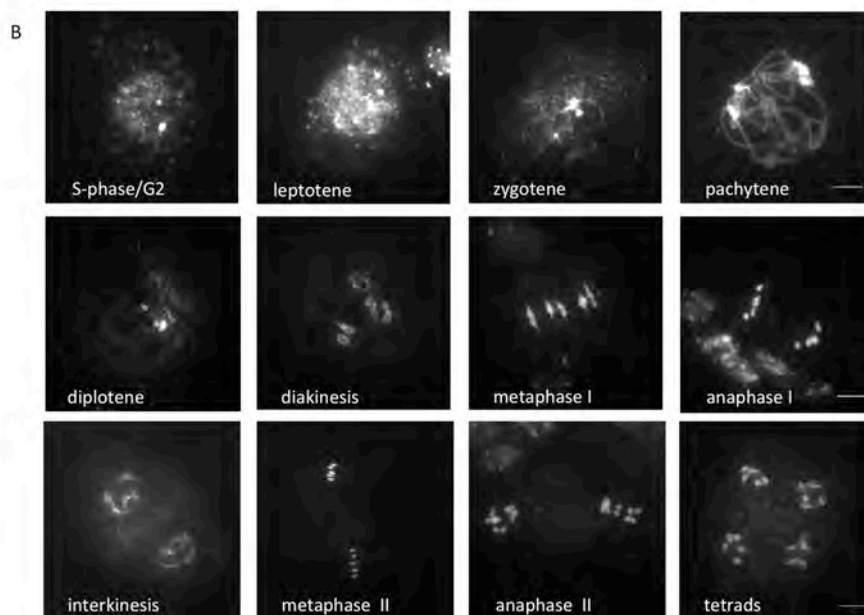
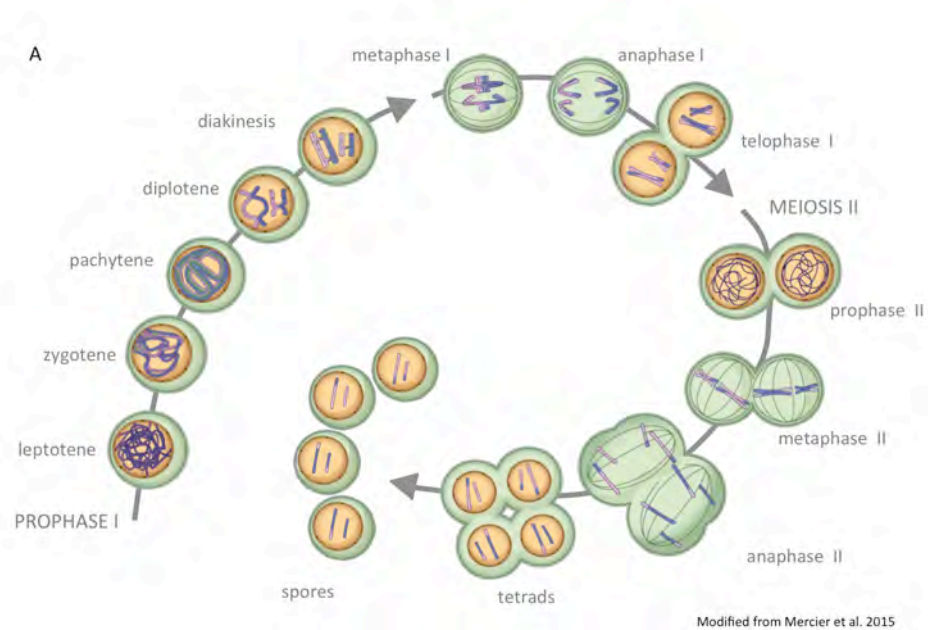


Figure 1.2 Progression of male meiosis in *Arabidopsis thaliana*

- A) Schematic representation of meiotic progression. Cytoplasm is green, nucleus is yellow and the homologous chromosomes are depicted in blue and pink. During prophase I homologs pair and synapse, COs are detectable at metaphase I, while exchange of DNA between homologs is visible from anaphase I, when homologs segregation take place. After metaphase II, sister chromatids divides and II four haploid spores are formed. The figure is modified from Mercier *et al.*, 2015.
- B) Cell spreads of WT Col-0. DNA was stained with DAPI to highlight chromosomes (in light gray). Scale bar is 10 μm . A more detailed description of cell spreads in found in the main text, chapter 1.1.2.

1.1.3 Chromosome dynamics and the role of cohesion in meiosis

As stated in the brief meiotic description in chapter 1.1, one of the most important outcomes of meiosis is balanced chromosome segregation resulting in four haploid cells. This is obtained by a complex interaction of events, including a correct establishment of COs and COs resolution, as well as an accurate deposition and removal of cohesin, the protein complex responsible of establishing cohesion between sister chromatids during mitotic and meiotic divisions.

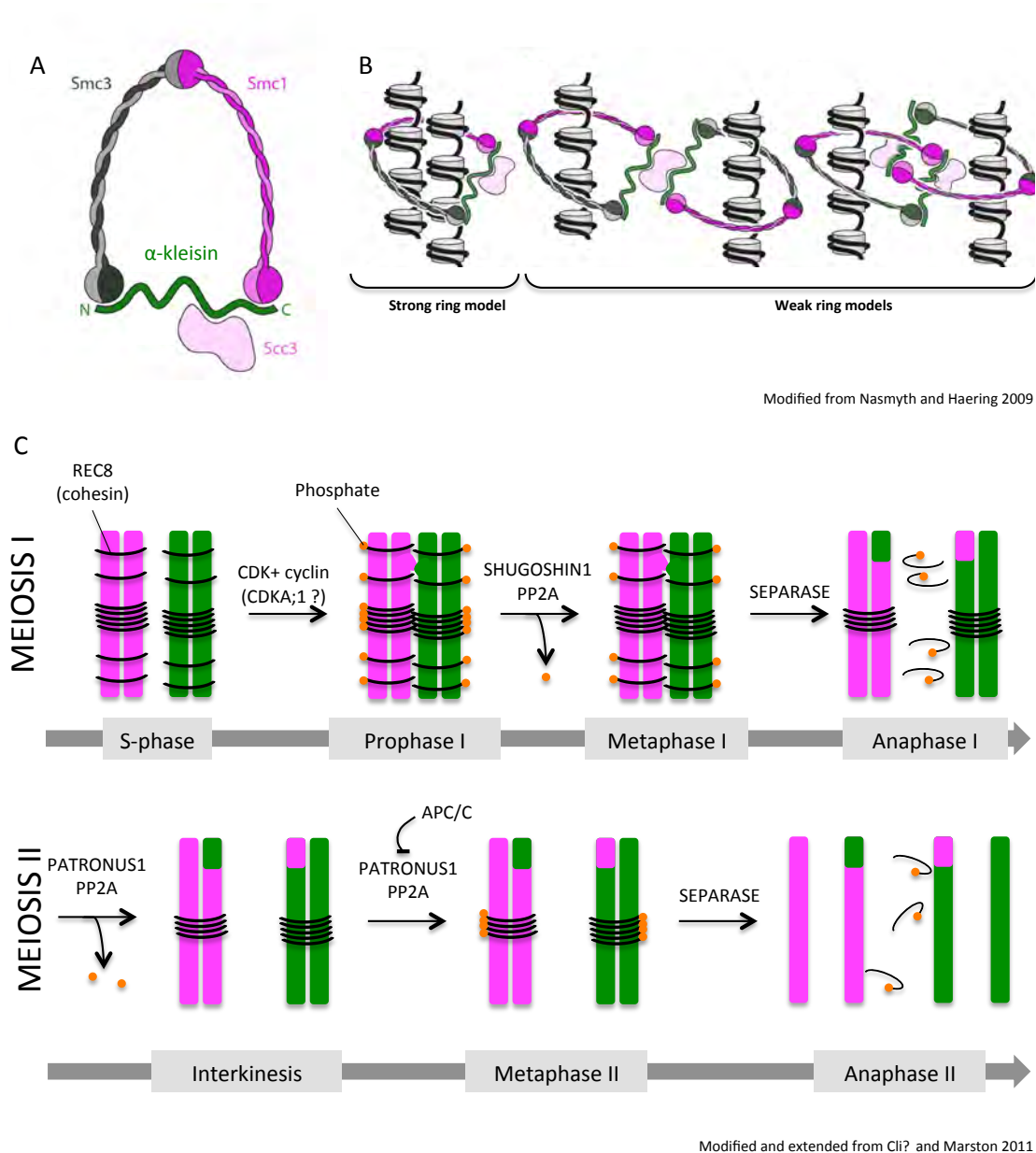
Cohesin is formed by four conserved subunits: SMC1, SMC3, SCC3 and an α -kleisin protein (Figure 1.3). The subunits assemble in a ring-like shape, which holds the chromatids together, either embracing both within the same ring (strong ring model) or establishing cohesin dimers, each one containing a single chromatid (weak ring model, reviewed in Nasmyth and Haering, 2009) (Figure 1.3). *Arabidopsis thaliana* genome encodes for four α -kleisins: SYN1, SYN2, SYN3, and SYN4, also known as REC8, RAD21.1, RAD21.2, and RAD21.3. Even though a certain level of redundancy has been observed (Schubert *et al.*, 2009), the four complexes, which differs by the kleisin subunit, are involved in different functions. This is shown by differences in mutant phenotypes (Schubert *et al.*, 2009) as well as by their expression in distinct tissues. REC8, in particular, is solely expressed in meiocytes (Cai *et al.*, 2003) and its null mutation affects spores formation, with substantial effects on plant fertility, while mitotic division and plant development do not show deficiency (Peirson *et al.*, 1997; Bai *et al.*, 1999).

Cohesin is deposited along chromosomes during S-phase (reviewed in Peters *et al.*, 2008), and it is maintained in position until the bipolar attachment of sister chromatids when finally its complete cleavage promotes their segregation. During meiosis cohesin requires a stepwise removal: at the end of prophase I REC8 is cleaved from the arm of the chromosomes allowing the resolution of COs, but remains loaded at the peri-centromeric areas, ensuring that sister chromatids do not segregate beforehand (Peters *et al.*, 2008; Nasmyth and Haering, 2009). The remaining cohesion is finally removed at the onset of anaphase II. Due to technical difficulties in the immunolocalization of REC8, which detected a strong signal from S-phase to metaphase I only (Cai *et al.*, 2003), it was doubted that in *Arabidopsis thaliana* REC8 was involved in the cohesion maintenance after the onset of anaphase

I. Only recently, the presence of REC8 after metaphase I has been proved by immunolocalization, confirming that the stepwise model could apply to plants as well (Cromer *et al.*, 2013; Yuan *et al.*, 2018; Yuan, 2018).

Both the cleavages are performed by the endopeptidase separase, which recognizes phosphorylated REC8 as a target (Katis *et al.*, 2010); thus the core element of the stepwise removal is tight control of REC8 phosphorylation and dephosphorylation (Figure 1.3). While there is no current evidence of the phosphorylating factor of REC8, it is well known that in *Arabidopsis thaliana* the protection of cohesion at anaphase I is performed by SHUGOSHIN 1 (SGO1) (Zamariola *et al.*, 2013; Cromer *et al.*, 2013), which directs the PROTEIN PHOSPHATASE PP2A to the centromeres, promoting dephosphorylation of REC8 (Yuan *et al.*, 2018) in a similar way to what was observed in yeast and animals (Clift and Marston, 2011); absence of SGO1 and PP2A results in early depletion of REC8 (Yuan, 2018; Yuan *et al.*, 2018), and consequently in chromosome mis-segregation. Additionally, another important protector of REC8, PATRONUS (PANS1) has been identified in plants, having a prominent role during interkinesis (Cromer *et al.*, 2013).

The meiotic role of REC8 and of the cohesin complex, in general, is not only restricted to the establishment chromatid cohesion. It has been proved instead that it is involved in homologs recognition and pairing, in the deposition of synaptonemal complex and in directing the kinetochore attachment (Bai *et al.*, 1999; Cai *et al.*, 2003; Chelysheva *et al.*, 2005).



Modified from Nasmyth and Haering 2009

Modified and extended from Cli? and Marston 2011

Figure 1.3 Cohesin structure and cleavage during meiosis

- Schematic representation of the cohesin ring complex.
- Cohesin can connect the two sister chromatids, either enclosing both the chromatids within the same ring (string ring model) or forming two rings, one per chromatids, which then interact and establish the connection (weak ring models).
- During meiosis, cohesin is cleaved in a two-steps manner, which is mediated by REC8 phosphorylation. At first cohesin is cleaved from the arms of the chromosomes, and remains at centromeres, protected by the action of SGO1, PP2A and PANS1. Only at the onset of the second anaphase cohesin is entirely removed, and sister chromatids separate.

1.1.4 Meiosis in polyploids

Polyploidy is a common condition among plants; its role of promoter of evolutionary flexibility and speciation is supported by evidence of whole genome duplication (WGD) in ancestors of monocots (Yu *et al.*, 2005; Jiao *et al.*, 2014) and angiosperms in general (Soltis *et al.*, 2007). Advantages of being polyploid lie in gene redundancy, which masks recessive alleles and has the potential to develop into gene paralogy (Comai, 2005), as well as in higher heterosis and vigor, which might foster polyploid survival in stress conditions (Comai, 2005; Sattler *et al.*, 2016; Peer *et al.*, 2017). The latter characteristic, together with the increased cell size, made polyploids interesting for breeding.

Even though polyploidization is a frequent event, its stabilization over generations is not (Peer *et al.*, 2017). More commonly, low ploidy levels are preferred, as exemplified by the experiment of Wang *et al.* where they proved genome instability in octaploids of *Arabidopsis thaliana* mutated for *TARDY ASYNCHRONOUS MEIOSIS (TAM)*. The mutation causes premature exit after meiosis I, and consequent generation of 2n gametes. The fourth generation of octaploid *tam*, did not show further genome doubling, on the contrary its progeny went back to a hexaploid state in 32% of the cases, while the remaining were distributed from diploids (2.4%) to octaploids (22%) and no higher ploidy level were observed (Wang *et al.*, 2010). Moreover, we know from numerous studies that neopolyploids can suffer from severe infertility, primarily caused by meiotic aberrations (reviewed in Ramsey and Schemske, 2002; Jenczewski and Alix, 2004; Comai, 2005; Zielinski and Mittelsten Scheid, 2012). From this observation raised the interest in studying meiotic regulation in polyploids organisms.

The major disturbance of meiosis in polyploids is caused by the formation of multivalents (association of more than two homologs) which results in difficulties in disentanglement of chromosomes association, errors in COs resolution, chromosome fragmentation, and ultimately in mis-segregation which induces aneuploidy and unviable gametes (Figure 1.4). Notably, the solution of these defects is fundamental to establish polyploidy over generations, and it is testified by the fact that neopolyploids are the most affected, while established lines present a regular

diploid-like meiotic division; epigenetics, as well as genetic, seems to play a role in this adaptation (Comai, 2005; Bomblies *et al.*, 2015; Pelé *et al.*, 2018)

Autopolyploids, which derive from a WGD event within a single species, and as a consequence have a double number of homologous chromosomes (Figure 1.4), are the most subjected to multivalents formation. It has been hypothesized that an increase in COs interference, and therefore a reduction in COs numbers but not their complete disappearance, would promote the formation of bivalents over multivalents (Bomblies *et al.*, 2015). This concept is supported by studies in *Arabidopsis arenosa*, which exists as diploid and as established natural tetraploid. Comparison between the genomes of the two populations revealed 39 differentiated regions, which encodes among others for eight meiotic genes involved in homologous recombination and synapsis: PRD3, ASY3, ASY1, REC8, ZYP1a, ZYP1b, SMC3 and PDS5 (Yant *et al.*, 2013).

Conversely, a second group of polyploids named allopolyploids has different solutions to the problem. Allopolyploids generate from hybridization followed by WGD; these concomitant events result in two or more diploid sets of homologous chromosomes, which are considered to be homoeologous one to the other (Figure 1.4). Homoeolog pairing is strongly restricted therefore in allopolyploids, compared to autopolyploids, the formation of multivalents is rare (Comai, 2005; Bomblies *et al.*, 2015; Pelé *et al.*, 2018). This phenomenon is regulated at a genetic level as demonstrated by the cases of the *Pairing homoeologous 1* locus (*Ph1*) in the allohexaploid *Triticum aestivum* (bread wheat, AABBDD; $2n=6x=42$). The *Ph1* locus contains a cluster of CYCLIN-DEPENDENT KINASES (CDKs) that control chromosome arrangement at premeiotic phases, as well as chromosome synapsis and COs formation. The absence of the *Ph1* locus induces homoeologous pairing and recombination. Similar evidence comes from the allotetraploid *Brassica napus* (AACC; $2n=4x=38$), in which a single gene was identified as primary responsible for the constraint: *PAIRING REGULATOR IN B. NAPUS* (*PRBN*) (reviewed in Jenczewski and Alix, 2004; Cifuentes *et al.*, 2010; Grandont *et al.*, 2013; Bomblies *et al.*, 2015). Curiously, since the low number of multivalents formed during allopolyploid meiosis, the strengthening of COs interference is not required, to the point that the number

of COs between homologs in allopolyploids seems to increase (Zielinski and Mittelsten Scheid, 2012; Grandont *et al.*, 2013)

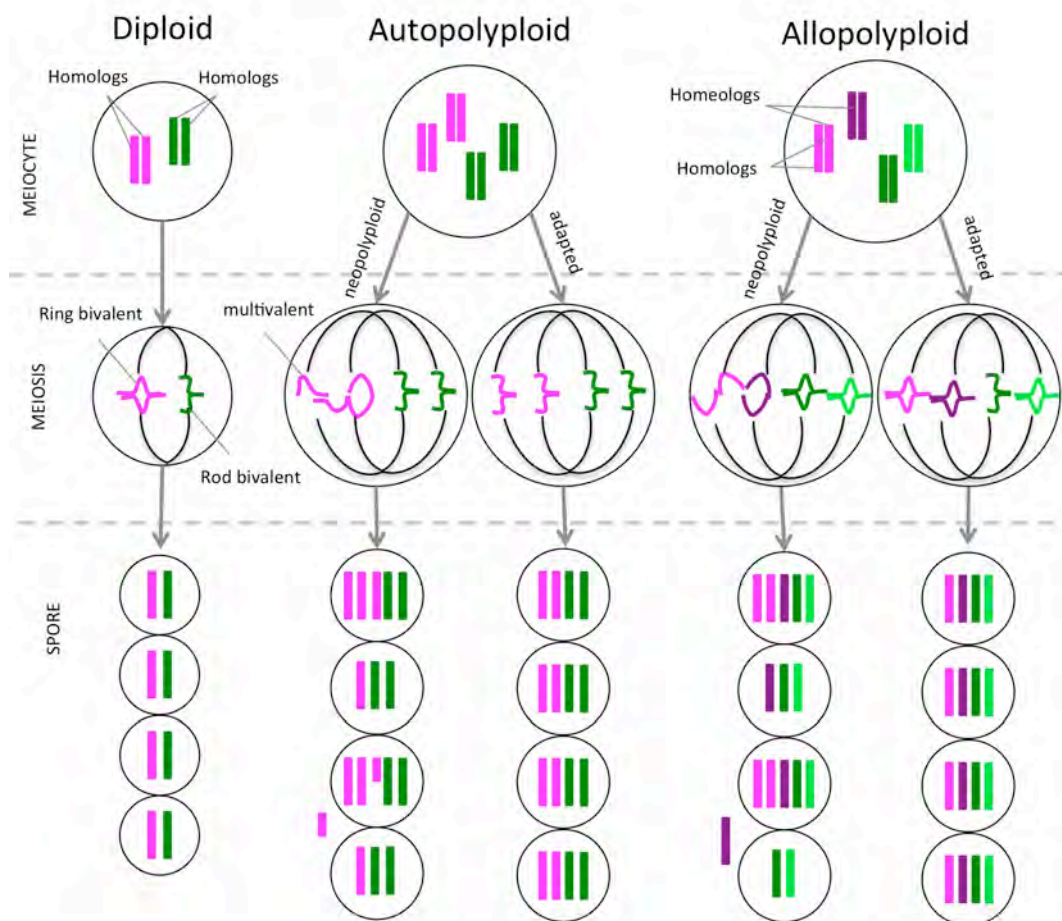


Figure 1.4 Meiotic defects and adaptation in polyploids

The figure illustrates the meiotic defects and the possible outcome of meiosis in diploid, autopolyploid and allopolyploid. Homologous chromosomes are presented in the same color (magenta and dark green) while homeologous chromosomes are colored with different tones (magenta/purple and dark/light green). During diploid meiosis, bivalents are formed in a ring shape (indication of two or more COs on the chromosome arms) or in a rod shape (only one CO is formed on one chromosome arm). Multivalents are easily formed during neopolyploid meiosis, and it results in the generation of unbalanced spores, chromosome fragmentation and aneuploidy. Established polyploids instead present a correct meiotic outcome, and balanced spores. This might be achieved with a reduction of CO number in autopolyploid (only rod bivalents) or with a strong restriction against homeologs pairing, in allopolyploids.

1.2 Time courses of plant meiosis

The course of meiosis and its consequent outcome (recombination, duration, gamete viability) can vary significantly depending on intrinsic characteristics of the organism, e.g., chromosome number, ploidy level, and gender; as well as depending on environmental factors, e.g. temperature and exposure to chemicals, both in plants (reviewed in Bennett, 1971, 1977; Bomblies *et al.*, 2015) and in animals (Allard and Colaiácovo, 2010; Zenzes *et al.*, 2001).

Among all, duration has been proven to be one of the most variable aspects: within the *Plantae* kingdom alone, meiosis can last from 16 hours in anthers of *Petunia* (Izhar and Frankel, 1973) up to 16.5 days in *Fritillaria meleagris* (reviewed by Bennett, 1977 and Table 1.1), or present an increase of 130 hours in female meiosis of *Lilium* hybrids compared with the male division (Bennett, 1977; Bennett and Stern, 1975). The main investigations about meiotic duration are dated back between 1950 and 1980. The majority of these works have been summarized by M.D. Bennett in his thorough review “*The time and duration of meiosis*” (1977), where a few common traits of the meiotic duration were stated for the first time:

- 1) Meiosis is always slower than the mitotic division of the same organism.
- 2) Prophase I is always the most extended phase.
- 3) The overall duration of meiosis is determined by the interaction of four main factors:
 - Environment, in particular temperature.
 - Genotype.
 - Nuclear DNA content.
 - Ploidy level.
- 4) The increase in duration of meiosis is due to a proportional increase of the length of every single phase, except for organisms that present developmental hold or, as more recent data prove, of single mutations of meiotic genes which are responsible for specific transitions during the division. For example in the case of *Atmlh3* and *Atmsh4*, involved in recombination, which cause a delay of prophase I (Higgins *et al.*, 2004; Jackson *et al.*, 2006).

Bennett's main conclusions have been re-proven and expanded by later experiments as illustrated in the following chapter. In particular, the influence of temperature and genotype have been assessed in the last decade.

1.2.1 Temperature and genotype effects on meiotic duration

Temperature effects can be quite drastic and influence many aspects of meiosis. Heat and cold shocks can alter the recombination rate (Bomblies *et al.*, 2015) and cause the arrest of meiotic progression (Draeger and Moore, 2017). Detailed experiments on the meiotic behavior at different temperature have been conducted on *Dasypyrum villosum* (Stefani and Colonna, 1996), *Endymion nonscriptus* (Wilson, 1959) *Secale cereale* and *Triticum aestivum* (Bennett *et al.*, 1971) bringing all at the conclusion that meiosis proceeds faster at higher temperatures (Table 1.1 and 1.2).

Implications of this information for breeding have been discussed by Stefani and Colonna, who hypothesized that incompatibility between hybrids of *Dasypyrum* and *Triticum* depends on different durations of prophase (9 hours longer in *Triticum turgidum*), and suggested that altering the temperature during meiosis could reduce the timing differences and increase the hybrid fertility (Stefani and Colonna, 1996). Another example is brought by Higgins *et al.*, where they correlate in *Hordeum vulgare* an altered spatiotemporal distribution of chiasmata with changes in temperature. In particular, higher temperature synchronizes the onset of recombination foci among the entire chromosome lengths, with no distinction between regions distal and proximal to centromeres. This phenomenon leads to rearrangement in the distribution of COs towards otherwise cold-spots, modifying the recombination landscape of barley (Higgins *et al.*, 2012).

The genotypic effects on meiotic duration can be analyzed under different aspects. At first, Bennett compares different varieties of the same species, concluding that plants sharing a large part of the genotype proceed at similar or identical speed, e.g. meiosis of the two cultivars of *Triticum aestivum* 'Chinese Spring' and 'Holdfast' lasts 24-25 hours when plants are grown at the same conditions. (Table 1.1, reviewed by (Bennett, 1977). On the other end, Bennett hypothesizes that mutations in single meiotic genes could influence meiosis, but the experimental means of the time were not advanced enough to bring clear evidence

to confirm this hypothesis. With the development of genetic tools such as T-DNA, it has been possible later on to verify it. A delayed and prolonged division has been found for example in the maize mutant *pam1*, (*plural abnormalities in meiosis 1*) (Golubovskaya *et al.*, 2002) and the *Arabidopsis thaliana* mutants *tam1* (Magnard *et al.*, 2001), *msh4* (*MutS homolog 4*) (delay of 8 hours in prophase) (Higgins *et al.*, 2004), and *mlh3* (*MutL homolog 3*) which shows a delay of 25 hours in first meiotic division, for an overall duration of meiosis of almost 60 hours (Jackson *et al.*, 2006).

1.2.2 Meiotic duration in polyploids

Another central point of Bennett's work was the study of polyploidy effects on meiosis (Bennett *et al.*, 1971; Bennett and Smith, 1972; Finch and Bennett, 1972; Bennett and Kaltsikes, 1973). Making use of cereal systems, which are present as diploid progenitors (*Triticum monococcum*, *Secale cereale* and *Hordeum vulgare*), and as tetraploids (*Triticum dicoccum*, *Secale cereale* and *Hordeum vulgare*), hexaploids or octaploids (different varieties of *Triticum aestivum* and the hybrid *Triticale*) Bennett and his collaborators observed that the duration of meiosis is shortened when the ploidy level becomes higher, e.g., meiosis of *Triticum monococcum* lasts 42 hours, while in its hexaploid relative *Triticum aestivum* meiosis lasts only 24 hours when grown at the same temperature (Bennett and Smith, 1972) (Table 1.1). This phenomenon was recorded in autopolyploids (*Hordeum vulgare*, Finch and Bennett, 1972) as well as in allopolyploids (*Triticale* and *Triticum aestivum*; Bennett *et al.*, 1971; Bennett and Smith, 1972) and could be considered counterintuitive since previous findings, as well as a comparison among the different species used in this study, described an increase in meiotic duration parallel to an increment in DNA content (Bennett, 1971; Bennett and Smith, 1972). The controversy of the data did not find an exhaustive explanation in the work of Bennett, and only recently a study conducted in *Triticum aestivum* proposed a regulatory mechanism based on observations of pre-meiotic association of centromeres in the hexaploid wheat, which were not recorded in the corresponding diploid (Martinez-Perez *et al.*, 2000).

It has to be noted that the work on cereals is focused exclusively on well-established polyploids, and therefore the shortening of meiosis could be a secondary

effect of the previously mentioned meiotic adaptation (chapter 1.1.4). Moreover an opposite trend was suggested by observations of meiotic progression of *Arabidopsis arenosa*; cell spreads of the diploid and tetraploid populations revealed that while the onset of meiosis was found in buds of the same size for both, the tetraploid buds hosting pollen were bigger than the diploid, showing a possible delay in meiosis (Higgins *et al.*, 2014).

1.2.3 Experimental procedures of time courses

Looking at the tables 1.1 and 1.2, and at the years of publication, together with the amount of information given, it becomes clear that after the review of Bennett and until early 2000, only a few works focused on the duration of meiosis.

The reason for this gap likely lies in technical issues. The basic experimental procedure relied on synchronicity of meiosis within the same flower bud or spikelet, and on tedious DNA labeling with radioactive compounds such as [³H]-thymidine, followed by autoradiography. The first attempts were based on relative timing, expressed in the frequency of cells found at a certain stage, within a specific position in the inflorescence or spike (Lindgren *et al.*, 1969). These types of experiments highlighted the differences of duration among the stages (e.g. In barley pre-pachytene and pachytene were the longest phases, followed by diplotene and telophase II and the position of the stages within the spikelet (Ekberg and Eriksson, 1965; Lindgren *et al.*, 1969), but often led to an imprecise or quite broad calculation of time.

A new rise of time courses as tools to study meiosis came after the introduction of immunolabelling techniques based on the modified thymine analog 5-bromo-2'-deoxyuridine (BrdU) (Gratzner, 1982) or 5-ethynyl-2'-deoxyuridine (EdU) (Salic and Mitchison, 2008). The usage of antibodies against the substitutive form of thymine, introgressed in DNA during replication, is much faster and less dangerous than the utilization of autoradiographic procedures. Armstrong was the first to describe a time course of plant meiosis using BrdU in *Arabidopsis thaliana*, being able to quantify the duration of each stage until diplotene (Armstrong *et al.*, 2003). This method allows the concomitant immunostaining of meiotic proteins and was applied as a tool to study mutant phenotypes and protein expression patterns in later

studies such as (Higgins *et al.*, 2004; Jackson *et al.*, 2006; Sanchez-Moran *et al.*, 2007). EdU was instead introduced a few years later either in combination with BrdU as presented by Higgins *et al.* in their time course of *Hordeum vulgare* (Higgins *et al.*, 2012), or to introduce a new cytological technique to study meiosis in *Arabidopsis thaliana* as in Stronghill *et al.* (Stronghill *et al.*, 2014) where they maintain the tridimensional structure of the pollen sacs, allowing the evaluation of more cellular features. In this study, they re-confirmed the duration of meiosis in WT male *Arabidopsis thaliana* to be around 22-24 hours as previously obtained by Armstrong and Sanchez-Moran (Table 1.2).

All the methods described above, independently on the labeling system, are based on fixation of meiocytes, and the actual time of each meiotic step is retro-calculated as an estimation of the distribution in the percentage of the meiotic stages over the samples, after a certain interval of times. This calculation has two major drawbacks: on one side it flattens the small asynchrony, which is present within the same pollen sac. This asynchrony was estimated to be 0.5 to 1 hour in *Petunia* by Izhar and Frankel, (Izhar and Frankel, 1973), and it is likely the reason why many time courses are not able to describe distinct phases duration from diplotene onwards (Armstrong *et al.*, 2003; Higgins *et al.*, 2012; Pacini and Cresti, 1978; Sanchez-Moran *et al.*, 2007; Stefani and Colonna, 1996; Stronghill *et al.*, 2014 and Table 1.2). The second drawback is the impossibility to disambiguate cases in which the meiotic division proceed at a different speed than in WT from cases in which the progression is arrested as in the mutant description of *pam1* (Golubovskaya *et al.*, 2002). Both problems can be solved applying live cell imaging techniques, as proven by data from Yu *et al.*, Nannas *et al.* on maize meiosis (Yu *et al.*, 2009; Nannas *et al.*, 2016). Yu and Nannas were able to define precisely the duration and progression of the second meiotic division, with a particular focus on anaphase II, which lasts less than 15 minutes (Table 1.1) and have been rarely recorded by fixed material (Nannas *et al.*, 2016; Yu *et al.*, 1997). Moreover, live cell imaging permits direct time calculation and, when performed for sufficient time, would bring new insights about meiosis of mutants, starting with the distinction between arrested and delayed progression, to the identification of their specific malfunctions and cytological effects.

Table 1.1

MONOCOT																			
plant specie	publication	temperature	overall duration of male meiosis	premeiosis	leptotene	zygotene	pachytene	diplotene	diakinesis	metaphase I	anaphase I	telophase I	metakinesis	prophase II	metaphase II	anaphase II	telophase II	tetrad	
<i>Allium cepa</i>	Vasil 1959	NOT GIVEN	95 hours	//	//	//	//	//	//	//	//	//	//	//	//	//	//	//	//
<i>Convolvulus majoris</i>	Bennett 1973	20°C	72 hours	//	//	//	//	//	//	//	//	//	//	//	//	//	//	//	//
<i>Diospyrum villosum</i>	Stefani and Colonna 1996	field in May field in July	35 ± 1.7 hours 22 ± 2 hours 136 ± 14.4 hours	//	//	//	15.5 hours 12 hours 6 hours	//	//	//	//	//	10.5 hours 6 hours 12 hours	//	//	//	//	8 hours 3.5 hours 6 hours	//
		5°C	88 ± 5.3 hours	//	//	//	69.5 hours	//	//	//	//	//	46 hours	//	//	//	//	//	22 hours
		10°C	29 hours	//	//	//	48 hours	//	//	//	//	//	20.5 hours	//	//	//	//	//	20 hours
		20°C	21 ± 0.7 hours	//	//	//	14 hours	//	//	//	//	//	10 hours	//	//	//	//	//	5 hours
		28°C	17 ± 0.7 hours	//	//	//	12.5 hours	//	//	//	//	//	5.5 hours	//	//	//	//	//	4.5 hours
		35°C	864 hours	//	//	//	30 hours	//	//	//	//	//	5 hours	//	//	//	//	//	3 hours
<i>Endymium nonscriptus</i>	Wilson 1959	0°C	360 hours	//	//	//	10 hours	//	//	//	//	//		//	//	//	//	//	//
		5°C	168 hours	//	//	//		//	//	//	//	//		//	//	//	//	//	//
		10°C	84 hours	//	//	//		//	//	//	//	//		//	//	//	//	//	//
		15°C	48 hours	//	//	//		//	//	//	//	//		//	//	//	//	//	//
		20°C	30 hours	//	//	//		//	//	//	//	//		//	//	//	//	//	//
		25°C	20 hours	//	//	//		//	//	//	//	//		//	//	//	//	//	//
		30°C	66 hours	//	//	//		//	//	//	//	//		//	//	//	//	//	//
		15-21°C	400 hours APPROXIMATE	//	//	//		//	//	//	//	//		//	//	//	//	//	//
<i>Fritillaria meleagris</i>	Barber 1942	12-15°C	96 hours	//	//	//		//	//	//	//	//		//	//	//	//	//	//
<i>Gasteria triana</i>	Straub 1937	NOT GIVEN	//	//	//	//		//	//	//	//	//		//	//	//	//	//	//
<i>Hordeum vulgare</i> unspecified variety	Lindgren et al. 1969	NOT GIVEN	//	//	5.30%	32.60%	19.90%	8%	19.50%	24.80%	2.40%	4.60%	13.00%	1.50%	7.20%	5.40%	13.60%	23.70%	
			//	//	//	//		7.50%	17.90%	24.10%	2.50%	4.70%	4.70%	1.60%	7.60%	5.80%	14.90%		
			//	//															
			39 hours	//															
<i>Hordeum vulgare</i> Sultan	Bennett and Finch 1971	20°C	39 hours	//	//	//													
<i>Hordeum vulgare</i> Ymer	Finch and Bennett 1972	20°C	39 hours	//	//	//													
<i>Hordeum vulgare</i> Ymer 4X	Finch and Bennett 1972	20°C	31 hours	//	//	//													
<i>Hordeum vulgare</i> Morex	Higgins et al. 2012	22°C	43 hours	//	//	//													
			43 hours	//															
			43 hours	//															
<i>Lilium candidum</i>	Sauvland 1956	NOT GIVEN	168 hours	//	//	//													
<i>Lilium henryi</i>	Pereira and Linkins 1963	NOT GIVEN	170 hours	//	//	//													
<i>Lilium hybrid: Black Beauty</i>	Bennett and Stern 1975	20°C	264 hours	//	//	//													
<i>Lilium hybrid: Sonata</i>	Bennett and Stern 1975	20°C	180 hours	//	//	//													
<i>Lilium longiflorum: variety unspecified</i>	Marquardt 1937	NOT GIVEN	96 hours	//	//	//													
<i>Lilium longiflorum: Nellie White</i>	Ito and Stern 1967	22°C	6492 hours	//	//	//													
<i>Lilium longiflorum: Croft</i>	Taylor and McMaster 1954	23°C	6240 hours	//	//	//													
<i>Lilium longiflorum: Floridi</i>	Erickson 1948	NOT GIVEN	72 hours -APPROXIMATE	//	//	//													
<i>Onithogalum virens</i>	Church and Wimper 1969	18°C	48 hours	//	//	//													
<i>Rhoeo discolor</i>	Vasil 1959	NOT GIVEN	88 hours	//	//	//													
<i>Secale cereale</i>	Bennett et al 1971	15°C	51 hours	//	//	//													
		20°C	39 hours	//	//	//													
		25°C	38 hours	//	//	//													
		20°C	126 hours	//	//	//													
<i>Secale cereale 4X</i>	Steinitz 1944; Taylor 1949; 1950; Beatty and Beatty 1953	NOT GIVEN	52 hours	//	//	//													
<i>Tradescantia pallidosa</i>	Steinitz 1944	NOT GIVEN	48 hours	//	//	//													
		18° to 23°	144 hours	//	//	//													
<i>Tradescantia reflexa</i>	Sax and Edmonds, 1953	NOT GIVEN	2160 hours	//	//	//													
<i>Trillium erectum</i>	Hotta and Stern 1963	1°C	1680 hours	//	//	//													
		2°C	960 hours	//	//	//													
		5°C	288 hours	//	//	//													
<i>Triticale turgidulum: durum</i>	Ito and Stern 1967	15°C	31 hours	//	//	//													
<i>Triticale: genotype A (CS/K7A)</i>	Bennett and Keltsikes 1973	20°C	21 hours	//	//	//													
<i>Triticale: genotype 4 (CS/K7A)</i>	Bennett and Smith 1972	20°C	22 hours	//	//	//													
<i>Triticale: genotype 6 (CS/Pret 7A)</i>	Bennett and Smith 1972	20°C	34 or 35 hours	//	//	//													
<i>Triticale: Rosecrans</i>	Bennett and Smith 1972	20°C	30 hours	//	//	//													
<i>Triticum dicoccum 4X</i>	Bennett and Smith 1972	20°C	31 hours	//	//	//													
<i>Triticum aestivum x Ae. Mutica</i>	Bennett, Dover and Riley 1974	20°C	35 hours	//	//	//													
<i>Triticum aestivum x Secale cereale</i>	Bennett 1973	20°C	43 hours	//	//	//													
<i>Triticum aestivum: Chinese Spring</i>	Bennett et al 1971	15°C	24 hours	//	//	//													
		20°C	18 hours	//	//	//													
<i>Triticum aestivum: Halfloft</i>	Bennett et al 1972	15°C	45 hours	//	//	//													
<i>Triticum monococcum</i>	Bennett and Smith 1972	20°C	24 or 25 hours	//	//	//													
<i>Tuboghnia violacea</i>	Taylor 1953	20°C	130 hours	//	//	//													
<i>Zea mays</i>	Hsu et al. 1988	NOT GIVEN	119.1 hours	//	43 hours	31 hours	12.2 hours	7.1 hours	7.2 hours	4.4 hours	1.6 hours	1.6 hours	1.1 hours	0.4 hours	3.9 hours	2.1 hours	2.8 hours	1 hour	
	Yu et al. 1997	25 ± 1°C	meiosis II: 5 hours	//	//	//	//	//	//	//	//	//	//	//	//	//	//	//	//
	Nemmas et al 2016	NOT GIVEN	anaphases: 12 min	//	//	//	//	//	//	//	12.7 ± 3.2 min	//	//	//	1.5 hours	//	//	11 ± 3.7 min	//

Table 1.2

Table 1.2 Duration of meiosis in Dicotyledons and gymnosperms

DICOTS																
plant specie	publication	temperature	meiosis duration overall	premeiosis	leptotene	zygotene	pachytene	diplotene	diakinesis	metaphase I/anaphase I	telophase I	interkinesis	prophase II	metaphase II/anaphase II	telophase II	tetrads
<i>Alliaria petiolata</i>	Bennett 1973	NOT GIVEN	24 hours	//	//	//	//	//	//	//	//	//	//	//	//	//
<i>Anthrinum majus</i>	Ernst 1938	NOT GIVEN	24 to 34 hours	//	//	//	//	//	//	//	//	//	//	//	//	//
<i>Arabidopsis thaliana: Ws</i>	Armstrong et al. 2003	18.5°-20°C	33 hours (24)	9	6	15.3										
<i>Arabidopsis thaliana: Col-0</i>	Sanchez-Moran et al. 2007	NOT GIVEN	32 hours (22)	10	7	12										
<i>Arabidopsis thaliana: Ler</i>	Stronghill et al. 2014	21°C	29 hours (22)	7	5	6	10	1	//	//	//	//	//	//	//	//
<i>Arabidopsis thaliana: Col-0 2X</i>	this thesis	21°C	35 hours (26.5)	8.5	1.5	6	10	3	1	1		1		4		
<i>Arabidopsis thaliana: Col-0 4X</i>	this thesis	21°C	51 hours (32.5)	19	1.5	7.5	11	3	1	1		1.5		6		
<i>Beta Vulgaris</i>	Bennett 1973	20°C	24 hours	//	//	//	//	//	//	//	//	//	//	//	//	//
<i>Capsella bursa-pastoris</i>	Bennett 1973	NOT GIVEN	18 hours	//	//	//	//	//	//	//	//	//	//	//	//	//
<i>Haplopappus gracilis</i>	Martham & Threlked	NOT GIVEN	24-36 hours	//	//	//	//	//	//	//	//	//	//	//	//	//
<i>Lycopersicon esculentum (Solanum lycopersicum)</i>	Bennett 1973	20°C	24-30 hours	//	//	//	//	//	//	//	//	//	//	//	//	//
<i>Lycopersicum peruvianum</i>	Pacini and Cresti 1978	NOT GIVEN	prophase 12 hours	//		12 hours										
<i>Petunia hybrida</i>	Izhar and Frankel 1973	15-17°C night /25-30°C day	16 hours	4	4	2	2	1	2	2	1		1		3	12
<i>Pisum sativum</i>	Bennett 1976	20°C	30 hours	//	//	//	//	//	//	//	//	//	//	//	//	//
<i>Veronica chamaedrys</i>	Bennett 1973	NOT GIVEN	20 hours	//	//	//	//	//	//	//	//	//	//	//	//	//
<i>Vicia faba</i>	Marquardt 1951	NOT GIVEN	72 to 96 hours	//	//	//	//	//	//	//	//	//	//	//	//	//
<i>Vicia sativa</i>	Bennett 1976	20°C	24 hours	//	//	//	//	//	//	//	//	//	//	//	//	//
GYMNOSPERM																
plant specie	publication	temperature	meiosis duration overall	premeiosis	leptotene	zygotene	pachytene	diplotene	diakinesis	metaphase I/anaphase I	telophase I	interkinesis	prophase II	metaphase II/anaphase II	telophase II	tetrads
<i>Pinus laricio</i>	Chamberlain 1935 (reported in Izhar et al. 1973)	NOT GIVEN	3 months	//	//	//	//	//	//	//	//	//	//	//	//	//

1.3 Imaging of meiosis

1.3.1 Live cell imaging setups

Three main setups have been used so far to follow meiosis live: wide-field, confocal and multi-photon microscopy.

Wide-field microscopy, often supported by deconvolution, provides an easy-to-handle system to obtain time-lapses and z-stacks of the division. The pairing of wide-field with a fluorescent light source (e.g., UV-lamp) allowed the employment of dyes and fluorophores fused to reporters to visualize cellular and nuclear elements, e.g., telomeres and centromeres (Tomita and Cooper, 2007) or synaptonemal proteins (Lee *et al.*, 2015). As an example, the functions of telomere bouquet in budding yeast *S.pombe* have been analyzed by wide-field microscopy. These works revealed its involvement in controlling the behavior of the microtubule-organizing center (Tomita and Cooper, 2007), as well as in creating a specialized sub-nuclear micro-environment that directs the assembly of meiotic centromeres (Klutstein *et al.*, 2015). Other works conducted both in yeast (Lee *et al.*, 2012) and in isolated mammal oocytes (Lee *et al.*, 2015; Shibuya *et al.*, 2014) dissected the rapid prophase movements of chromosomes, showing that they follow different dynamics over the meiotic division and that they are responsible for the formation of correct synapsis and recombination events.

While for single cell imaging (unicellular organisms, or isolated meiocytes) the wide-field microscope is a good option, for more complex samples confocal laser scanning microscopy (CLSM) is more adequate. By setting up a pinhole in front of the detector, the signal from the off-focal plane can be filtered, restituting images with a high signal/noise ratio. This allows the observation of thicker specimen that could be scanned a series of optical sections. Consequently, confocal microscopy has been successfully applied to study homolog pairing in *S.pombe* (Chacón *et al.*, 2016), *C. elegans* (Rog and Dernburg, 2015; Wynne *et al.*, 2012), *Drosophila melanogaster* (Christophorou *et al.*, 2015), and mammalian oocytes and spermatocytes, which can be visualized *ex vivo* within cultured embryonic ovaries and tubules (Enguita-Marruedo *et al.*, 2018). Likewise, chromosome segregation in mammal oocytes has been analyzed by confocal microscopy: kinetochores could be tracked for over 8

hours, revealing that the bi-oriented attachment of homologs is established after a lengthy try-and-error process (Kitajima *et al.*, 2011); microtubules organizing centers and actin elements of the cytoskeleton have been shown to be relevant for spindle formation and correct segregation (Schuh and Ellenberg, 2007; Holubcová *et al.*, 2013; Mogessie and Schuh, 2017), as well as it was confirmed by live cell imaging of fetal mouse oocytes that cohesin establishment is maintained without detectable turnover and that its loss in older oocytes remains uncorrected, leading to formation of aneuploid and non-viable gametes (Burkhardt *et al.*, 2016).

A further advantage of confocal microscopy is the usage of lasers as a light source, allowing the precise selection of excitation wavelength. This opened the way to procedures such as FRAP, as presented in the study of Gigant *et al.* By applying photobleaching to the cytoskeleton reporter GFP:NMY2, they were able to detect a change in the spindle dynamics of oocytes which carried a mutation in the kinesin-13, proving its involvement in the formation of meiotic spindles of *C. elegans* (Gigant *et al.*, 2017).

At last, two-photon microscopy has been used to image meiosis in *C. elegans*. Two-photon microscopy uses infrared light as excitation source, which allows deep penetration in the tissues. Coupling two-photon technology with the FLIM/FRET technique Llères *et al.*, were able to visualize at a nanoscale level the compaction of prophase chromosomes within *C. elegans* ovaries, and to link its regulation to the action of condensin I and II (Llères *et al.*, 2017).

1.3.2 Live cell imaging of plant meiosis

In contrast to the study of meiosis in other organisms, research in plants is only in its infancy to explore the power of live imaging. So far, only five studies are published that employ two different approaches to describe chromosome movements and MTs rearrangements in maize meiocytes (Yu *et al.*, 1997; Nannas *et al.*, 2016; Higgins *et al.*, 2016; Sheehan and Pawlowski, 2009) as well as chromatin reprogramming in *Arabidopsis thaliana* (Ingouff *et al.*, 2017).

The system developed by Yu *et al.* 1997, re-adapted in the works from Nannas *et al.*, 2016 and Higgins *et al.*, 2016, is based on wide-field fluorescent microscopy of isolated maize meiocytes; the cells are cultured in liquid medium, which offers the

advantage of easy treatment with dyes as Syto12 to mark chromosomes whereas other cellular elements could be visualized with fluorescent reporters such as the fusion protein CFP: β -TUB1 for microtubules.

While this set up is easily applicable, its usage is restricted to the study of short meiotic phases such as metaphase and anaphase: meiocytes could be maintained alive for a maximum of 9 hours (Yu *et al.*, 1997) and were imaged over periods of 80 minutes or less (Nannas *et al.*, 2016), failing to reconstitute information about the longer prophase. Nonetheless, important knowledge could be gained about the regulation of meiotic spindles, which could not be revealed by fixed specimen. For example, the work of Nannas described the existence of asymmetrical anaphases, which correct off-center positioning of the spindles in anaphase I and II, and the appearance of phragmoplast equidistant from the chromosomes instead of in the spindle mid-zone, providing a backup system for failure in completing chromosomes segregation (Nannas *et al.*, 2016).

The second approach is based on multiphoton microscopy. Exploiting its great focus depth, which reaches 200 μ m, meiocytes can be imaged without the need of isolation. This set up has been successfully applied to maize anthers cultured in liquid medium (Sheehan and Pawlowski, 2009) and on *Arabidopsis thaliana* inflorescences, embedded in solid medium and dissected with a vibratome (Ingouff *et al.*, 2017). Samples could be maintained alive for periods longer than 30 hours and imaged for 24 hours (maize anthers in Sheenan and Pawlowski, 2009, no time indications for Ingouff *et al.*, 2017). Sheenan and Pawlowski were able to observe and analyze chromosome movements similar to the one described for yeast, *C. elegans*, and mammals, revealing the presence of different dynamics characterizing zygotene and pachytene stages (Sheehan and Pawlowski, 2009). Ingouff *et al.*, instead, were interested in investigating chromatin reprogramming during *Arabidopsis thaliana* reproduction, and revealed that methylation levels are very stable except for a significant decrease of the signal upon egg cell maturation. Since in their study Ingouff *et al.*, aim to follow the complete sexual development of the plant, meiosis was considered a single unit, without distinction among sub-phases, and therefore their resolution of the cell division was minimal.

2 Objectives

Over the last years, the study of biological processes has been incredibly fostered by live cell imaging, which disclosed the complex dynamics underlying events such as cell proliferation, pattern formation, and cell death. Differently than in other topics, in the field of meiosis plants has lacked behind yeast or other animals, counting only a handful number of publications using live cell imaging approaches (Yu *et al.*, 1997; Sheehan and Pawlowski, 2009; Nannas *et al.*, 2016; Higgins *et al.*, 2016; Ingouff *et al.*, 2017).

As a consequence, the description of the dynamics of the meiotic division has been restricted to the application of cytochemical methods such as cell spreads and immunolocalization, which are based on fixed material. While these techniques have been and continue to be, very informative, they did not allow fully capturing the nature of meiosis, characterized by specific chromosome movements during pairing and segregation, or by the fast dynamics of protein re-location.

The first aim of this study was, therefore, the establishment of a live cell imaging technique to follow the entire meiotic division in anthers of *Arabidopsis thaliana*. The technique should fulfill three main requisites: long-time imaging (and hence maintenance of sample viability for a long time) to follow the complete division, chromosomal resolution in imaging to distinguish chromosomes and cellular structures, and finally simplicity in its execution to make the method available for other researchers.

Secondly, a system to unequivocally describe the images and allow for a quantitative description of the obtained data should be developed.

Finally, I was interested in the application of the new method, paired to the analysis set up, to perform a comparison between the time course of male meiosis in wild type *Arabidopsis thaliana*, in diploid and tetraploid populations.

3 Results

3.1 Technique establishment

Live cell imaging of plants benefited greatly from CLSM application; for example confocal microscopy has been used to study mitosis and cell differentiation in root apical meristem (RAM) (e.g., in Komaki and Schnittger, 2017) and in shoot apical meristem (SAM) (e.g., in Hamant *et al.*, 2014; Gruel *et al.*, 2016) of *Arabidopsis thaliana*. Conversely, it has not been applied so far to observe plant meiosis. In the first chapter of the “Results” section a new method is introduced.

3.1.1 Sample isolation and mounting

The selection and preparation of optimal material are of key importance to perform live imaging. To facilitate the handling of the sample the whole procedure was performed under a dissection microscope with a magnification of 4X. An inflorescence was cut from a five to six weeks old plant and laid down on a support of 1% agarose dissolved in MilliQ water. Under our growth conditions (Material and Methods section 6.1), wildtype-like flower buds undergoing meiosis are 0.3-0.5 mm long and present a round shape (Figure 3.1); therefore all flowers larger than 0.5mm were removed at the pedicel with the use of tweezers (Figure 3.1A).

CLSM has a typical penetration depth of 70-100 μm , which allows imaging through the four cell layers that enwrap the pollen mother cells (PMCs) within the anther, but not to penetrate the sepals. Thus, to obtain clear images of male meiocytes, it was necessary to remove the uppermost sepal of the flower bud; in this way, two of the six anthers are exposed and directly accessible to the objective (Figure 3.1C₁ and C₂). After the sepal removal, the inner organization of the floral organs is disclosed, giving a further hint about the staging: in flower primordia undergoing meiosis, petals are visible, but they do not overlap with the anthers which in turn have the same length of the gynoecium (Figure 3.1C₂). This developmental stage corresponds to stage 9 in the description from Smyth *et al.* 1990 (Smyth *et al.*, 1990).

Conversely, all the small flowers, presumably not containing any meiocytes yet, were clipped away (Figure 3.1B) to obtain a single bud attached to a few millimeters of its stem. The sample was transferred and anchored onto a small petri dish (diameter of 35 mm) filled with Apex Culture Medium (ACM) (Hamant *et al.*, 2014). Further stabilization was obtained using a drop of 2% agarose in MilliQ water distributed around the flower head.

If the flower bud was not at the correct stage, either one of two strategies was followed: when the flower presented a more advanced developmental stage (e.g., long petals), it was clipped, and the very next flower of the inflorescence was isolated; when the flower was too young it was possible to mount it on ACM, seal the petri dish and let it grow at the same growth conditions of the mother plant until the correct developmental stage was reached.

To assess the sample viability on ACM, flower buds were isolated and mounted on the medium as in preparation for imaging, with the removal of the uppermost sepal. The petri dish containing the samples were sealed and repositioned in the same growth chamber as the mother plant, to assure the maintenance of the environmental conditions. Flower bud growth was monitored throughout one week (Figure 3.1 D).

The organs of the flowers presented a development from stage 9, (Figure 3.1 D, DAY 0) to stage 15 (Figure 3.1 D, DAY 7), within a similar timeframe (7 days versus 6.5 days) as previously published in Smyth *et al.* 1990 (Smyth *et al.*, 1990).

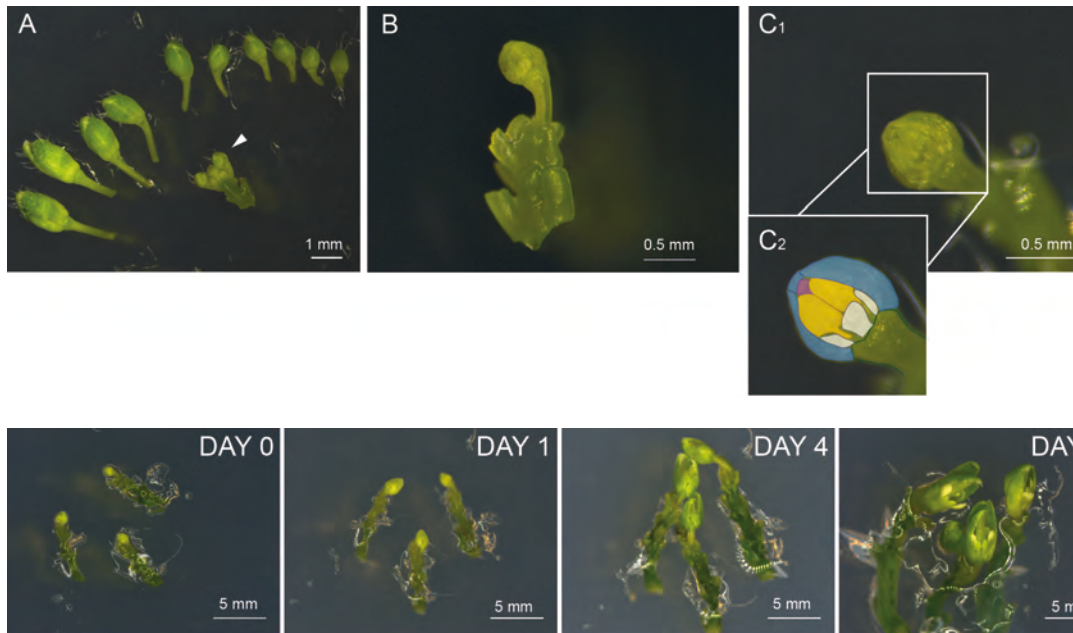


Figure 3.1 Sample isolation and viability

The three main steps of sample preparation are illustrated:

A) At first, an inflorescence is dissected. All the older flowers are removed, while the younger flower buds are kept attached to the stem. The white arrowhead indicates a flower bud at a meiotic stage.

B) After the removal of the uppermost sepal and the validation of the correct developmental stage of the selected flower, all the smaller flower buds are clipped away.

C₁) The sample is anchored into ACM with the exposed anthers facing up.

C₂) Magnification of the flower bud in C₂); the different floral organs are highlighted: in blue sepals, in white petals, in yellow anthers and in pink the gynoecium.

D) Monitoring of flower growth and development on ACM. The 3 flowers present a normal growth over a period of 7 days: the floral organs and the stem elongate in a constant manner from day 0 to day 7, confirming their viability on the medium.

3.1.2 Microscope set up

Upright CLSM ZEISS 780 and 880 were equipped with 40X water dipping objectives, which can be submerged directly into water; thus bypassing the use of cover glasses.

This set up allows mounting the sample on solid medium in a small petri dish, as described in 3.1.1, leaving it free to grow and expand without constraint in the vertical direction, but at the same time offering an anchoring system to avoid flotation.

Other magnification lenses such as 20X and 63X were tested for the purpose, but the 40X objective was finally selected since I could visualize the entire flower structure without sacrificing resolution when zooming onto single meiocytes (**Figure 3.2 B₁**). Once ready, the petri dish containing the sample was positioned on the microscope stage and stabilized with double-sided tape. The petri dish was then

filled with autoclaved water, and left in position for a period of minimum half an hour, to ensure that the medium would absorb the water, and avoid later on further movements due to medium swallowing.

Such a microscope set up applies to several investigations, and therefore the settings for image acquisition could be adjusted according to with the purpose. In the context of this dissertation, I applied the technique to perform time courses of the entire meiotic division, on flower buds expressing GFP and TagRFP fusion proteins; thus the main concern was to balance image resolution, with temporal resolution and sample upkeep.

Images were acquired as a series of z-stack. The interval time was set between minimum 3 and maximum 15 minutes, depending on the observed meiotic phase. The z-stacks were composed by six focal planes, with 50 μm distance. This interval in the z-dimension allowed the buffering of small vertical movement of the sample, assuring that the same meiocytes would be captured during the whole data acquisition. When more than flower bud was mounted on the same petri dish, their different positions were saved using the multi-position function of ZEN software, and each of them was automatically re-focused at each time point, using the auto-focus function based on fluorescence.

Argon laser (λ 488) and DPSS 561-10 laser (λ 561) were used as the source of excitation wavelengths for GFP and TagRFP respectively; their intensity was adjusted according to with the sample emission, but in general, was never exceeding 10% for the Argon laser and 4% for the DPSS 561-10 laser. It was essential to keep it as low as possible to not compromise the sample viability. The emitted signals were firstly filtered through the Beam splitter MBS 488/561. Green and red fluorescence were recorded in two channels by sequential line mode filtered respectively for 498-550 nm and 578-649 nm; an additional third channel was used to collect the auto-fluorescence of chloroplasts, and filtered for 680-750 nm. The pinhole was set at 1 Airy Unit, and scan time did not exceed 0.7 μsec pixel dwell. The bidirectional function was on, and averaging was performed on two lines. Images were 1024x1024 pixels.

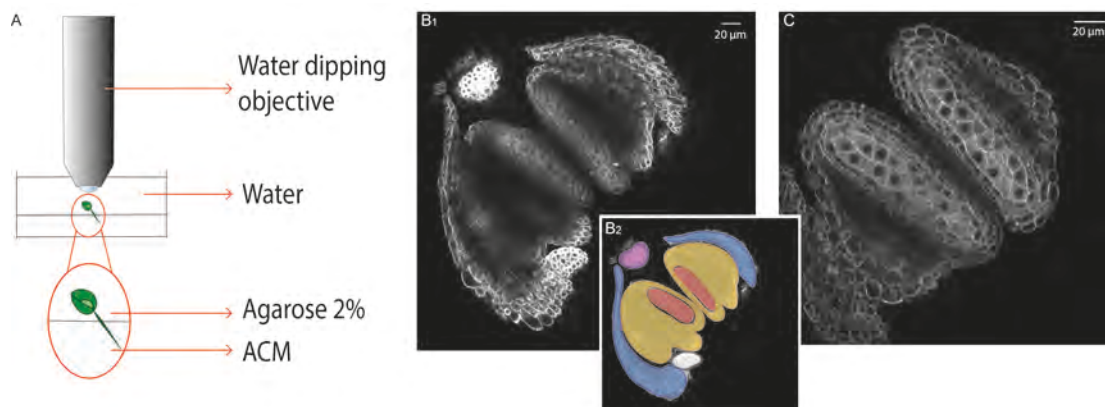


Figure 3.2 Microscope set up

Example of microscope set up and sample visualization.

- A) The sample (in green) is mounted in a small petri dish containing ACM. The petri dish is filled up with distilled water and the objective is immersed directly into the water.
- B₁) Overview of a flower bud carrying TUB4-RFP reporter, under the 40X water dipping objective.
- B₂) Identification of floral organs of the flower bud in B₁: in blue sepals, in white a petal, in pink the tip of the gynoecium and in yellow 2 anthers. Within the anthers pollen sacs are highlighted in red.
- C) Zoom in on the anthers of B, on a different focal plane. Meioocytes occupy the inner part of the anther and are recognizable by their regular shape and the big central nucleus.

3.2 Selection of reporter lines

A typical set up for live cell imaging of cell divisions is concomitant use of a marker for chromatin, such as histone fusion protein, with a marker that highlights microtubules to monitor chromosome and spindle behavior (two examples to follow plant meiosis can be found in Peirson *et al.*, 1997; Nannas *et al.*, 2016). Additionally, I was interested in a meiotic-specific marker, to unequivocally identify meiocytes even at early stages of meiosis when their size and shape are not yet very distinct.

I identified as a good candidate among the reporters available in our laboratory the *GFP* fusion to *REC8* $PRO_{REC8}:REC8:mEGFP$, generated by Dr. Shinichiro Komaki (Prusicki *et al.*, 2018).

REC8 accumulation has been detected by immunolocalization studies starting from pre-meiotic S-phase until the onset of anaphase I (Cai *et al.*, 2003). Moreover, seen its role as α -kleisin subunit in the meiotic cohesin complex, it localizes along the entire length of the chromosomes during prophase I, allowing the detection of chromosome dynamics and synapsis state until the end of metaphase I.

Therefore I decided to utilize *PRO_{REC8}:REC8:mEGFP* as a marker for chromatin during meiosis. I found that the reporter line only accumulates in meiocytes and its localization pattern is consistent with the previous description (Cai *et al.*, 2003)(Figure 3.3 A).

Moreover, the *REC8* reporter allowed us to estimate the sensitivity of the imaging procedure. While *REC8* is removed from chromosomes arms at the end of meiosis I to allow the resolution of cross-overs, a small fraction remains at the centromeres to maintain sister chromatid cohesion (Yuan *et al.*, 2018). The detection of the centromeric fraction of *REC8* has been challenging by immunolocalization studies (Cai *et al.*, 2003; Yuan *et al.*, 2018). When I followed the first meiotic division, I observed the remaining *REC8:GFP* at centromeres indicating that the here presented live cell imaging system is highly sensitive (Figure 3.3 B).

As cytoskeleton marker, I selected a fusion protein of the TUBULIN β SUBUNIT 4 (*TUB4*) with TagRFP expressed under the *RPS5A* promoter (*PRO_{RPS5A}:TagRFP:TUB4*), generated and kindly provided by Dr. Takashi Ishida (Kumamoto University, Japan). The expression of *PRO_{RPS5A}:TagRFP:TUB4* is not cell-specific, and therefore not only allows a straightforward recognition of meiotic phases such as metaphase and anaphase, but permits as well the observation of the complete structure of the anther, and consequently the study of the behavior of other cell layers constituting the pollen sac, e.g., the tapetum.

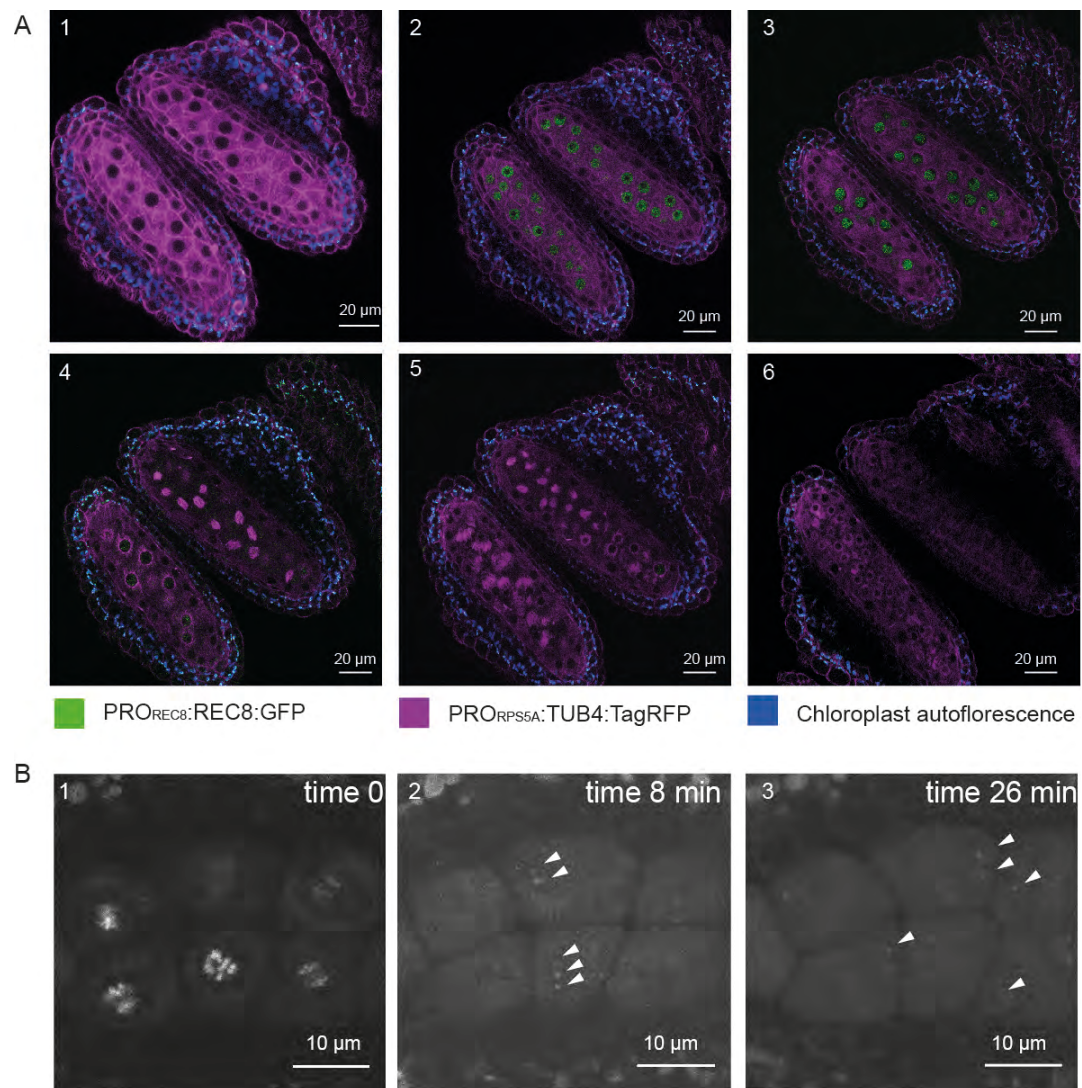


Figure 3.3 Expression pattern of *PRO_{REC8}:REC8:mEGFP* and *PRO_{RPS5A}:TagRFP:TUB4* in the *KINGBIRD* line

- A) The figure depicts the localization of *PRO_{REC8}:REC8:mEGFP* and *PRO_{RPS5A}:TagRFP:TUB4* over the course of entire meiosis in a flower of the *KINGBIRD* line. A₁:premeiosis; A₂: leptotene; A₃: zygotene; A₄: diplotene in the lower anther and metaphase I in the upper anther; A₅: telophase I in the lower anther and late prophase II-metaphase II transition in the upper anther; A₆: tetrads.
- B) REC8-GFP localization after metaphase I (B₁) in a *PRO_{REC8}:REC8:mEGFP*-only plant. The white arrowheads in B₂ and B₃ indicate centromeric REC8.

3.2.1 Functionality of the *PRO_{REC8}:REC8:mEGFP* and the *PRO_{RPS5A}:TagRFP:TUB4* reporter

To assure that the fusion protein *PRO_{REC8}:REC8:mEGFP* was functional, I performed a rescue assay. Homozygous plants of the REC8 T-DNA insertion line SAIL_807_B08 (*rec8*^{-/-}) present a normal vegetative growth, but are completely sterile, with short siliques and pollen and seed abortion rates at almost 100% (Figure 3.4 A-E). A close

look to meiotic progression reveals all the typical phenotypes previously described for *rec8* homozygous plants: irregular chromosome condensation and pairing at prophase I, chromosome fragmentation, presence of univalents, and chromosome mis-segregation resulting in the formation of unbalanced gametes, micronuclei and polyads (Figure 3.4 F, Bai *et al.*, 1999). The introgression of *PRO_{REC8}:REC8:mEGFP* construct into *rec8* *-/-* background fully restored fertility, with the plant growing elongated siliques, and having a similar level of pollen and seed production as wild-type plants (figure 3.4 A-E). Cell spreads of *PRO_{REC8}:REC8:mEGFP* revealed a normal meiotic progression, with correct chromosome pairing at prophase and absence of polyads after telophase II (Figure 3.4 F). Overall, I could confirm the functionality of the reporter *PRO_{REC8}:REC8:mEGFP*.

Mutations in tubulin genes, including the Arabidopsis *β -tubulin 4* (TUB4), are known to have a semi-dominant effect (Ishida *et al.*, 2007). I wanted to verify that the introgression of the marker would not behave as a dominant or semi-dominant negative itself, inducing an abnormal phenotype at a meiotic level. Therefore I checked the progression of meiosis using the cell spread technique in plants carrying *PRO_{RPS5A}:TagRFP:TUB4* in a wild-type Columbia background. The analysis revealed that meiosis progresses normally, ruling out the possibility of a negative effect of the construct, and revealing no artifact formation during the cell division (Figure 3.4).

3.2.2 The KINGBIRD line

To maximize the information coming from chromosome conformations and microtubules rearrangements I combined the lines *PRO_{REC8}:REC8:mEGFP* and *PRO_{RPS5A}:TagRFP:TUB4*. The resulting double reporter line is referred to as *Kleisin IN Green microtuBules In ReD (KINGBIRD)*. The separated excitation and emission spectra of the two fluorochromes allowed the reliable and concomitant detection of both reporters (Figure 3.3 A) No meiotic defects and no reduction in fertility were observed in this line as well (Figure 3.4 A-E).

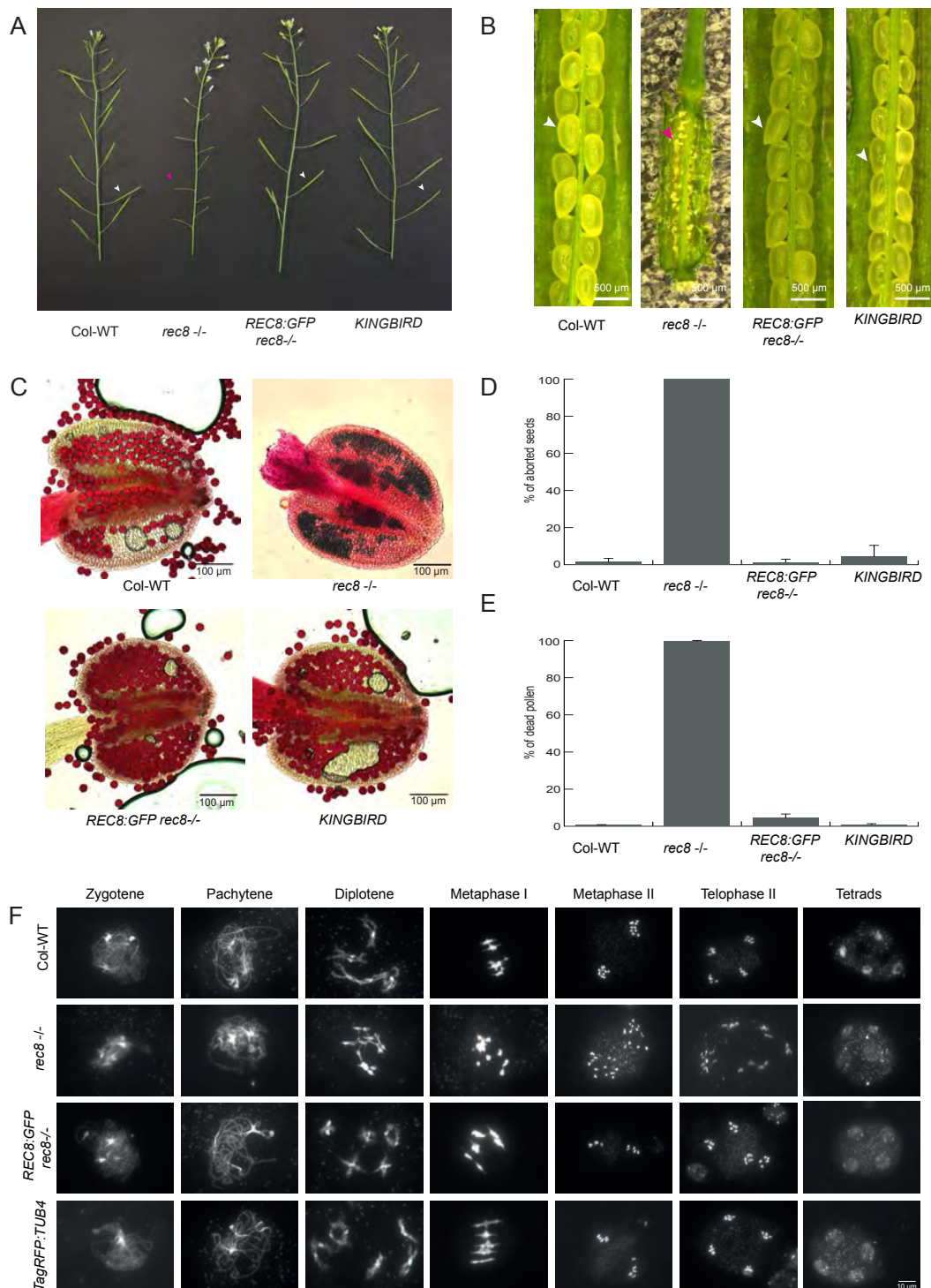


Figure 3.4 PRO_{REC8}:REC8:GFP, PRO_{RPSA5}:TgRFP:TUB4 and the *KINGBIRD* line have wild-type phenotype

Branches of Col-0 WT, *rec8*^{-/-}, *REC8:GFP* in *rec8*^{-/-} background, *KINGBIRD* in Col-0 WT background. While *rec8*^{-/-} shows short, thin and sterile siliques (magenta arrow head), *REC8:GFP* and *KINGBIRD* present WT-like, elongated and thick siliques (white arrow heads). Open siliques of Col-0 WT, *rec8*^{-/-}, *REC8:GFP* in *rec8*^{-/-} background, *KINGBIRD* in Col-0 WT background, Col-0 WT, *REC8:GFP* and *KINGBIRD* form round, turgid and fully developed seeds (white arrow heads), whereas *rec8*^{-/-} presents dry and aborted seeds (magenta arrow head).

Anthers stained with Peterson staining (Peterson et al. 2010). Col-0 WT, *REC8:GFP* and *KINGBIRD* only produce viable pollen, while high rates of aborted pollen (blue) are visible inside *rec8*^{-/-} pollen sacs.

Rate of seed abortion (%).

Rate of aborted pollen in (%).

Selection of main meiotic phases from the cell spreads of Col-0 WT, *rec8*^{-/-}, *REC8:GFP* in *rec8*^{-/-} background, and *TagRFP:TUB4* in Col-0 WT background. *rec8*^{-/-} presents defects from diplotene onwards: univalents, miss-segregation of chromosomes, formation of micronuclei and unbalanced tetrads. The meiotic progression is restored in *rec8*^{-/-} expressing *REC8:GFP* and it is not disrupted in *TagRFP:TUB4* in Col-WT background. Both of the constructs generated balanced and viable gametes.

3.3 A landmark system for male meiosis of *Arabidopsis thaliana*

The mathematical analysis of the data presented in this section has been obtained in collaboration with Emma Mathilde Keizer, Rik Peter van Rosmalen and Christian Fleck, from the Department of Agrotechnology and Food Sciences, Laboratory of Systems and Synthetic Biology, Wageningen University & Research, Wageningen, The Netherlands. Their work is acknowledged by the abbreviation (WUR) over the course of the manuscript.

3.3.1 Cell features description and co-occurrence

Using the *KINGBIRD* reporter line, I was able to distinguish five cellular features of the meiocytes: cell shape, nucleus position, nucleolus position, microtubule array (MTs), and chromosome state (condensation and pairing/synapsis). During the progression of meiosis, each of these features undergo major changes and gives rise to the conformations illustrated in **Figure 3.5 A**. These conformations are detectable in a distinct and unidirectional order; therefore they could be coded by ascending numbers to facilitate the downstream analysis, e.g., the nucleolus can be undetectable (conformation 1), centrally located (conformation 2), peripheral (conformation 3) or absent (conformation 4)(**Figure 3.5**).

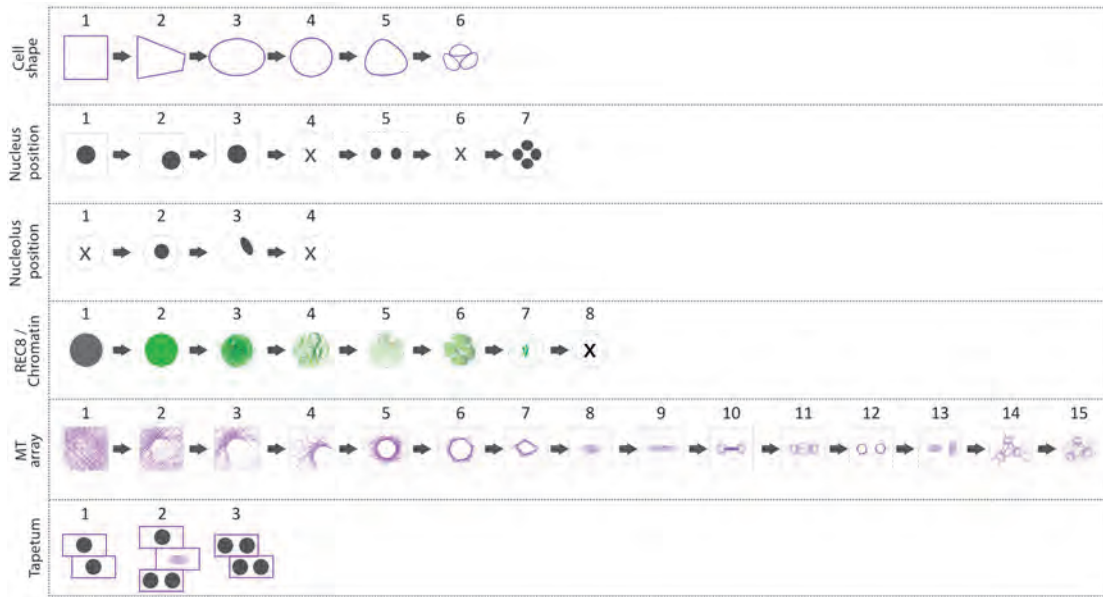
Importantly, the selected markers recapitulated previously described changes in nucleolus position and microtubule cytoskeleton, corroborating that the imaging system did not affect meiosis (Peirson *et al.*, 1997; Stronghill *et al.*, 2014; Wang *et al.*, 2004b; Yang *et al.*, 2006).

In addition to the five features of the meiocytes, the sample preparation, which keeps anthers intact, provided the possibility to follow the differentiation of the surrounding tissues, especially the tapetum cells. These are in direct contact with the meiocytes and are thought to be necessary for their nourishment and support (Pacini and Cresti, 1978). A key feature of tapetum cells in many plants species, including *Arabidopsis thaliana*, is that they become poly-nucleated through endomitosis, i.e., a cell cycle variant in which cytokinesis is skipped (Jakoby and Schnittger, 2004). The poly-nuclearization of tapetum cells was clearly visible in the *KINGBIRD* line, possibly representing a sixth cell feature next to the five meiotic features as presented above and previously suggested as a criterion to judge meiosis (Stronghill *et al.*, 2014; Wang *et al.*, 2004b), I, therefore, coded for three possible configurations of the tapetum: mono-nucleate (1), transitory state, with part of the tapetum showing spindle (2), complete poly-nuclearization of the tapetum (3) (**Figure 3.5 A**).

Observing a first set of time-lapses gave rise to the hypothesis that some of the conformations of the different morphological features are coupled and/or appear in a specific order, e.g., the nucleolus dissolves only after the nucleus has moved to one side of the meiocyte and returned to a central position. To assess the nature of these associations, I analyzed a subset of cells (n=169 from 35 anthers) from 126 time-lapses, assigning a combination of numbers that represents the conformation of each feature at each time point when a frame was taken, e.g. the conformation 1-1-2-2-1-1 describes a meiocyte that is rectangular in shape, has a centrally located nucleus with a centrally located nucleolus, with not yet paired chromosomes, an evenly distributed microtubule array and surrounded by a mono-nucleate tapetum (**Figure 3.5.A**). In the following, I call a combination of all feature configurations at a certain time point, a *cellular state*.

At first, conformation co-occurrence was tested mapping the frequency of their paired appearance at 10,671 time points (WUR). The heat-map in **Figure 3.5.B** illustrates the results of the analysis: the darker the blue color, the tighter is the correlation between features and the higher is the frequency of co-appearance of two configurations. The results confirm the hypothesis that the majority of the features follow a precise developmental path and that some of their conformations are strictly coupled, e.g., cell shape 1 and nucleus position 1, while other conformations never appear at the same time point, e.g., nucleolus position 2 and MTs array 6. In particular, the tapetum cells relate only to a certain extent with the developmental program of the other five features, having looser co-occurrence than expected (**Figure 3.5.B**). I, therefore, decided to proceed in the analysis of the cellular states omitting the sixth feature and focusing on the meiocytes only.

A



B

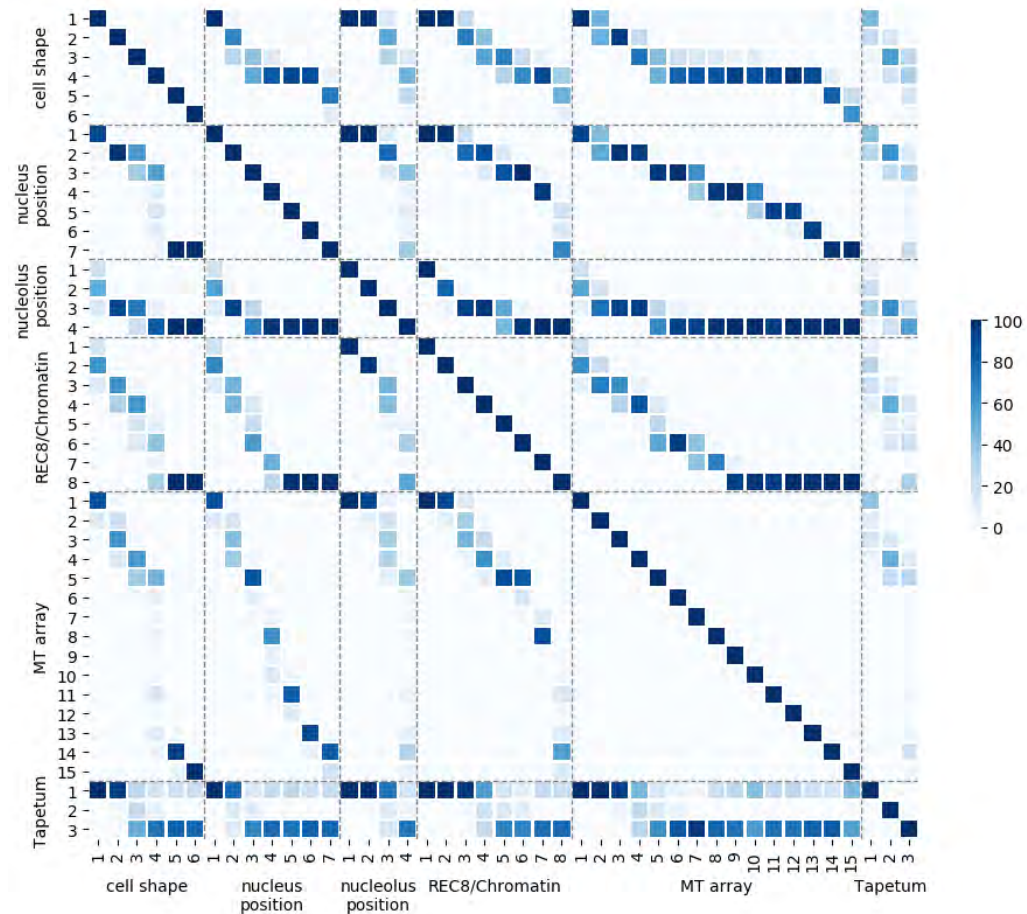


Figure 3.5 Conformations of cellular features

- A) The figure illustrates the different conformations that each of the five cellular features and the tapetum cells can acquire during meiotic progression. Each state is indicated by a number, which has been used as a code in the following analysis
- B) Heat-map illustrating the co-occurrence of configurations of cellular features. The frequency of the co-occurrence is expressed in percentage on a scale from 0 to 100, where 0 is a light blue square and 100 is the darkest blue. The heat map was realized by Rik P. van Rosmalen (WUR)

3.3.2 Assessment of cellular states and definition of neighboring score

The data set used to analyze the configuration co-occurrence was then refined with the removal of the tapetum cells, resulting in cellular states described by only five digits corresponding to the configuration of cell shape, nucleus position, nucleolus position, chromosome condensation and synapsis, and microtubule array.

The updated data set presented within the 10,671 time points the appearance of only 101 different cellular states, out of the more than 20,000 theoretically possible; their frequencies were distributed in a very dispersed range (from 0.01% to 21.14% of the total number of observations) (Annex 1). I realized at this point that an assessment of these states based on their direct frequency was highly biased by the duration of the respective state i.e. combinations of features that depict long phases such as pachytene are present in higher number of time points than combinations depicting short phases, e.g. metaphase I.

Hence, to identify significantly distinct cellular states within the observed data, together with the support of collaborators from WUR, we determined a *neighboring score*, which quantifies the representation of a certain state compared to its surrounding and not to the complete division.

The neighboring score was defined as:

$$Score = \frac{count(state) - mean(count(neighboring\ states))}{standard\ deviation(count(neighboring\ states))}$$

where *count* indicates the number of observations of a state, and *neighboring states* is the group of surrounding cellular states selected for the comparison.

The definition of neighboring state is based on empirical observations. At first I excluded from being neighbors, states that differentiated of more than one digit for the same feature (e.g. the states 4-5-4-8-10 is neighbor of 4-5-4-8-11, but not of 4-5-4-8-12), affirming as a consequence, that these two states were distant enough in the progression to not belong to the same developmental phase. In the same way, I excluded from the definition all the cases in which all the five features switch concomitantly, since this situation was never observed in the data set (e.g. the states

3-2-3-5-5 and 4-3-4-6-6 are not neighbors). Conversely, in this data set I could observe one, two, three or four features turning configuration simultaneously. The occurrence of the events was extrapolated within a maximum interval time of 15 minutes, to test if a pattern was recognizable (WUR) (Figure 3.6). The events showed an uneven distribution, with the majority of the changes happening for one single feature (69.6% considering an event as one, independently by the number of features that switched simultaneously), followed by the change in two features (24.5%), three features (5.5%) and four features (less than 0.5%). This analysis revealed that the majority of the switch events interested a maximum of two features (94 %); I therefore opted to define neighbors as in the following: *neighbor of a cellular state is a cellular state that is one transition away (-1 or +1) for at least one, and at most two, features compared to another.* With this, 2-2-3-4-4, for example, is a neighbor of 2-2-3-4-3 and of 3-2-3-4-3, but not of the cellular state 2-2-3-4-2 neither of 3-2-3-3-3.

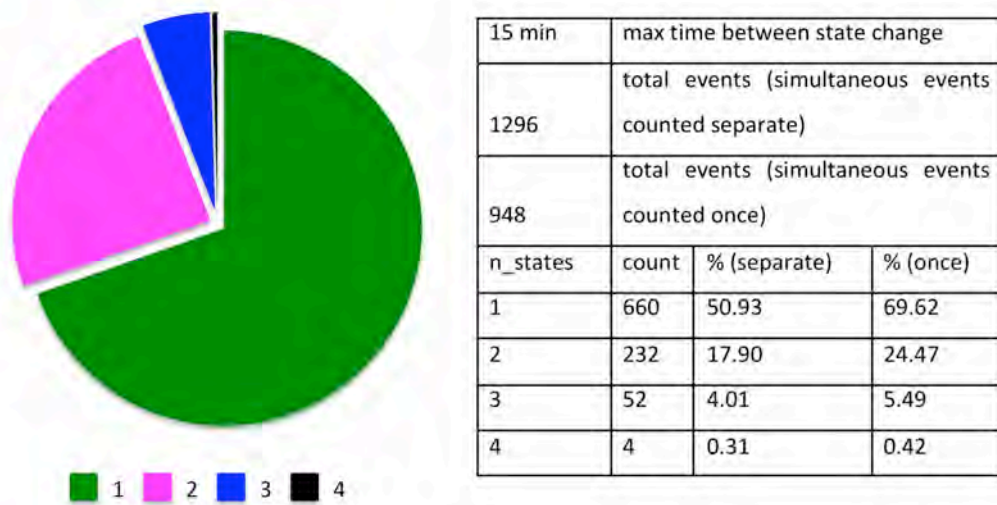


Figure 3.6 Percentage of simultaneous exchanges of cellular features

The pie graph illustrates the percentage of events in which one, two, three or four cell features changed simultaneously within 15 minutes of interval time. The percentage has been calculated on a total number of 948 events, each event consists in a time-point in which one or more features changed. The table on the side reports the percentage and number of events (calculation done by Emma M. Keizer and Rik P. van Rosmalen (WUR))

3.3.3 A Landmark system

The neighboring score was then calculated for all the observed states (Figure 3.7 and Annex 1, WUR). Notably, for this analysis, were only considered as neighbor states these states that were actually noted in the dataset and not the complete palette of possible features combinations.

The analysis revealed 11 distinct cellular states that differed from the neighbors with a neighboring score higher than one. This score denoted that they occur at least one standard deviation more frequently than the mean of their neighboring states (Figure 3.7). The results of the neighboring score analysis were reproduced and confirmed by bootstrapping (Annex 2 WUR,).

The 11 outstanding cellular states (A1-A11) are henceforth called meiotic *landmarks* (Figure 3.7, Figure 3.8 and Annex 1). The states between landmarks are defined as *transition states* and often represent alternative routes to the next landmark (Figure 3.7), e.g., the cell shape may first change from rectangular to trapezoidal, and then the nucleus moves from a center position to a position at the side of the cell, or the nucleus moves first and then the cell shape changes. However, the nucleus is finally always located at the smaller side of the trapezoidal cell defining the new landmark state. This new system, based on landmarks and transition states, applied to the original data set could cover the 97.2% of the time points, with 72.5% falling on a landmark, and 24.7% on a transition state; only 2.8% of the cellular state found in the dataset could not be assigned.

The new landmark system described here can be roughly assigned to the classical phases of meiosis with A0 and A1 correlating with S-phase, G2 and early leptotene, A2 with late leptotene, A3 and A4 with early and late zygotene, A5 and A6 with early and late pachytene, A7 with diplotene, A8 with metaphase I, A9 with interkinesis, A10 with metaphase II and finally A11 with telophase II (Figure 3.8). However, it has to be noted that their alignment of with the classically defined stages remains imprecise. For example, zygotene is defined by the beginning of the chromosomal synapsis, a cell feature that could not clearly be resolved in our analysis. Thus, I cannot clearly mark the beginning of zygotene in our study. However, as more meiotic reporter lines are generated, for instance for the lateral

or central elements of the synaptonemal complex, synapsis can be resolved with great resolution in the future.

Taken together, I conclude that cellular differentiation steps of meiosis can be variable but then converge on distinct cell states (landmarks). The qualitative assortment of the landmarks, possibly their order as well as their duration and the degree of variability (transition state number and duration), represent a new system to describe meiosis.

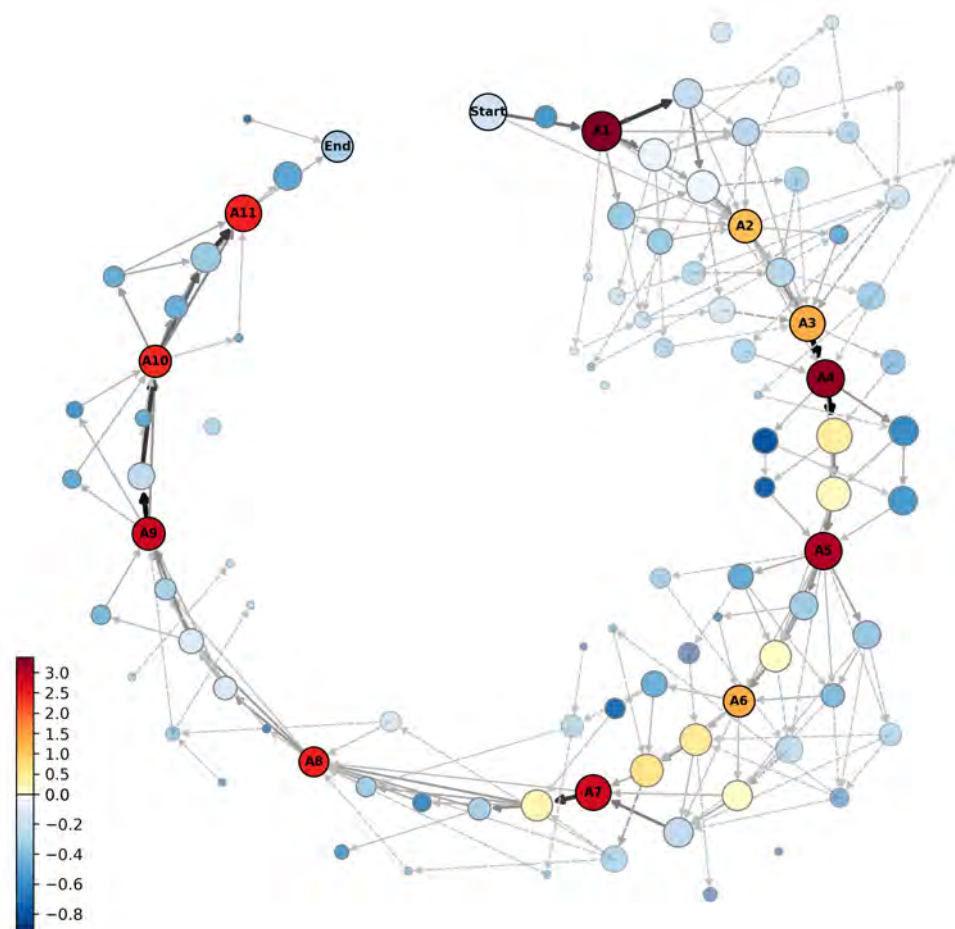


Figure 3.7 Map of meiotic cellular states

Meiosis represented as a progression of cellular states. Each circle signifies an observed cellular state and the arrows are observed transitions between these states. The size of circles depicts the frequency of appearance of each cellular state while the color represents their *neighboring score*. Cellular states that have a score higher than 1 (dark yellow to red) are defined as *landmarks* and were assigned a name (A1-A11). Landmarks are highlighted by outlined circles and their names are written in the center. The intensity of the line color of the arrows specifies which are the predominant paths taken by a male meiocyte undergoing meiosis. Notably, the arrows indicate progression from one state to the following one only when the transition was seen within 15 minutes interval time, therefore the presence of non-connected circles. *Map by Rik P. van Rosmalen (WUR).*

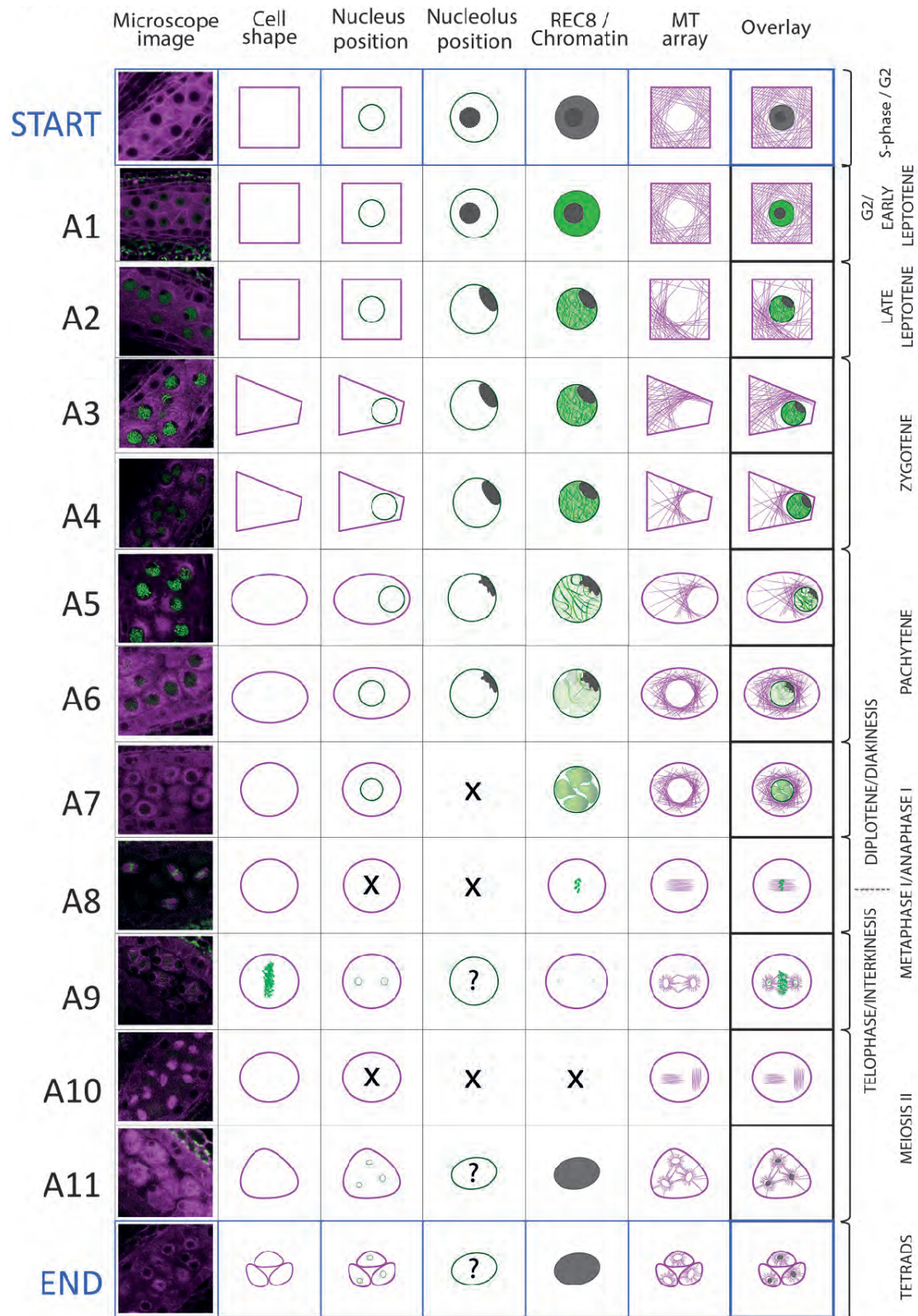


Figure 3.8 Landmark scheme

Illustration of the 11 here identified meiotic landmarks of male meiosis, A1-A11, and the combination of the parameter states that represent them. The first column provides a microscopy picture of meiocytes depicting each stage. The state of each parameter is separately shown in the following columns, the right-most column (Overlay) present their combination. On the right side, the classical stages of meiosis are assigned to each Landmark

3.3.4 The case of the Nuclear Envelope breakdown

The break-down of the nuclear envelope in diplotene is an important hallmark of meiosis (Wijnker and Schnittger, 2013). Indeed, I could observe the break-down (state seven among the MT arrays, Figure 3.9). However, the nuclear envelope break-down was not part of a landmark state (Figure 3.9). First, the break-down progresses rapidly, i.e., within minutes. Thus, with a sampling interval of one frame, every 10 minutes it was only captured in 22 out 10,671 analyzed time points. Moreover, the break-down of the nuclear envelope appeared to happen with a looser combination of feature states, e.g., the cell could appear oval or round, as well as at different chromosome condensation levels (Figure 3.9). For these reasons, a clearly defined landmark fulfilling the criteria was not reached. To keep the landmark definition consistent, I decided against adding it retrospectively.






STATE	FEATURES COMBINATION	COUNTS	PERCENTAGE	NEIGHBORING SCORE
	3 4 4 7 7	1	0.01	- 0.55
	4 3 3 6 7	1	0.01	- 0.50
	4 3 4 6 7	10	0.10	- 0.30
	4 3 4 7 7	4	0.04	- 0.57
	4 4 4 7 7	6	0.05	- 0.33

Figure 3.9 Cellular states at the nuclear envelope breakdown

The table illustrates the 5 different cellular states that can be identified with the nuclear envelope break down. The nuclear envelope breakdown is indicated by the MTs state 7, after the breakage of the circular pre-spindle structure, but before the formation of the spindle. Seen its high variation, and the fast speed of the events that characterize this meiotic hallmark, the neighboring score obtained by the states is very low, preventing its classification as landmark.

3.4 Tetraploid generation

Polyploidization has been recognized as a wide-spread phenomenon in many eukaryotes, especially in plants (Comai, 2005). However, the presence of multiple sets of homologous chromosomes, especially in autopolyploid species, is a challenge for the faithful pairing of homologs and their balanced segregation in meiosis.

Besides the obvious difficulties in the distribution of equal numbers of chromosomes to avoid aneuploidy the increased chromosome number might also affect other aspects of meiosis (Grandont *et al.*, 2013; Zielinski and Mittelsten Scheid, 2012). Early works by Bennett, summarized in his review *Time and Duration of Meiosis* (Bennett, 1977) revealed that established lines of polyploid plants such as cereals have a shortened meiosis in comparison to diploid sister plants (e.g., in *Secale cereale* diploid meiosis was calculated to last 51 hours versus 38 hours of tetraploid meiosis (Bennett, 1971)). Moreover, polyploidy might alter the recombination landscape by mechanisms that are just now being understood (Blary *et al.*, 2018; Leflon *et al.*, 2010; Pecinka *et al.*, 2011). Hence, detailed cytological analysis of the effects of polyploidy is required to understand its molecular effects.

3.4.1 VIGS treatment and KINGBIRD tetraploids

Genome doubling is traditionally induced by treating plants with colchicine (Blakeslee and Avery, 1937). However, not all plants are susceptible to colchicine and treatment with colchicine is known to cause aneuploidy (Yu *et al.*, 2009). To this end, I decided to apply an alternative method to generate polyploids. The method relies on Virus-induced gene silencing (VIGS), a post-transcriptional silencing approach that offers the possibility to obtain the desired phenotype directly and, at the same time, avoid the use of stable transgenes/mutants that will be otherwise transmitted to the offspring (Burch-Smith *et al.* 2004). The method was established in our laboratory by Calvo-Baltanás who designed a construct to knock down *OMISSION OF SECOND MEIOTIC DIVISION 1 (OSD1)* (Calvo-Baltanás, 2019). The lack of OSD1 results in the formation of diploid male and female gametes due to an exit after the first meiotic division, and therefore generates tetraploid progeny (d'Erfurth *et al.*, 2009; Iwata *et al.*, 2011).

Plants expressing *PRO_{REC8}:REC8:mEGFP* and *PRO_{RPS5A}:TagRFP:TUB4* were separately treated with the binary vectors pTRV1, which carries the viral genes necessary for infection, and *pTRV2* VIGS vector, which harbors an insert containing a homologous sequence to *OSD1*, named as *pTRV2-AtOSD1* (Figure 3.10). As a positive control for the infection, plants were treated with a VIGS construct to silence *PHYTOENE DESATURASE (PDS)* (*pTRV2-AtPDS*), which causes visual photobleaching upon silencing and can be correlated to the success infection rate (Burch-Smith *et al.*, 2006; Padmanabhan and Dinesh-Kumar, 2009) (Data not shown). Next, I identified plants producing diploid gametes as a result of *OSD1* silencing by using cell size as a proxy to differentiate between diploid (large) and haploid (small) pollen grains (Figure 3.10).

Flowers of each reporter line presenting diploid pollen were then reciprocally crossed, and the tetraploid nature of the resulting F1 of the re-constituted *KINGBIRD* reporter line was confirmed by flow-cytometer (Figure 3.10). F2 tetraploid seeds were then collected, and F2 plants were used for time course experiments. The meiotic defects of tetraploid plants can lead to the formation of aneuploid progeny. To confirm that the live cell imaging experiment was conducted on authentic tetraploid, a few inflorescences per plant were fixed and used for cell spreads and chromosome counting (Figure 3.10)

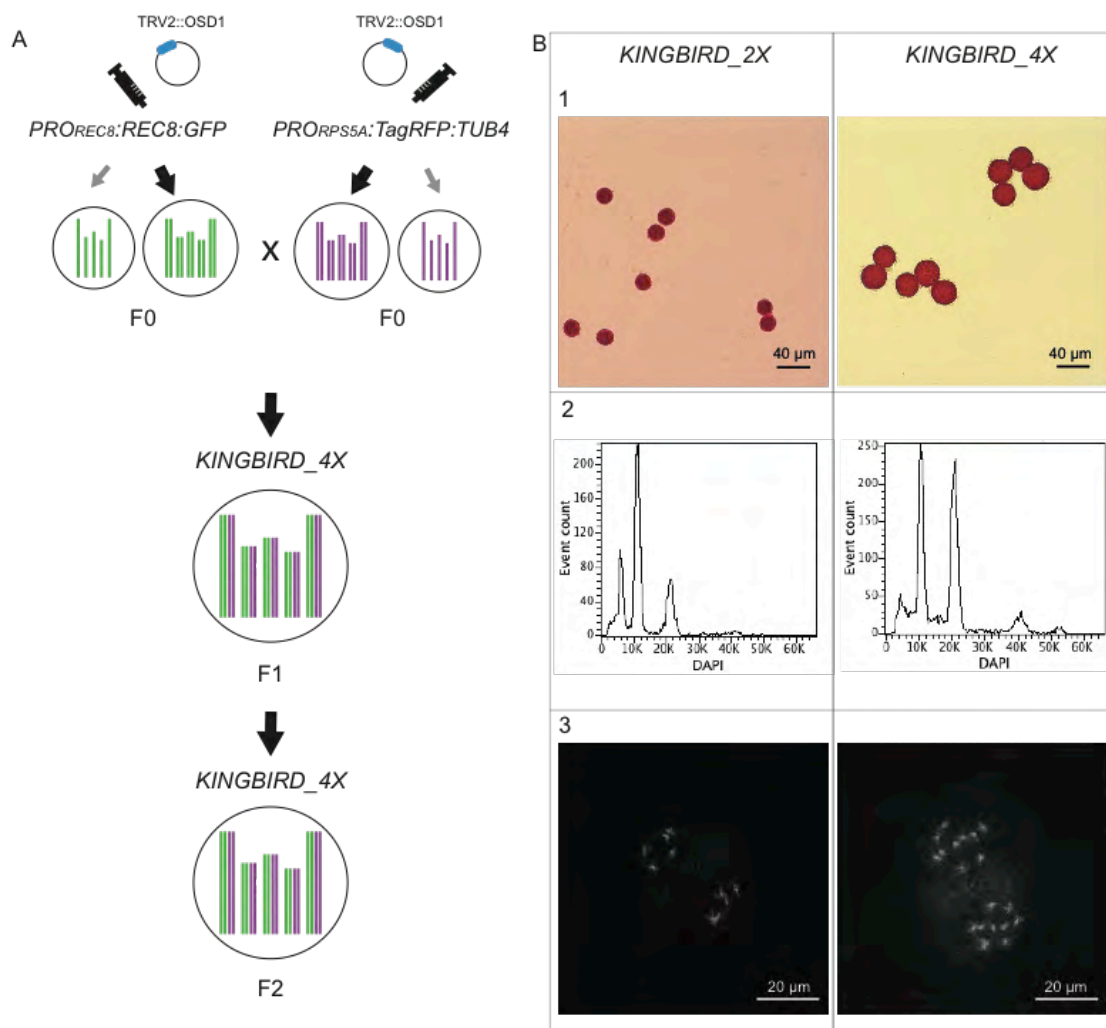


Figure 3.10 Generation of tetraploid of *KINGBIRD* reporter line

- A) Scheme of VIGS treatment and neo-tetraploid generation. F2 generation was used to perform time course experiment.
- B) Examples of the different ways used to check for tetraploidization:
1. Peterson staining to assess pollen size and viability, used to check the effect of VIGS treatment on flowers of F0. Tetraploid pollen (*KINGBIRD_4X*) has a diameter twice as long as the diploid.
 2. Flowcytometer results used to check the outcome of F1. The diploid plant show peaks at 1C, 2C and 4C, while the tetraploid has peaks at 2C, 4C and 8C.
 3. Cell spreads and chromosome counting. The two cells are in prophase II. The diploid PMCs contain 5 chromosome each, while the tetraploid PMCs contain 10 chromosomes. Both of the cells show balanced segregation.

3.4.2 Meiosis of the F2 tetraploid *KINGBIRD* line progresses through the same landmarks as diploid plants

The observation of 91 time-lapse capturing the progression of meiosis in the second generation of the tetraploid *KINGBIRD* line led to the conclusion that the landmark system described for the diploid meiosis could be re-applied unvaried to the new specimen. An example of the outlook of meiotic progression in tetraploid is shown in Figure 3.11.

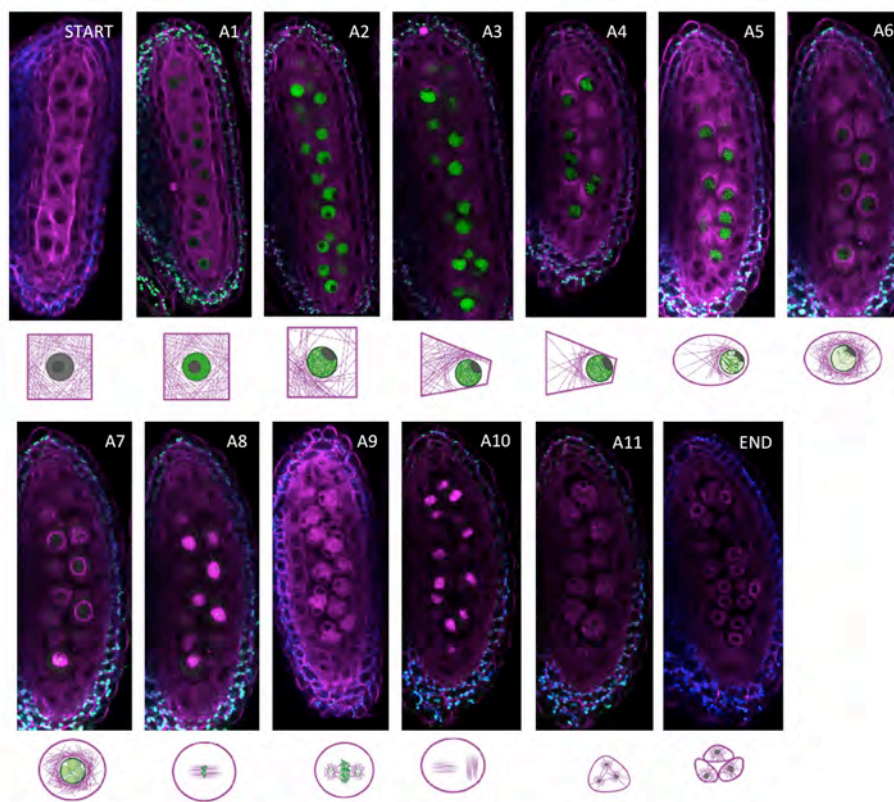


Figure 3.11 Progression of meiosis in *KINGBIRD* 4X anthers

Each picture represents the outlook of the 11 landmarks in *KINGBIRD* 4X meiocytes as they progress through meiosis in one pollen sac; below each picture a schematic depiction of the landmark according with the system presented in chapter 3.3. The landmark system extrapolated from the diploid data set can be applied unvaried to meiosis in tetraploid plants. Signal from $PRO_{REC8}::REC8::mEGFP$ is depicted in green and the signal from $PRO_{RPS5A}::TagRFP::TUB4$ is in magenta.

3.5 Time course of meiosis in diploid and tetraploid KINGBIRD lines

3.5.1 Diploid time course

The duration of meiosis in male *Arabidopsis thaliana* has been described by previous works, and it is known to be set around 30 hours (Armstrong *et al.*, 2003; Sanchez-Moran *et al.*, 2007; Stronghill *et al.*, 2014); in order to test whether the imaging procedure might affect meiotic progression, I decided to determine the length of the division with the live cell imaging set up. An advantage of live cell imaging is that it offers the possibility to follow the progression of meiosis in single cells, allowing a direct calculation of the time course, which does not rely anymore on complicated counting of percentages and relative times as for the EdU and BrdU experiments.

While long time-lapses with more than 30 hours containing all meiotic stages could occasionally be obtained, they were rarely fully informative due to loss of focal plane, induced by water evaporation and sample growth. Hence I selected 58 time-lapses capturing subsection of the meiotic division ongoing in 21 anthers. Each time-lapse could be considered as a contig, and their sum provided a complete description of entire meiosis. To faithfully judge the duration of a landmark, the minimal length of one time-lapse had to be long enough to capture at least two transitions of sequential landmarks, with each landmark covered at least four times (Annex 6). For this analysis, the transition states between two landmarks were added in the time estimate of the preceding landmark.

Each meiocyte was manually annotated and tracked over the different time-lapses, and a landmark was manually assigned to each visible cell, at each time point, based on its outlook, and noted on an excel file (an example in Figure 3.12). When a cell, due to sample movement, was not recognizable at a specific time point, an “n” staying for “non- visible” was noted. The file was then used as input for a costumed software designed by Dr. Felix Seifert (CropSeq, GmbH, Hamburg, Germany), which reconstitute as output the time each cell spent in a certain landmark. Over the complete set of data recorded 47 time lapses resulted informative, showing the progression of meiosis of 17 anthers, and 136 cells (from 1 to 19 meiocytes per anther, more details in Annex 3 and Annex 5).

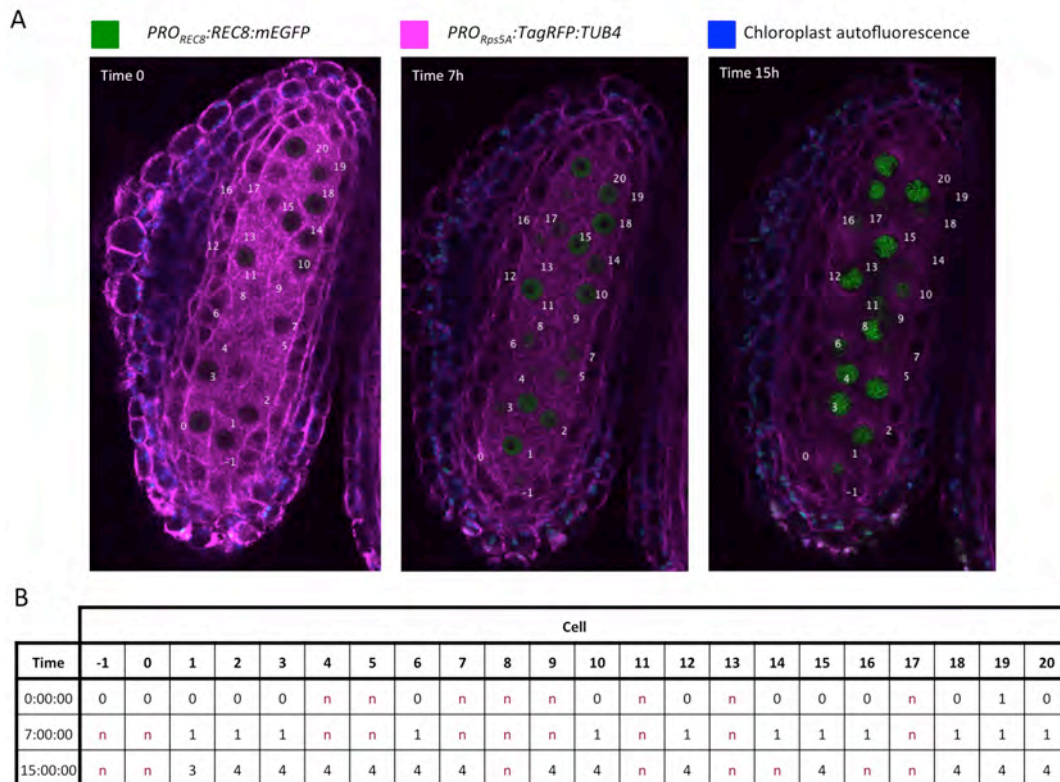


Figure 3.12 Example of time course analysis procedure

- A) Time lapses of *KINGBIRD* anthers were corrected for xyz shift (Material and Methods chapter 5.8). Each cell was manually annotated, in order to recognize it at each time point of the time lapses.
- B) An Excel sheet, having on the vertical axis the time point and on the horizontal axis the cell identification number, was filled with the landmark number present by each cell at each time point. When the cell was not visible, an n was inserted in the table.

Considering the single cell analysis, the total duration of meiosis resulted to be 35 hours. This value includes the length of landmark A1 (8 hours in total), which correlates with the onset of REC8 expression, and overlaps with S-G2 phase until early leptotene. Prophase, as expected, resulted in being the longest phase (minimum 20 hours) with late leptotene (A2) lasting 1.5 hours, zygotene (A3-A4) 6 hours, pachytene (A5-A6) 9.5 hours and diplotene and diakinesis (A7) together 3 hours. Importantly, we could also resolve meiotic phases thereafter and determine metaphase I and anaphase I (A8) together with 1 hour, telophase I, interkinesis and prophase II (A9) with 1 hour and meiosis II (A10-A11) all together with 4 hours (Figure 3.12, Annex 3 and Annex 6).

tested for the appearance of BrdU and EdU in meiotic chromosome configurations (Armstrong et al., 2003; Sanchez-Moran et al., 2007; Stronghill et al., 2014). In these experiments, male meiosis in *Arabidopsis thaliana* was judged to last approximately 22 to 24 hours with leptotene spanning between five and seven hours, zygotene and pachytene together lasting between 16 and 21 hours, and the rest of meiosis from diplotene onwards spanning approximately three hours. The application of live cell imaging delivered a similar time frame of the meiotic phase lengths. I found meiosis to proceed at roughly the same speed: respectively, the whole meiotic division lasts between 2 and 4 hours longer compared to previously published studies (Armstrong et al. 2003 and Sanchez Moran et al. 2007), and my prophase calculation is 2 hours shorter than shown by Stronghill et al. 2014. Moreover, I could observe that the sum of the individual phases as a result of several movies matched very well the estimate resulting from long movies that spanned entire meiosis. For example, the duration of short and later landmarks, such as A8 to A10 have similar durations in cells that have been observed for shorter times (e.g. flowers 1, 2 and 27 in Annex 3) and in cells that have been observed for several hours prior undergoing these landmarks (e.g. flowers 3 and 29 in Annex 3). This information corroborates the conclusion that the technique here developed does not affect the progression of meiosis. Besides, I could gain resolution exactly in these later stages. Time courses based on cell spreads such as the one performed with BrdU and EdU techniques could not calculate precisely the duration of each the last meiotic phase, often grouping the stages from diplotene onwards. This is due to the loss of synchronicity of meiocytes within the same pollen sac, which results in the appearance on the same slide of meiocytes in stages from diplotene to tetrads, impeding the discrimination of the duration of each phase. Being able to follow the same cell over time with live cell imaging solved this problem, resulting in the increase of temporal resolution.

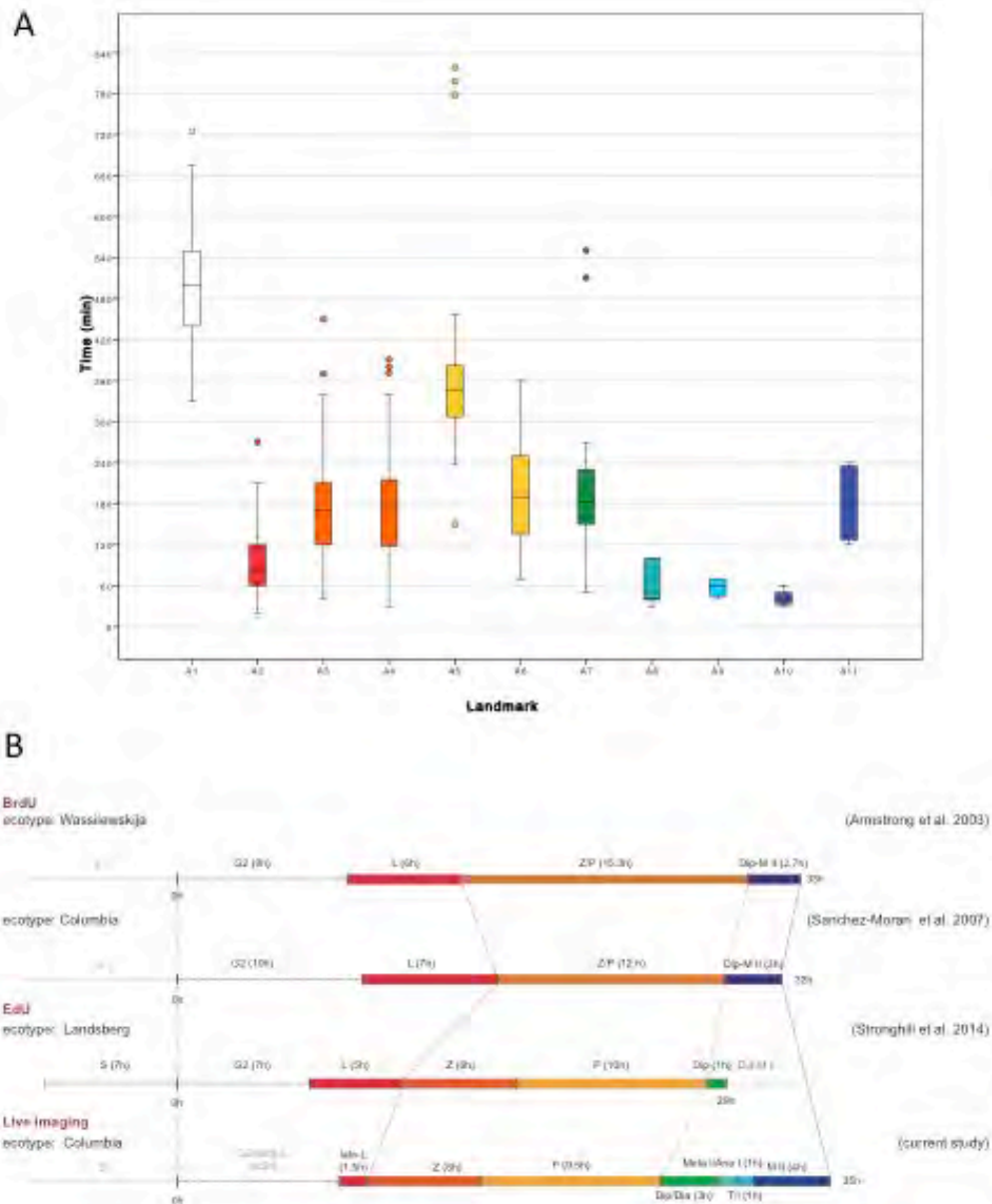


Figure 3.13 Time course of male meiosis I anthers of *Arabidopsis thaliana*

A) Box plot illustrating the duration of each landmark in minutes. Outliers are illustrated with a dot. The color code for each landmark refers to the meiotic phase: white (A1) is S-phase/G2, red (A2) is late leptotene, orange (A3, A4) is zygotene, yellow (A5, A6) is pachytene, green (A7) is diplotene/diakinesis, aquamarine (A8) is metaphase I/anaphase I, light blue (A9) is telophase /interkinesis, dark blue (A10, A11) is the second meiotic division.

B) Comparison of meiotic timelines obtained with different techniques: BrdU and EdU staining, followed by sample fixation, versus live imaging. S stands for S-phase; L for Leptotene, Z for Zygotene, P for Pachytene, Dip for Diplotene, Dia for Diakinesis, Meta I/ Ana I for Metaphase and Anaphase I, T/I for Telophase and Interkinesis, M II for second meiotic division. The duration of each phase is indicated in hours for all the time courses, Time 0 has been set as the initiation of leptotene.

3.5.2 Tetraploid time course and comparison

To calculate the time course of the tetraploid population of the *KINGBIRD* line, the second generation of *KINGBIRD* 4X was selected as sample of interest, and their ploidy level was corroborated via cell spreads as illustrated in chapter 3.4.1 and Figure 3.10. The same conditions used for *KINGBIRD* 2X were used; flowers of both the populations (2X and 4X) were mounted on the same petri dishes and observed in parallel. Among the data collected for the *KINGBIRD* 4X, 27 anthers over 91 time-lapses were analyzable and resulted informative (Annex 5). The analysis was executed as described for the diploid line in chapter 3.5.1.

The results obtained showed that overall meiotic division in neo-tetraploid plants lasts 51 hours, 16 hours more than in diploid plants (Figure 3.14, Annex 4 and 6). A closer look reveals that the increase in the duration depends mainly on the extension of the landmark A1, which starts with the first appearance of PRO_{REC8}:REC8:mEGFP and terminates in late leptotene. A1 contributes alone in the increase of 10 hours, while the remaining 6 hours are distributed over the other ten landmarks, with the most substantial increase in landmark A11 (ca. 2 hours), which correspond to the second meiotic division (Figure 3.14, Annex 4 and Annex 6). Even though the difference of the average duration of these landmarks appeared to be relevant, the standard deviation values revealed a high internal variation in both the populations. I then tested the results for statistic significance. First, the samples had to be grouped by anthers, averaging the duration of each landmark within a pollen sac, and among different pollen sac in second place. In this way, the number of samples per each landmark was reduced, and they presented a non-normal distribution; therefore the Mann-Whitney U test was chosen for the comparison (Annex 7) (WUR). The test revealed that only the landmark A9, with a p-value pair to 0.008, was significantly different between the diploid and tetraploid populations, while the other landmarks had p-values between 0.1 (A11) and 0.7 (A5), confirming the null hypothesis to be true (Figure 3.14 A, Annex 7). Hence, I concluded that no difference between the duration of diploid and neo-tetraploid duration could be detected within the dataset. The differences scored for landmark A1 was not comparable by statistic, since all the cells came from the same sample.

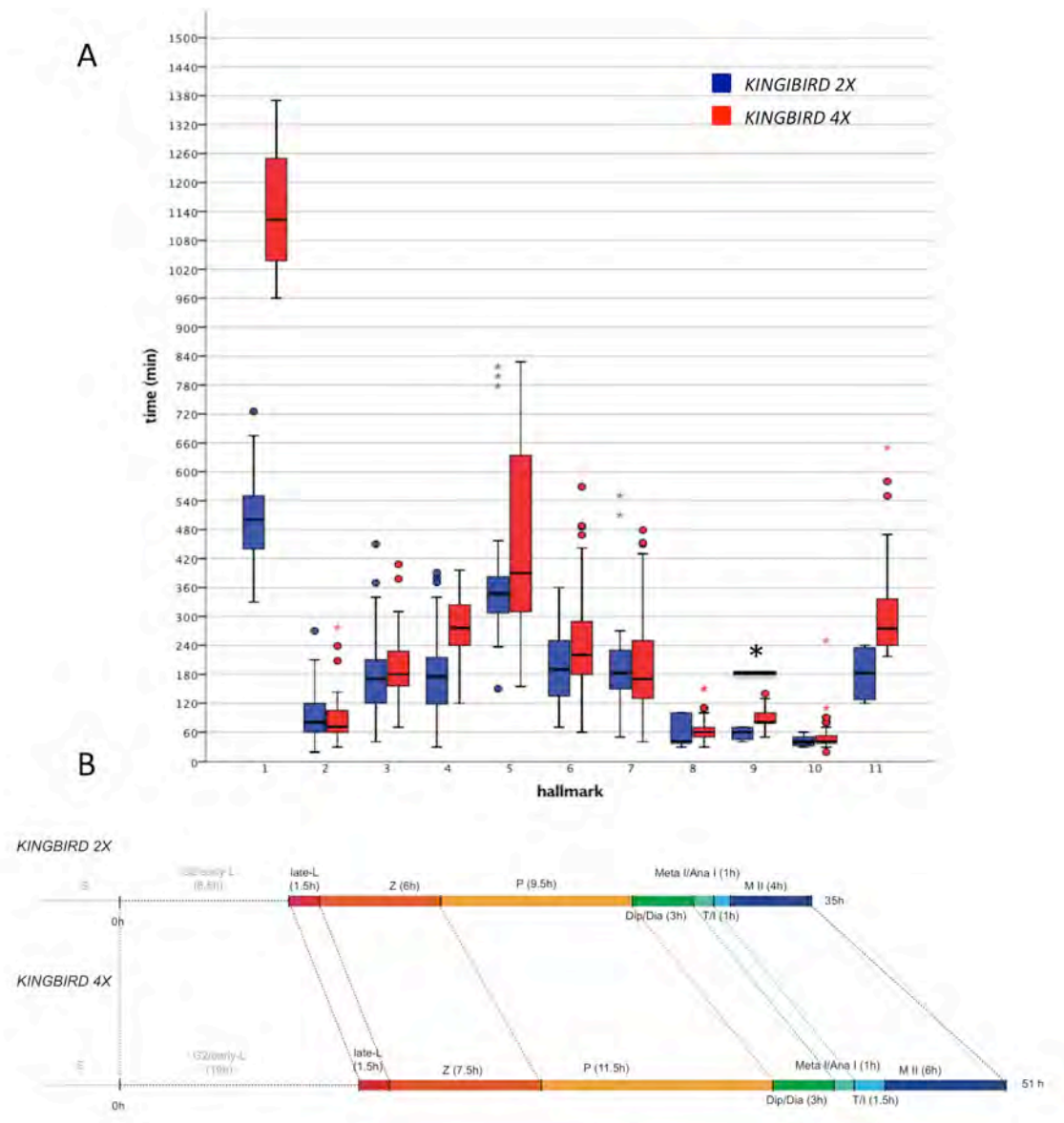


Figure 3.14 Comparison between diploid and tetraploid time course

A) Box plot illustrating the duration of each landmark in minutes for the diploid (in blue) and tetraploid (in red) population of *KINGBIRD*. Outliers are illustrated with a dot or a star. The landmark A9 is significantly longer in tetraploid (pValue= 0.008).

B) Comparison of the meiotic timelines obtained for diploid *KINGBIRD* (2X) and tetraploid (4X). S stands for S-phase; L for Leptotene, Z for Zygotene, P for Pachytene, Dip for Diplotene, Dia for Diakinesis, Meta I/ Ana I for Metaphase and Anaphase I, T/I for Telophase and Interkinesis, M II for second meiotic division. The duration of each phase is indicated in hours for all the time courses, Time 0 has been set as the initiation of leptotene.

3.6 Towards new applications

3.6.1 Screen of reporters and generation of new crossed lines

The microscope set up here introduced is not limited to the imaging of the only KINGBIRD line but can be applied to follow a broad spectrum of reporter lines. In our laboratory many were available and could be in three different categories:

- 1) Reporters of constitutively expressed genes, which encodes for structural elements of the cell such as nuclear envelope (SUN domain-containing protein 1, SUN1), and histone variants (H2A and H2B and the centromeric histone variant CENH3).
- 2) Reporters of cell-cycle related genes such as cyclins (CYCB3, Solo Dancers SDS, TAM) and protein involved in DNA repair (recombinase A RAD51, ring between ring 1 RBR1)
- 3) Reporters of meiotic-specific genes such as the components of the synaptonemal complex (Asynaptic 1, ASY1, asynaptic 3, ASY3, and Zipper 1, ZYP1).

I proceeded therefore with the screening of some of these lines to check whether the constructs are expressed during meiosis when the result was positive, the plants were crossed to generate double reporters that could be used in future to deepen the study of meiosis and to extend the landmark reference system (Figure 3.15 and Annex 8).

3.6.2 KINGBIRD2 and its introgression in mutant backgrounds

A new construct for *PRO_{REC8}:REC8:mEGFP* and *PRO_{RPS5A}:TagRFP:TUA5* was cloned in laboratory by Dr. Shinichiro Komaki and named *KINGBIRD2* (unpublished). The two reporters were encoded by sequential sequences on the same plasmid, and therefore inserted in the same genomic locus after plant transformation, limiting the segregation of the alleles in the following generations. This characteristic is of great help when working in a mutant background, or with a third reporter in addition, since it enhances the chances of finding the three (or more) alleles of interested combined. Moreover, since TagRFP:TUA5 has signal in roots, the selection of plants carrying the construct does not need to be performed on growing medium, it is instead sufficient to check for tubulin RFP expression in roots (e.g., fluorescent

binocular) limiting the usage of herbicide that might have a stronger effects on mutants than on WT plants. The construct was checked for expression in WT plants (Figure 3.15) and later introgressed by floral dip in five T-DNA lines of *Arabidopsis thaliana* Col0 (Annex 8) which are mutated for three different genes, or family of redundant genes, involved in plant development and meiosis regulation:

1. The gene At1G77390, encoding for *CYCLIN A;1*, mainly known as *TARDY ASYNCHRONOUS MEIOSIS (TAM)*, which is responsible for the progression transition G2/MI and MI/MII (Magnard *et al.*, 2001; Wang *et al.*, 2004a). The mutant phenotype presents delay in meiosis I, with asynchronous meiocytes and an early exit from meiosis due to cytokinesis after the first division, which brings to the generation of dyads and later tetraploid pollen (Magnard *et al.*, 2001).
2. The triple and quadruple mutant of the *KIP-RELATED-PROTEIN (KRP)* redundant genes (*krp4,6,7* and *krp3,4,6,7*), which inhibit CDKA;1 regulating the entry in meiosis, and resulting in increased number of meiocytes (Zhao *et al.*, 2017).
3. The gene At4G35520, which encodes for *MUTL PROTEIN HOMOLOG 3 (MLH3)*, involved in COs formation. Plants carrying a null mutation of *mlh3* presents reduced fertility, polyads formation, and prolonged prophase I (Jackson *et al.*, 2006).

All the mutants described above present phenotypes that affect the timing of meiosis but do not present arrests in its progression, resulting into the formation of partially viable pollen; a live cell imaging approach to study their functionality could, therefore, reveal new insights into their regulation.

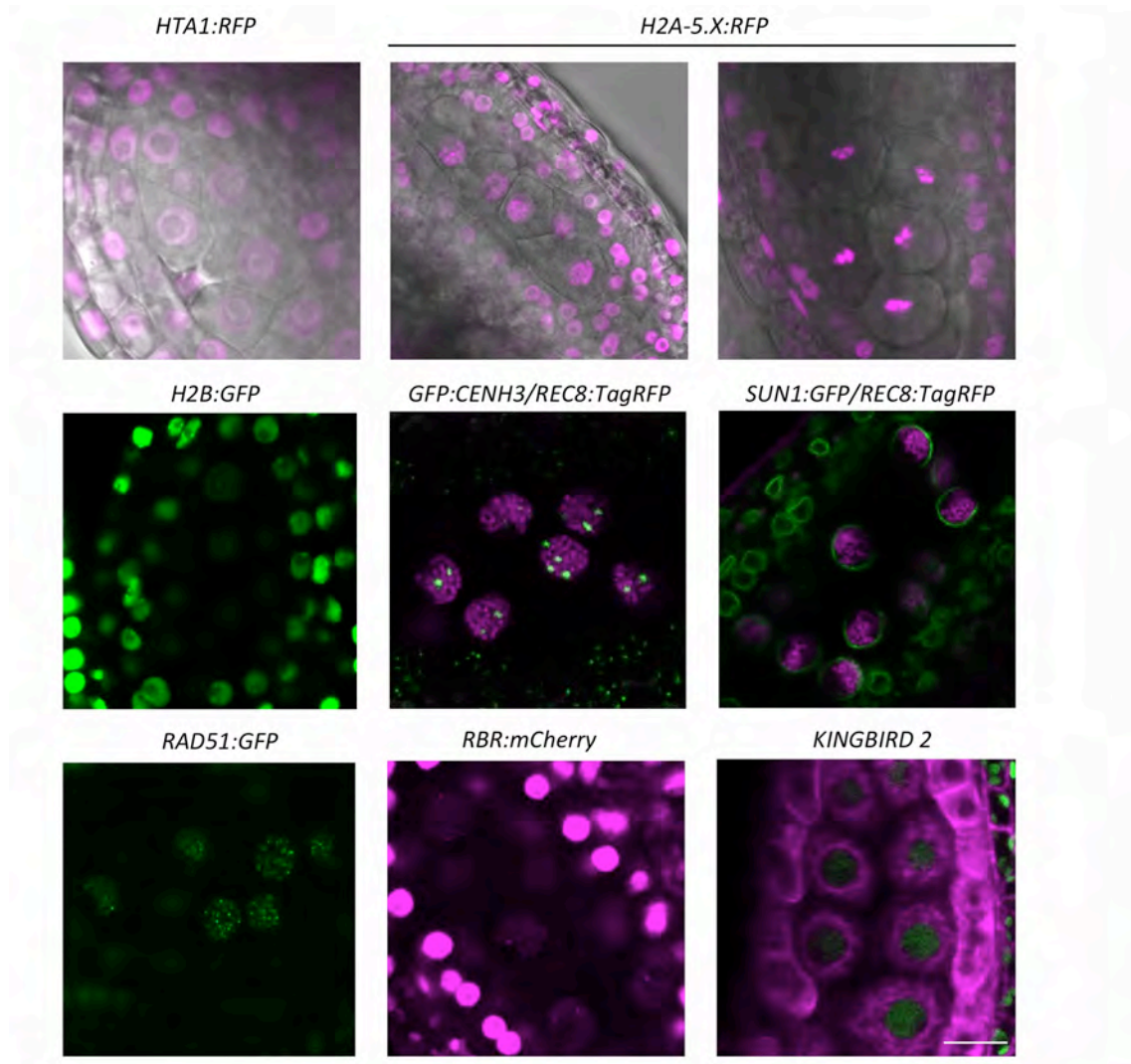


Figure 3.15 More reporters are available to study meiosis

The figure shows a few examples of fluorescent reporters that are available to study male meiosis in *Arabidopsis thaliana*. The fluorescence from GFP is depicted in green, while RFP, Tag-RFP and mCherry are in magenta. Different meiotic stages could be imaged: *HTA:RFP*, *H2B:GFP* are in pre-meiotic stage; the first picture of *H2A.5.X:RFP*, *GFP:CENH3/REC8:TagRFP* and *SUN1:GFP/REC8:RFP* are in zygotene, the second picture of *H2A.5.X:RFP* is at metaphase; the *KINGBIRD 2* line is at diplotene (landmark A6); a meiotic stage cannot be assigned precisely to *RAD51:GFP* and *RBR1:mCherry*, since little is still known on their localization in vivo, but likely the two anthers present an early prophase stage. The scale bar is 10 μm .

3.6.3 Generation of $PRO_{REC8}:REC8:mNG$

The imaging of live meiosis in plants has to consider two main aspects: the long duration of the division, and the deep localization of the meiocytes. The microscopy technique here presented offers a good solution to cope with both the hindrances; nonetheless, it is just a starting point to further optimization. A direction that could be taken to improve the quality of the data is to explore the performance of different fluorophores and test for their signal intensity and resistance to photobleaching.

In 2013, Shaner *et al.* synthesized a novel fluorescent protein derived from the *Branchiostoma lanceolatum* LanYFP. The new protein, named mNeonGreen (mNG), fluoresces in the green spectrum with sharp excitation peak at λ 506 nm, and emission peak at λ 517 nm; it has been described as more than 2.5 times brighter than mEGFP, has a higher photostability (158s vs. 150s), increased resistance to acid pH (pK_a^h of 5.7 vs. 6.0) and has a faster folding (less than 10 min vs. 25 min) (Shaner *et al.*, 2013). Seen its physical characteristics mNG could be a valid alternative to the more classic EGFP and mEGFP. Moreover, it has been proved to have high FRET and FLIM performances (Shaner *et al.*, 2013; Mastop *et al.*, 2017) opening the live cell imaging technique here described to new applications.

I was interested in testing the performance of mNG with our imaging conditions; therefore I generated the chimera $PRO_{REC8}:REC8:mNG$, to have a comparison with the established reporter $PRO_{REC8}:REC8:mEGFP$.

The cloning strategy of $PRO_{REC8}:REC8:mNG$ is described in Leyk, Bachelorarbeit 2016, UHH (Leyk, 2016). The DNA sequence of mNG (GenBank KC295282) was codon-optimized for plants (DNA Cloning Service E.K, GmbH, Hamburg, Germany). The destination vector pGWB501-REC8-Smal-mNG, carrying the C-terminal fusion protein:REC8:mNG under the expression of *REC8* endogenous promoter, was then transformed in *Agrobacterium tumefaciens* and introgressed by floral dip in *Arabidopsis thaliana* Col0, WT, and SAIL_807_B08 (*rec8*+/-) background.

3.6.4 Performance of $PRO_{REC8}:REC8:mNG$

Five different lines (named line 1 to line 5) were obtained from a first screen of $PRO_{REC8}:REC8:mNG$ introgressed in *rec8* +/- background, and regrown to T2 to check

their performance in homozygous *rec8*^{-/-} background. Seeds from lines 1,2,3, and 5, germinated on Hygromycin MS plates, while line number 4 did not produce viable seedlings. Plants carrying homozygous T-DNA insertion for *rec8* mutant allele were selected for testing *PRO_{REC8}:REC8:mNG* performance.

At first, isolated flower buds were mounted on microscope slides and checked for signal. Different conditions were tested to find the microscope set up that fits best mNG fluorescent spectrum. The protein was excited by the Argon laser set on three different wavelengths (λ): 488 nm, 496 nm, and 514 nm, and showed the highest intensity at 488 nm. This λ was then selected to perform live cell imaging experiments (Figure 3.16)

Samples were then mounted on a petri dish as presented in chapter 3.1.1 together with flower buds carrying *PRO_{REC8}:REC8:mEGFP* and meiosis was followed live over 48 hours.

PRO_{REC8}:REC8:mNG localized correctly during the complete prophase I (Figure 3.16) showing a clear signal over the entire data acquisition, in the same intensity and resolution range as the signal of *PRO_{REC8}:REC8:mEGFP*. However, I could not perform a more detailed comparison between the two fusion proteins due to the failure to rescue in the four analyzed lines carrying *PRO_{REC8}:REC8:mNG* on a homozygous mutant background for *rec8*. The four lines showed different degrees of sterility, with short siliques and pollen abortion (Figure 3.16), revealing that the construct, independently from its insertion locus is not fully functional. Given that REC8 sequence is the same in both constructs, the reason of the only partial rescue should lie in the mNG protein itself, albeit its structure is very similar to the one of mEGFP, with even a slightly shorter amino acid sequence (236 AA against the 239 of mEGFP) and slighter lighter molecular mass (26.6 kDa against 27 kDa of mEGFP). The construct cloned has a linker of 19 AA between REC8 and mNG, which was designed to give more mobility to the fluorochromes. It might be, on the contrary that its presence causes a disturbance to REC8, which even though able to localize correctly over the entire prophase (Figure 3.16) does not have full functionality. Shorter linker (up to a minimum of 3 AA) have been successfully used in our laboratory, and therefore should be tested in this context.

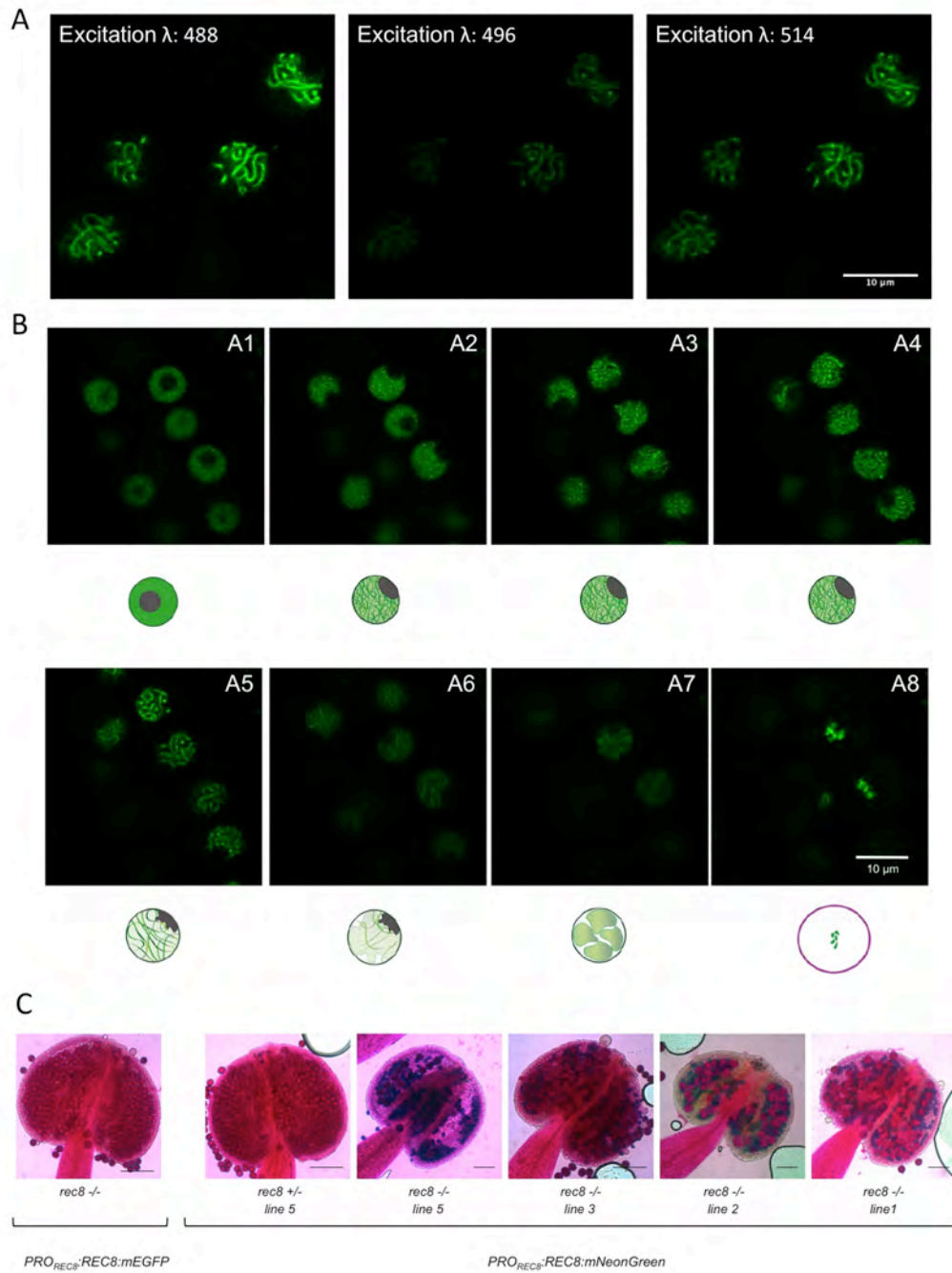


Figure 3.16 $PRO_{REC8}:REC8:mNG$ performance

- A) $PRO_{REC8}:REC8:mNG$ expression in meiocytes of line 1 at pachytene stage. The protein was tested using different wavelength in the green-yellow spectrum (488, 496, 514). The best performance and the brightest signal was detected exciting with Argon laser at 488 nm
- B) Localization of $PRO_{REC8}:REC8:mNG$ over meiosis in a flower bud of line 3. The protein shows the same pattern detected for $PRO_{REC8}:REC8:mEGFP$, from A1 to A8 as illustrated by the drawings below the pictures, showing normal localization of REC8 protein until metaphase I.
- C) Petersen staining of $PRO_{REC8}:REC8:mNG$. The construct, contrary to $PRO_{REC8}:REC8:mEGFP$, does not rescue $rec8^{-/-}$ sterility. Dead pollen grains (in blue) are detected in four of the five transgene lines obtained, with different rates depending on the insertion locus (line 5 is the most sever, line 3 presents the lighter phenotype). The second picture from the left shows the anther of a heterozygous plant. No dead pollen is observed. More reporters are available to study meiosis

4 Discussion

4.1 Strengths and limitations of the microscope set up

The core of this thesis is the establishment of a live cell imaging technique to observe the progression of meiosis in plants. Previous attempts conducted in maize and *Arabidopsis thaliana* required complicated handling and advanced tools or were not able to follow complete meiosis, thus limiting the power of live cell imaging. The protocol presented in this thesis is based on a conventional confocal microscope, which nowadays could be easily found in research centers and universities. Moreover it requires only minimal sample handling. Two main expedients were used in this set up: the usage of a water dipping lens, which allows acquiring images without a coverslide, and the mounting of the flower bud on a solid medium. As a result, entire meiosis could be recorded as it progresses in individual meiocytes, which are left unperturbed within their pollen sac.

Samples were imaged over a maximum of 48 hours. These relatively long durations of data acquisition present a risk of photodamages. Moreover, the flower bud was submerged in water during the complete imaging procedure resulting in a hypoxic condition. Therefore, the viability and the stress of the samples, together with the maintenance of optimal conditions, was one of the main concerns. However, the results obtained in this thesis revealed that the technique does neither impair duration nor progression of the different phases of meiosis.

A strength of the microscopy setup presented here is its high modularity. For example, it is possible to adjust the acquisition settings according with the purpose of the experiments, reducing or increasing the interval time between scans. Very short meiotic events such as nuclear envelope break down or anaphases could be caught minimizing the interval time and acquiring the images for a short duration (e.g. less than one hour). In addition, the choice of *Arabidopsis thaliana* as model system presents, among other advantages, that is easily transformable (Somerville and Koornneef, 2002). This characteristic allows the usage of multiple fusion proteins of meiotic regulators to GFP or other fluorescent proteins as reporters

without the need to rely on chemical staining and dyes. Thus, diverse processes in meiosis could be monitored; examples from our laboratory include RAD21, CDKA;1, TAM, SWITCH 1 (SWI1) and SGO1 as well as ASY1, ASY3 and ZYP1 as elements of the synaptonemal complex (Viola Kuttig, Kostika Sofroni, Chao Yang, Franziska Böwer and Dr. Yuki Hamamura, unpublished data or in revision).

Given the great advantages of a live cell imaging system for plant meiosis, it is easy to speculate on multiple future applications of the technique. On one side the full potential of confocal microscopy could be explored, performing experiments as Förster Resonance Energy Transfer (FRET) to investigate protein interactions. For instance, an interesting target for these analyses could be the CDKA;1-cyclins complexes, which control the progression of mitosis and meiosis in a similar way (Wijnker and Schnittger, 2013). The description of an hypomorphic allele of *cdka;1* mutant, which compromises sporophytic growth, and yet is viable, revealed a key role of CDKA;1 in meiosis (Dissmeyer *et al.*, 2007). Moreover, eight cyclins of *Arabidopsis thaliana* (*CYCA1;2/TAM*, *CYCA2;1*, *CYCA2;2*, *CYCA3;2*, *CYCA3;3*, *CYCA3;4*, *CYCB3;1* and *SDS*) are expressed during male meiotic phases (Bulankova *et al.*, 2013). Some of them, as *CYCB3;1* which localizes on meiotic spindles at metaphases, follow an exact pattern of expression, while some others, like *SDS*, do not show any relation with a specific meiotic phase. Interestingly, previous works conducted in mammalian cells imaged a biosensor based on FRET to reveal the specific activity of the Cdk1-cycB1 complex during mitosis (Gavet and Pines, 2010), and meiosis (Daldello *et al.*, 2018). The biosensor was constituted by a donor and an acceptor fluorescent protein, linked by a phosphorylation site specific for the kinase, and by a phosphobinding domain. When the linker is phosphorylated by the Cdk1-cycB1 complex, the biosensor changed conformation, altering the FRET efficiency, which is then detected as a change in emitted signal. A similar biosensor could be designed to visualize the activity of specific CDKA;1/CYC complexes. When paired to the live cell imaging method, it could enlighten how meiotic progression is regulated, and clarify the different timeframe of several cyclins.

On the other side this microscope set up is limited to acquire 2D images over time, while to thoroughly analyze cellular dynamics, such as chromosomes trajectories and movements during prophase, a third spatial dimension is preferable.

To perform efficient 3D time-lapse it is necessary to increase the resolution in the z dimension, without losing speed in image acquisition, and preserving the cells from excessive phototoxicity. Z-piezo drive, combined with either resonant scanner or spinning-disk scanner, could be a good solution to this matter. Alternatively, another option to tackle this challenge is the usage of Light Sheet Fluorescent Microscopy (LSFM). LSFM is finding its way into plant developmental studies thanks to its fast data acquisition and to the lower out of focus excitation, which reduces the photobleaching effect, and enhance resolution without the need of pinhole (Ovečka *et al.*, 2018; Komis *et al.*, 2018). Images of the entire flower bud or pistil of *Arabidopsis thaliana* could be acquired by LSFM (Ovečka *et al.*, 2018). The limiting factor of LSFM is the resolution power, which is still lower than the one of confocal microscopy (around 770 nm vs 350 nm for the XY axes and reaches a maximum of 2µm vs 770 nm for the z-axis), and would not allow to distinguish in such a fine way chromosomes and microtubule pattern (Ovečka *et al.*, 2018). Nonetheless the imaging field is advancing very fast, and the resolution power of LSFM has been already improved to a confocal level by the application of lattice technology (Chen *et al.*, 2014), which allows a resolution of 370 nm in the z dimension, and maintains the speed of acquisition pair to 100 frames per seconds (Ovečka *et al.*, 2018). Lattice LSFM has been so far applied to observe leaves of *Arabidopsis thaliana* as a proof of concept for an increase in resolution (Liu *et al.*, 2018), but more can be expected in the near future.

4.2 Live cell imaging application to study meiosis in crops

A compelling possible development of the live cell imaging method is its re-adaptation to follow meiosis in crops. As previously stated, the manipulation of meiosis has great potential to improve crop breeding. Therefore, knowledge gained from *Arabidopsis thaliana* can be translated into to the most economically relevant plant species barley, wheat, maize, potato, tomato, cabbages, oilseed rape, etc. Techniques to introduce fluorescent reporters in dicots such as potatoes, and oilseed rape or in monocots as rice and maize are developing fast, and the generation of reporter lines is becoming easier. *Brassica napus*, due to its similarity with *Arabidopsis thaliana* in the flower structures, could be easily pursued. For instance,

the glycine-rich protein GRP17:GFP reporter, which is a major component of the pollen coat, has been expressed in anthers of *Brassica napus*, and imaged by stereo fluorescent microscopy (Suzuki *et al.*, 2013). This study revealed the migration of tapetal cells between pollen grains after meiosis, and set a precedent in observing anthers of Brassica. Other examples are the chimera CFP: β -TUB1, stably introgressed in maize, which has been used to image maize meiosis in isolated meiocytes (Nannas *et al.*, 2016; Higgins *et al.*, 2016), or the reporter for histone H2B (H2B:mCherry), introgressed in rice. H2B:mCherry has been successfully imaged in rice roots (Bureau *et al.*, 2018), and it could be possibly used to visualize chromatin during meiosis.

Still, main adaptations needs to be done to the imaging procedure and to the sample mounting, to finally obtain clear time lapses of meiosis in crops. Anther size of crop species can be bigger than for *Arabidopsis thaliana*, e.g. cereals; moreover meiosis can take longer (Table 1.1), and therefore the samples might have different needs to be kept alive. Nonetheless the first step toward maize and potato live cell imaging of meiosis have been done in our laboratory by Martina Balboni and Dr. Yuki Hamamura (unpublished data) confirming that the method could be extended and optimized to other plants.

4.3 The landmark system

The images acquired via live cell imaging restituted a different picture of meiocytes than the one obtained by cell spreads. Importantly, cells maintained their spatial organization, usually destroyed by other techniques, which has two major implications: first, it was required to establish a new reference system to identify meiotic stages unequivocally, and secondly, new interesting details of meiocytes cytology emerged. The establishment of a new reference system has been initiated by the characterization of the *KINGBIRD* line. The *KINGBIRD* line revealed five morphological features of male meiocytes, i.e., cell shape, position of the nucleus, position of the nucleolus, REC8 localization along with information about chromatin state, and microtubule array. I used these cellular features not only to attribute meiotic stages to cytological samples, as previously done (Ross *et al.*, 1996; Peirson *et al.*, 1997; Armstrong and Jones, 2003; Stronghill *et al.*, 2014), but also I could

assess how they connect to each other. The assessment of the relative frequency of cellular states with neighboring score revealed that meiotic progression could be described as a network of transition states, converging at different moments of the division into 11 prominent states, named landmarks. While landmarks represent stable combinations of features, that were observed identical in more samples, the transition states presented a higher degree of variability, indicating that each meicyote can follow multiple pathways to finally assume the same landmark (Figure 4.1 A). This observation reveals that the cellular features are all interconnected but that the stringency of their reciprocal interactions varies between meicyotes and within meiotic phases.

4.4 Towards an atlas of meiosis

While variation, to a certain extent, is intrinsic of biological samples, it would be interesting to test how much does the map of the cellular states vary, and which singular features would be more affected by different extrinsic elements, i.e. environmental cues as high or low temperatures, or under altered intrinsic conditions, i.e. when a meiotic regulator is mutated. We could expect for examples that the variability of transition states is enhanced when the plant is subjected to temperature changes (Figure 4.1 B). Increases in temperature are known to accelerate meiosis (Wilson, 1959; Stefani and Colonna, 1996), this could lead to less accuracy in the division control, and therefore different cellular states could be observed. In other cases instead, heat seems to cause a stop in meiotic progression as it appears in wheat (Draeger and Moore, 2017). Moreover, it is known that heat and cold treatments change microtubule rearrangements inducing polyploidy, or alter the deposition of the synaptonemal complex (Morgan *et al.* 2017, Modliszewski *et al.* 2017). Both the effects could induce aberration in the feature morphology and therefore could alter the way they combine into cellular states. The stability of the landmarks could be affected as well, shifting the equilibrium of the model that I obtained from WT dataset towards different cellular states (Figure 4.1 C). A complete change in the landmark landscape could also be possible. For instance, some landmarks are expected to disappear: a straight-forward example is the loss of A11 in *tam* or *osd* mutants, where a premature exit from meiosis is observed

(d'Erfurth *et al.*, 2009; Wang *et al.*, 2010; d'Erfurth *et al.*, 2010)(Figure 4.1 D). However, it is likely that more subtle and unexpected changes in the duration/composition of the landmark system exist in other meiotic mutants. Moreover, the landmark system presented here, which is based on a comparison between observed states, could be extended by the insertion of new feature combinations, leading to a new map of cellular states, with new landmarks (Figure 4.1 E).

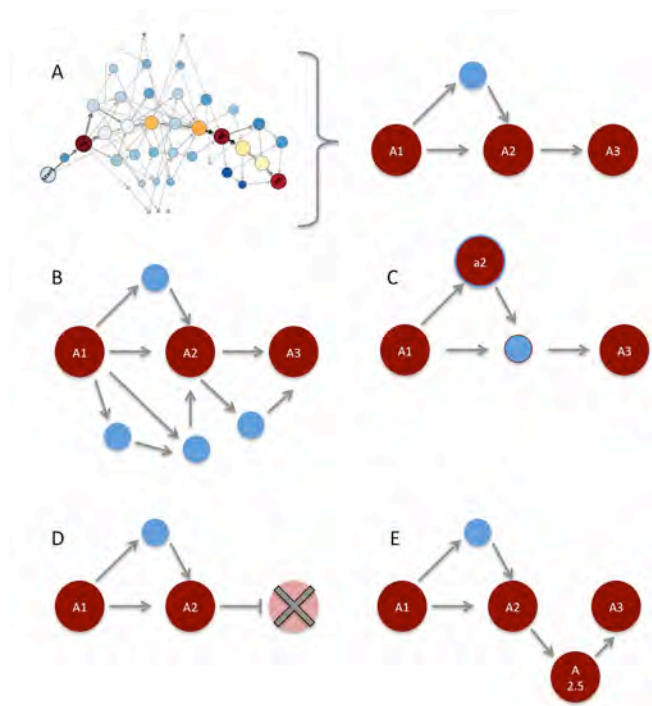


Figure 4.1 Possible changes of the landmark system

The figure is a schematic representation of the possible changes of the landmark system, expected when performing the neighboring score analysis on mutants or in different environmental conditions. The red circles identify landmarks, while the blue circles identify transition states.

- A) Schematic representation of the landmark system, as obtained from the current analysis of WT plants.
- B) Possible variation 1: increase in number of transition state (increase in the system variability).
- C) Possible variation 2: a transition state becomes more relevant than the closest landmark, and they switch role in the system.
- D) Possible variation 3: a landmark is depleted.
- E) Possible variation 4: new landmarks are added.

The different landmark systems could, therefore, become a very efficient way to identify and quantify meiotic defects. This leads to the second possible application of the landmark system, which aims to draw an atlas of plant meiosis on the track of what has been done for human mitotic cells (Cai *et al.*, 2018). Cai *et al.* describe a

model of mitotic division of human cells, mainly based on chromosome volume and position. They sub-divided mitosis in 20 sub-stages, each characterized by a specific profile of features as I did for *Arabidopsis thaliana* meiocytes. Cai *et al.* went further and standardized the mitotic time, describing a general spatiotemporal cellular context of mitosis, which was then used to map the localization and dynamics of 28 well known mitotic proteins. In the same way, we could use the landmark system as an atlas of male WT meiosis, providing a new tool to study protein dynamics and interactions.

4.5 Single cell imaging reveals new insights into meiotic timing and tissues synchronization

Live cell imaging allows following the same single cell as it proceeds through meiosis, and thus it permits direct observation of changes within the same sample rather than a comparison between different phases captured in different cells. This not only disclosed details about morphological variability, as introduced in the previous chapter (chapter 4.2, Discussion), but also it allowed a direct time calculation of the duration of meiosis per cell. Moreover I could observe the relation that is established between meiocytes or between meiocytes and the surrounding tissues. Cell spreads analysis revealed that meiocytes of *Arabidopsis thaliana* are synchronous until the end of prophase I. The synchronicity is lost at the onset of metaphase I, and cell spreads coming from the same flower bud display multiple phases, from diakinesis to tetrads (Armstrong *et al.*, 2003; Stronghill *et al.*, 2014). With the application of live cell imaging, I could refine the duration of these shorter and not synchronous phases. Furthermore, it was possible to verify the origin of asynchronicity and at which time of the division it appears. I observed that even though different anthers of the same flower bud are going through meiosis within the same day, they present some delay one in respect to the other. The same is observed between pollen sacs of the same anther. Secondly, I could detect the presence of asynchronicity among meiocytes of the same pollen sac as well: cells on one pole of the anther proceed first to metaphase I, generating a gradual wave that reaches the opposite pole of the anther with a delay of ca. 15 minutes (ongoing work). The delay is then maintained during all the following phases. The gradient

starts equally from the distal or from the proximal end of the anther. This phenomenon has not been described so far, and therefore further research should be carried out to determine its function and regulation. In 1972 Ito and Stern observed that isolated meiocytes lose their synchronicity faster than meiocytes that are cultivated in anthers (Ito and Stern, 1967), suggesting that the contact among meiocytes is fundamental in regulating the timing of meiosis. One possible explanation is that it could reflect a hormonal response, implying a possible involvement of auxin transport and signaling. Auxin is involved in many developmental processes of the plant, and have been proven as important regulator for post-meiotic divisions, pollen maturation and tapetum dehiscence (Cecchetti *et al.*, 2008; Yang *et al.*, 2013; Yao *et al.*, 2018). In the same way, it might be interesting to investigate its role in regulating meiosis.

On the other side, auxin transporters and YUCCA genes do not show expression of GUS reporters of fluorescent chimera in anthers at a meiotic stage (Yao *et al.*, 2018). Moreover, the fact that the gradient seems to come from at least two different directions possibly is in contrast with the classic model of auxin transport, and therefore other factors might determine the delay. At the beginning of meiosis, all the gametes in a pollen sac form a syncytium connected by plasmodesmata. The cytoplasmic channels are blocked at the end of prophase I by callose deposition at the cell wall (Heslop-Harrison, 1966; Ünal *et al.*, 2013). The closure of plasmodesmata causes molecular isolation of the future gametes, and it could have a role in the protection against drought or environmental stresses. The newly acquired isolation might induce the loss of synchrony among meiocytes; therefore it might be interesting to monitor callose deposition and the timing of plasmodesmata closure during meiosis, and verify if it follows a similar gradient. Callose deposition could be as well involved in the lack of fine tune between tapetum cells and meiocytes. Cytoplasm extrusions similar to the one connecting meiocytes, establish connections between tapetal cells and meiocytes, but they loose connection before the end of meiosis I (Echlin, 1971). I demonstrated here, analyzing the feature correlation, that meiosis progresses to a certain extent independently of tapetum cell development. Polynucleated tapetum cells are not found before A4/zygotene, and conversely, when all tapetum cells are poly-

nucleated, meiosis has progressed into A7/diplotene. However, endomitosis only loosely correlates with any of the meiotic stages between A4 and A7. Considering that plasmodesmata put in contacts meiocytes and tapetum cells, the same scheme followed by the dis-regulation among meiocytes could potentially play a role in the loss of communication and coordination between meiocytes and tapetum.

4.6 Time course in 2X and 4X

Previous analyses of polyploid species indicated that early stages of prophase I, i.e., leptotene, proceed faster than in diploid species (Bennett, 1971; Bennett and Kaltsikes, 1973; Bennett, 1977). A more recent paper instead suggested that prophase is slower in tetraploid of *Arabidopsis arenosa* than in the diploid population (Higgins *et al.*, 2014). The time courses of diploid and tetraploid populations of *KINGBIRD* restituted a controversy result. Looking at the average duration of landmarks, it appears that meiosis in neotetraploid is slowed down in two central moments of the division: during S-phase and at the transition between meiosis I and II. The lengthening of S-phase could be correlated to the increased DNA content of polyploid plants, which would then require longer time to duplicate. Although the difference seems relevant, no statistic could be performed, since all the observations came from the same flower bud. The lengthening of later meiotic events is instead significant and it refers in particular to the landmark A9. A9 represents the transition between the first and the second division, and its timing includes all the phases from telophase I to the end of prophase II. These steps of meiosis have not been studied thoroughly so far. An hypothesis is that the meiotic defects described for neotetraploid generations such as multivalent formation and consequent breakage of chromosomes or formation of chromosomes bridges and laggards and isolated chromosomes have an effect on telophase and dyad formations. It is debatable, though, the fact that these later stages are more affected than metaphase I and anaphase I, where no significant lengthening is detected. A possible reason why an alteration in meiotic timing is present only after metaphase I could be the fact that plants have very relaxed Spindle Check Point (SAC) (Komaki and Schnittger, 2017). Moreover, no previous data have been collected about the duration of meiosis in the presence of these types of defects so that no proper

comparison can be defined. Since the second meiotic division is described as very similar to a mitotic division (d'Erfurth *et al.*, 2009; Wijnker and Schnittger, 2013), it would be interesting to check if any delay in tetraploid mitosis could be observed. Nonetheless, before proceeding to further investigation, the current results should be re-validated, with an increased number of samples.

4.7 Future perspectives

I introduced here a novel system to investigate meiosis in plants. The system is built by a technical component, that is the microscopy method, and by an analytical component, the landmarks. Each component could be employed singularly or in combination, therefore broadening the experimental perspectives of meiotic research as discussed in the previous chapters. Nonetheless, to exploit the full potential of the technique, it will be fundamental in the near future to develop an automatized protocol for data analysis. The manual annotation of cells and of cell features over many hours of observation has been a lengthy process, greatly limiting the dataset that could be analyzed. Tools to perform data analysis and image processing advanced at the same pace of microscopy, and they are more and more accessible via user-friendly interfaces and free plugins. The coupling of technique such as cell tracking and cell profiling, guided by deep learning approaches have been applied to study animal development such as *C.elegans* (Kainmueller *et al.*, 2014) or to medical research as a tool to identify carcinogenic cells and drug effects (Matuszewski *et al.*, 2018). The development of a machine learning procedure to process the images could incredibly speed up the analysis of our data set and thus make the live images acquisition together with the landmark system a powerful approach to deepen our knowledge on plant meiosis.

5 Material and Methods

5.1 Plant material and growth conditions

The *Arabidopsis thaliana* (L.) Heynh plants used in this study were all derived from the Columbia (Col-0) ecotype. NASC (Nottingham, UK) provided the T-DNA insertion lines of *rec8* (At5g05490, SAIL_807_B08), and *tam1-2* (At1g77390, SAIL_505_C06) from Syngenta (Ag, Basel, Switzerland), *mlh3-1* (At4g35520, SALK_015849) and *mlh3-2* (At4g35520, SALK_041465) from the SALK institute for Biological Studies (La Jolla, CA, USA). The triple and quadruple mutants *krp4,6,7* and *krp3,4,6,7* were generated and described in Zhao *et al.*, 2017.

All seeds were surface-sterilized with chloride gas, sown on MS plates (Annex 9) and stored 3 days at 4 °C in the dark for stratification. 25 mg/L Hygromycin B was added to the plate when required for selection. For germination, plates were transferred to long-day condition (16 h day/8 h night regime at 22 °C/18 °C). After germination, plants were transferred to soil and grown under short-day conditions for 2 weeks (12 h day/12 h night regime at 21 °C/18 °C), and then transferred to long-day conditions until seed production.

5.2 Genotyping

Seven to ten days after transfer to soil, the plant DNA was extracted by magic buffer protocol. The necessary number of wells in a 96 deep-well polypropylene block were prepared with one metal bead and filled with 250 µl of magic buffer (Annex 9). The smallest leaf of the rosette was clipped with forceps and located in a well. The block was shaken for three minutes (MM300, Retsch, Haan) and then centrifuged at 2500 rpm for 1 minute. 100 µl of DNA in magic buffer were aliquoted, transferred into a PCR plate and stored at -20°C.

All genotypes were determined by polymerase chain reaction (PCR) with the primers indicated in Annex 10. 1 µl of extracted DNA was used as template for PCR amplification. The mastermix for the PCR reaction was prepared as follow:

- 7.5 μ l DreamTaq Green PCR mastermix (Thermofisher scientific)
- 0.5 μ l of 10 μ M Forward /LB primer
- 0.5 μ l of 10 μ M Reverse/RB primer
- 5.5 μ l Nucelase Free Water
- 1 μ l extracted DNA

The lid of the thermocycler was pre-heated at 99°C, and the program set as follow:

- 94°C, 3 min
 - 94°C, 30 sec
 - 55°C, 30 sec
 - 72°C, 1 min
 - 72°C, 5 min
 - 16°C, hold
- } X 30 cycles

To genotype *REC8 WT* allele in *PRO_{REC8}:REC8:GFP* and *PRO_{REC8}:REC8:mNG* line, the GreenTaq was substituted by Terra PCR Direct polymerase Mix (Takara), and the thermocycle run as follow:

- 95°C, 2 min
 - 98°C, 10 sec
 - 60°C, 15 sec
 - 68°C, 3.5 min
 - 68°C, 2 min
 - 16°C, hold
- } X 35 cycles

5.3 Cloning of PRO_{REC8}:REC8:mNG

The cloning procedure of PRO_{REC8}:REC8:mNG has been previously described in detail in Leyk 2016, Bachelorarbeit (Leyk, 2016), and will be here briefly summarized. To generate the *PRO_{REC8}:REC8:mNG* construct, a 711 bp fragment from the B812p35s-LNeon vector, containing the newly synthesized mNG gene (sequence in Annex 11), was amplified with the primers *Smal*-mNeon-F and *Smal*-mNeon-R (Annex 10). Two *Smal* sites were inserted by the PCR: one in front of the molecular linker, which encodes for 19 AA before the start codon, and the second one right after the stop codon of mNG. The new fragment was cloned into pHSG399 for amplification. The

construct was then cut out by *Sma*I digestion and ligated to the linearized entry vector pENTR-CTer-SmaI-REC8 followed by LR recombination reaction into the destination vector pGWB501 (Nakagawa *et al.*, 2007) (Annex 11). The vector pGWB501-REC8-SmaI-mNEON was then transformed into the *Agrobacterium tumefaciens* GV3101 strain (pMP90).

5.4 Plant transformation and crossing

The transformation of *Arabidopsis thaliana* was performed with the floral dip method (Clough and Bent, 1998). The *Agrobacterium tumefaciens* carrying the plasmid of interest was cultured in 15 ml liquid LB (Annex 9) with antibiotics, overnight (ON) at 28°C, shaking at 165 rpm. The following day, flowering plants (4 to 5 weeks old) were prepared for transformation: all the siliques and open flowers were clipped away, leaving only young closed flower buds attached at the inflorescence. The ON culture of *Agrobacterium tumefaciens* was then centrifuged at 4000 rpm for 10 minutes at room temperature, and the pellet was resuspended in 15 ml solution of 5% Sucrose and 0.02% Silwet-77 in Millipore water. Closed flowers were coated with the bacterial suspension by using a pipette. After bacteria distribution, plants were closed in a humidified plastic bag for 2 days, and then transferred in a growth chamber at standard growth conditions until seeds collection.

The crosses, were performed on flowering plants 5-6 weeks old. Flowers of the female parent were emasculated 1 day before anthesis. Under a dissecting microscope the closed flower buds were gently opened using fine forceps, and anthers were cut off, while all the remaining organs were left intact. The following morning, emasculated flowers were hand-pollinated and marked. Plants were then transferred at standard growth conditions until seeds collection.

5.5 VIGS

5.5.1 VIGS treatment

The protocol for incubation and inoculation was previously described in Nimchuck *et al.*, 2000 and readapted in Calvo-Baltanas *et al.*, 2018.

Plant transformation of $PRO_{REC8}:REC8:GFP$ and $PRO_{RPS5A}:TagRFP:TUB4$ was done by leaf agro-infiltration at the stage of five leaves rosette. *Agrobacterium*

tumefaciens GV3101 (pMP90) carrying the vectors pTRV2-OSD1, pTRV2-PDS and pTRV1 were cultured in 2ml YEB medium (Annex 9) with 50 µg/ml antibiotics (gentamycin and kanamycin) at 28°C, ON, shaking at 165 rpm. The following day, 150 µl of culture were inoculated in 3 ml of YEB + antibiotics and grown for 13 hours at 28°C, shaking at 165 rpm. The bacteria were then centrifuged at 5000 rpm for 5-15 minutes, resuspended in 3 ml of Induction medium (Annex 9) and grow for 5-7 hours at 23°C. shaking at 165 rpm. After a maximum of 7 hours, bacteria were centrifuged at 5000 rpm for 5-15 minutes, and resuspended in 10-12 ml of Infiltration medium (Annex 9), to an optimal OD600 of 0.4. The Agrobacteria carrying pTRV2-OSD1 or pTRV2-PDS were mixed to the culture of pTRV1 in a 1:1 ratio. The final solution was infiltrated into the leaves using a 5 ml syringe without needle. Plants were then kept at standard growing conditions.

5.5.2 Selection of VIGS treated plants

Selection of infected flower material was done by evaluation of pollen ploidy and pollen size, as described in Calvo Baltanas *et al.*, 2018. One anther per flower was stained with Peterson staining (Annex 9) and checked for pollen size (section 5.6.2, material and methods). Flowers showing diploid pollen were either emasculated to be used as female parent or used as pollinator. Crosses were performed as explained in section 5.4 of material and methods. The F1 offspring was selected on Hygromycin B for *PRO_{REC8}:REC8:GFP*; 7 to 10 days after germination, seedlings were screened on MS plates to check for fluorescence signal from *PRO_{RPS5A}:TagRFP:TUB4* at dissecting microscope equipped with a fluorescence detection system (e.g. Olympus MVX10, coupled with U.V. light source X-cite series 120 Q). The ploidy level of the F1 was tested by flow cytometry (CyFlow Ploidy Analyzer, Sysmex PARTEC, Görlitz, Germany) and tetraploid F1 plants grown for F2 seeds production. F2 plants have been used for imaging of tetraploid microspore mother cells.

5.6 Phenotype evaluation

5.6.1 Evaluation of seed abortion

To assess the rate of seeds abortion, three siliques per plant, from three different plants per line were used. The siliques were selected based on their position along the stem, in order to analyze material at the same developmental stage. Siliques were positioned on a double side tape on a slide and checked under a dissecting microscope (Stemi2000, Carl Zeiss GmbH, Oberkochen, Germany). They were cut along the septum with a fine needle and the valves were opened. Viable and aborted seeds were then scored.

5.6.2 Pollen viability test

Pollen viability and pollen size were assessed as described in Peterson (Peterson *et al.*, 2010). A drop of Peterson stain (Annex 9) was released on a polylysine microscope slide, anthers were cut from an open flowers and tapped on the drop of stain to facilitated pollen release. Anther were finally immersed in the stain, and covered by a cover slide 18x18 mm. Slides were then positioned on a pre-heated hotplate at 80°C for 2-5 minutes and screened for pollen viability using the light microscope (Axioskop, Carl Zeiss GmbH, Oberkochen, Germany) and 20X-40X objectives. To check the rescue of *rec8* phenotype in *PRO_{REC8}:REC8:GFP* and *KINGBIRD*, 1500 pollen grains from 6 different flowers and three different plants were counted per line.

5.6.3 Cell spreads

Cell spreads of *PRO_{REC8}:REC8:GFP*, *PRO_{RPS5A}:TagRFP:TUB4*, *KINGBIRD (2X)*, and F2 of *KINGBIRD (4X)*, were made as described in Ross *et al.* 1996. Inflorescences of 4-6 weeks old plants were harvested, fixed on ice in 7-9 ml of EtOH/Acetic acid 3:1 in 15 ml falcon tube and incubated for 24 hours at 4°C. The following day, the inflorescences were washed 3X in 70% EtOH and stored at 4°C until needed in 7-9 ml of 70 % EtOH. At the moment of cell spreads preparation, flower buds were isolated from the inflorescence and transferred into a 24 –well plate, grouped by size. The flower buds were washed 3X in 900 µl Millipore water and finally covered by 900 µl of 0.01 M Citrate Buffer (Annex 9) for 5 minutes. The citrate buffer is then substituted with 600 µl of Enzyme mix (Annex 9), and the sample is incubate at 37°C

for 3 hours, in moisturized conditions. Flower buds were then positioned on a microscopy slide with a drop of enzyme mix (Annex 9), and smashed in 15 μ l of 45% Acetic acid with the help of a bended needle or cannula. 5 μ l of 45 % Acetic acid were added to the slide, which was placed on a hotplate pre-heated at 46°C for 30 seconds. The slide was finally rinsed with a solution of EtOH/Acetic acid 3:1, dried on the hotplate, stained with 18-20 μ l of DAPI in Vectashield (Vector Laboratories, INC, Burlingame, CA, USA) and covered with a cover-slide 20x24mm. Cell spreads were then screened and imaged using the fluorescence microscope Zeiss Axio Imager 2, equipped with a 63X oil immersion objective.

5.7 Confocal Microscopy

5.7.1 Still pictures

Still images of meiocytes were acquired using the inverted confocal microscope Leica TSC SP8 and LAS X software (Leica Mikrosysteme Vertrieb GmbH, Wetzlar, Germany). Inflorescences of *Arabidopsis thaliana* were cut and positioned on a microscope slide held by double side tape. Up to six flowers at meiotic stage (0.4-0.6 mm) were isolated and dissected: under a dissection microscope (e.g. Zeiss Stemi2000 and Stemi508) each flower bud was opened with a fine tweezer (Dumoxel 0203-4-PO) and sepals were removed to visualize the anthers. The flower buds were then transferred into a drop of tap water on a microscope slide and covered with a coverslide 18x18 mm. Pictures were captured with a 40X water immersion objective. mEGFP and mNG were excited at λ 488 nm, and detected at λ between 498-550 nm. TagRFP was excited at λ 561 nm and detected at λ between 578-650 nm. Autofluorescence from chloroplasts was highlighted in blue using excitation at λ 488, and detection at λ between 680-750 nm.

5.7.2 Live cell imaging

Time lapses were acquired using a Zeiss LSM 880 or a Zeiss LSM 780 confocal microscope and ZEN 2.3 SP1 software (Carl Zeiss GmbH, Oberkochen, Germany). Flowers of 0.4-0.6 mm were isolated and prepared as described in the results section 3.1.1. Up to 4 samples were positioned on the same petri dish and cultured in ACM (Annex 9, Hamant *et al.*, 2014). During image acquisition the petri dish was filled

with autoclaved water and placed under a W-plan-Apochromat 40X/1.0 DIC objective (Carl Zeiss GmbH, Oberkochen, Germany). mEGFP and mNG were excited at λ 488 nm, and detected at λ between 498-550 nm. TagRFP was excited at λ 561 nm and detected at λ between 578-650 nm. Autofluorescence from chloroplasts was highlighted in blue using excitation at λ 488, and detection at λ between 680-750 nm. Time lapses were acquired as series of Z-stacks (6 planes, 50 μ m distance). Interval time varies from a maximum of 15 minutes to a minimum of 3, depending on sample conditions. The functions “Autofocus” and “Automatized positions” were used to acquire images. Room temperature and sample temperature were controlled and stabilized at 18 °C and 21°C respectively.

5.8 Time lapses processing and analysis

Time lapses obtained in the .czi format were converted into sequential images by Image J (Fiji version 1.52b, <https://imagej.net/Fiji>). They were then opened with MetaMorph Version 7.8.0.0 software (Molecular devices LLC., San Jose, CA, USA) and one focal plane was selected from all z-stacks over the whole time series using the function “Review Multi Dimensional Data”, the file was exported as .tiff stack file. XY drift was then corrected using the plugin “HyperStackReg v05” of Fiji, selecting ‘Solid Body’ as transformation parameter. Brightness and contrast were adjusted and the file was finally converted into an RGB file by Fiji. Cells were manually annotated on Fiji over the time lapse.

5.9 Quantitative analysis of live cell imaging data

5.9.1 Landmark extraction

Data set annotation

A subset of the analyzable male meiocyte was described at every time point by assigning manually a value for each of the five features assessed. A total of 169 meiocytes from 35 anthers were annotated, leading to a total of 18,531 data points spanning more than 3,269 hours. For 7,860 observations one or more of the features could not be annotated with a well-defined state, with 5,893 observations not having a single feature recognizable. The resulting dataset, consisting in 10,671 time

points, was used to determine the co-occurrences of feature states and the landmarks.

All analysis of the dataset was done using the Python programming language (Version 3.6, Python Software Foundation, <https://www.python.org>) (WUR)

Data preprocessing (WUR)

The manually created data set contains a description of the state of each of the 5 features that were recorded in individual cells with 15 minute intervals. In some cases, the time between consecutive measurements was more than 15 minutes. In these cases, we inserted an unmeasured data point ('n') for each cell feature such that time between measurements was equal and at most 15 minutes for each recorded time course. This was done to ensure that unmeasured periods are noted as unmeasured properly and to decrease the risk to assign any unrealistic transitions. The combination of the state of each of the 5 cellular features makes up the cell state. Transitions from one cell state to another occur when one or more feature switch to a new state.

Cell state co-occurrence (WUR)

To create the co-occurrence heat map, the number of times a combination of two feature states occurred in the same cell at the same time point was counted. Since some time courses were measured with different temporal resolution (e.g. 10 minute intervals versus 15 minute intervals), we first resampled the data points from all time courses to have the same time between measurements. Co-occurrence counts were normalized by the total number of counts in the column, including the counts where the state of the 2nd feature could not be measured. This means that in the upper triangular part of the matrix, the counts are normalized for the total occurrence of the first feature (all feature sections per row together sum up to 1) while in the lower triangular part of the matrix for the second feature, each column sums up to 1.

Bootstrapping (WUR)

To assess the robustness of the selected landmarks and thus our theoretical framework, we performed a bootstrapping procedure on our data set. The total set

of observations was randomly sampled with replacement to obtain a data set 1.5 times the size of the original data set. Scores for each state in this data set were calculated using the procedure described in the previous paragraph. This process was repeated 1000 times to obtain estimates for the mean value, standard deviation and quantiles of the score of each cellular state.

5.9.2 Meiotic time course calculation

Dataset annotation and time calculation

A second dataset was annotated solely using the landmark system for the comparison of the calculation of the time course of diploid and tetraploid *KINGBIRD* lines. The timing of image acquisition and the landmark attribution for each cell at each time point was done manually on Excel. Landmarks were described using numbers from 0 to 12 with a trailing “s” when the landmark was appearing for the first time. An “n” was assigned to the cell when not visible at a certain time point. All the starting points appearing later than 15 min after the previous recorded landmark were discarded. Files in the CSV format were created for each anther. The duration of each landmark was automatically extracted from the CSV files using a custom software from Dr. Felix Seifert (CropSeq bioinformatics, GmbH, Hamburg, Germany) based on consecutive landmark transitions. This resulted in a dataset of 327 landmark durations from 136 meiocytes of 17 different anthers for *KINGBIRD 2X* and in a database of 592 landmark durations, from 238 meiocytes of 27 different anthers for *KINGBIRD 4X*.

Statistical analysis (WUR)

Mann-Whitney U test was applied to compare the diploid and tetraploid datasets. Samples were grouped by anthers, averaging the duration of each landmark within a pollen sac, and among different pollen sacs in second place.

Statistical analysis of the dataset was done using the Python programming language (Version 3.6, Python Software Foundation, <https://www.python.org>).

References

- Allard, P. and Colaiácovo, M.P.** (2010). Bisphenol A impairs the double-strand break repair machinery in the germline and causes chromosome abnormalities. *PNAS* **107**: 20405–20410.
- Armstrong, S.J., Franklin, F.C.H., and Jones, G.H.** (2003). A meiotic time-course for *Arabidopsis thaliana*. *Sex Plant Reprod* **16**: 141–149.
- Armstrong, S.J., Franklin, F.C.H., and Jones, G.H.** (2001). Nucleolus-associated telomere clustering and pairing precede meiotic chromosome synapsis in *Arabidopsis thaliana*. *J Cell Sci* **114**: 4207–4217.
- Armstrong, S.J. and Jones, G.H.** (2003). Meiotic cytology and chromosome behaviour in wild-type *Arabidopsis thaliana*. *J. Exp. Bot.* **54**: 1–10.
- Bai, X., Peirson, B.N., Dong, F., Xue, C., and Makaroff, C.A.** (1999). Isolation and Characterization of SYN1, a RAD21-like Gene Essential for Meiosis in *Arabidopsis*. *Plant Cell* **11**: 417–430.
- Barakate, A., Higgins, J.D., Vivera, S., Stephens, J., Perry, R.M., Ramsay, L., Colas, I., Oakey, H., Waugh, R., Franklin, F.C.H., Armstrong, S.J., and Halpin, C.** (2014). The Synaptonemal Complex Protein ZYP1 Is Required for Imposition of Meiotic Crossovers in Barley. *The Plant Cell* **26**: 729–740.
- Bennett, M.D.** (1971). The duration of meiosis. *Proc. R. Soc. Lond. B* **178**: 277–299.
- Bennett, M.D.** (1977). The time and duration of meiosis. *Phil. Trans. R. Soc. Lond. B* **277**: 201–226.
- Bennett, M.D., Chapman, V., Riley, R., and S, F.R.** (1971). The duration of meiosis in pollen mother cells of wheat, rye and Triticale. *Proc. R. Soc. Lond. B* **178**: 259–275.

- Bennett, M.D. and Kaltsikes, P.J.** (1973). The Duration of Meiosis in a Diploid Rye, a Tetraploid Wheat and the Hexaploid Triticale Derived from Them. *Can. J. Genet. Cytol.* **15**: 671–679.
- Bennett, M.D. and Smith, J.B.** (1972). The effects of polyploidy on meiotic duration and pollen development in cereal anthers. *Proc. R. Soc. Lond. B* **181**: 81–107.
- Bennett, M.D. and Stern, H.** (1975). The Time and Duration of Female Meiosis in *Lilium*. *Proceedings of the Royal Society of London. Series B, Biological Sciences* **188**: 459–475.
- Blakeslee, A.F. and Avery, A.G.** (1937). METHODS OF INDUCING DOUBLING OF CHROMOSOMES IN PLANTS By Treatment With Colchicine. *J Hered* **28**: 393–411.
- Blary, A. et al.** (2018). FANCM Limits Meiotic Crossovers in Brassica Crops. *Front. Plant Sci.* **9**.
- Bomblies, K., Higgins, J.D., and Yant, L.** (2015). Meiosis evolves: adaptation to external and internal environments. *New Phytologist* **208**: 306–323.
- Bulankova, P., Akimcheva, S., Fellner, N., and Riha, K.** (2013). Identification of *Arabidopsis* Meiotic Cyclins Reveals Functional Diversification among Plant Cyclin Genes. *PLOS Genet* **9**: e1003508.
- Burch-Smith, T.M., Schiff, M., Liu, Y., and Dinesh-Kumar, S.P.** (2006). Efficient Virus-Induced Gene Silencing in *Arabidopsis*. *Plant Physiology* **142**: 21–27.
- Bureau, C., Lanau, N., Ingouff, M., Hassan, B., Meunier, A.-C., Divol, F., Sevilla, R., Mieulet, D., Dievart, A., and Périn, C.** (2018). A protocol combining multiphoton microscopy and propidium iodide for deep 3D root meristem imaging in rice: application for the screening and identification of tissue-specific enhancer trap lines. *Plant Methods* **14**: 96.
- Burkhardt, S., Borsos, M., Szydlowska, A., Godwin, J., Williams, S.A., Cohen, P.E., Hirota, T., Saitou, M., and Tachibana-Konwalski, K.** (2016). Chromosome

- Cohesion Established by Rec8-Cohesin in Fetal Oocytes Is Maintained without Detectable Turnover in Oocytes Arrested for Months in Mice. *Curr Biol* **26**: 678–685.
- Cai, X., Dong, F., Edlmann, R.E., and Makaroff, C.A.** (2003). The Arabidopsis SYN1 cohesin protein is required for sister chromatid arm cohesion and homologous chromosome pairing. *Journal of Cell Science* **116**: 2999–3007.
- Cai, Y. et al.** (2018). Experimental and computational framework for a dynamic protein atlas of human cell division. *Nature* **561**: 411.
- Calvo-Baltanas, V.** (2019). Control of meiosis using virus-induced gene silencing.
- Calvo-Baltanas, V., Wijnen, C.L., Lukhovitskaya, N., Snoo, C.B. de, Hohenwarter, L., Jong, H. de, Schnittger, A., and Wijnker, E.** (2018). Efficient reverse breeding by VIGS-mediated transient crossover reduction. *bioRxiv*: 459016.
- Cecchetti, V., Altamura, M.M., Falasca, G., Costantino, P., and Cardarelli, M.** (2008). Auxin Regulates Arabidopsis Anther Dehiscence, Pollen Maturation, and Filament Elongation. *The Plant Cell* **20**: 1760–1774.
- Chacón, M.R., Delivani, P., and Tolić, I.M.** (2016). Meiotic Nuclear Oscillations Are Necessary to Avoid Excessive Chromosome Associations. *Cell Reports* **17**: 1632–1645.
- Chambon, A., West, A., Vezon, D., Horlow, C., Muyt, A.D., Chelysheva, L., Ronceret, A., Darbyshire, A., Osman, K., Heckmann, S., Franklin, F.C.H., and Grelon, M.** (2018). Identification of ASYNAPTIC4, a Component of the Meiotic Chromosome Axis. *Plant Physiology* **178**: 233–246.
- Chelysheva, L. et al.** (2005). AtREC8 and AtSCC3 are essential to the monopolar orientation of the kinetochores during meiosis. *Journal of Cell Science* **118**: 4621–4632.
- Chen, B.-C. et al.** (2014). Lattice light-sheet microscopy: Imaging molecules to embryos at high spatiotemporal resolution. *Science* **346**: 1257998.

- Christophorou, N., Rubin, T., Bonnet, I., Piolot, T., Arnaud, M., and Huynh, J.-R.** (2015). Microtubule-driven nuclear rotations promote meiotic chromosome dynamics. *Nature Cell Biology* **17**: 1388–1400.
- Cifuentes, M., Grandont, L., Moore, G., Chèvre, A.M., and Jenczewski, E.** (2010). Genetic regulation of meiosis in polyploid species: new insights into an old question. *New Phytologist* **186**: 29–36.
- Clift, D. and Marston, A.L.** (2011). The Role of Shugoshin in Meiotic Chromosome Segregation. *Cytogenet Genome Res* **133**: 234–242.
- Clough, S.J. and Bent, A.F.** (1998). Floral dip: a simplified method for *Agrobacterium*-mediated transformation of *Arabidopsis thaliana*. *The Plant Journal* **16**: 735–743.
- Comai, L.** (2005). The advantages and disadvantages of being polyploid. *Nature Reviews Genetics* **6**: 836–846.
- Crismani, W., Girard, C., and Mercier, R.** (2013). Tinkering with meiosis. *J Exp Bot* **64**: 55–65.
- Cromer, L., Jolivet, S., Horlow, C., Chelysheva, L., Heyman, J., De Jaeger, G., Koncz, C., De Veylder, L., and Mercier, R.** (2013). Centromeric Cohesion Is Protected Twice at Meiosis, by SHUGOSHINs at Anaphase I and by PATRONUS at Interkinesis. *Current Biology* **23**: 2090–2099.
- Daldello, E.M., Luong, X.G., Yang, C.-R., Huhn, J., and Conti, M.** (2018). Cyclin B2 is required for progression through meiosis in mouse oocytes. *bioRxiv*: 441352.
- Dernburg, A.F., McDonald, K., Moulder, G., Barstead, R., Dresser, M., and Villeneuve, A.M.** (1998). Meiotic Recombination in *C. elegans* Initiates by a Conserved Mechanism and Is Dispensable for Homologous Chromosome Synapsis. *Cell* **94**: 387–398.
- Dirks, R. et al.** (2009). Reverse breeding: a novel breeding approach based on engineered meiosis. *Plant Biotechnol J* **7**: 837–845.

-
- Dissmeyer, N., Nowack, M.K., Pusch, S., Stals, H., Inzé, D., Grini, P.E., and Schnittger, A.** (2007). T-Loop Phosphorylation of Arabidopsis CDKA;1 Is Required for Its Function and Can Be Partially Substituted by an Aspartate Residue. *The Plant Cell* **19**: 972–985.
- Draeger, T. and Moore, G.** (2017). Short periods of high temperature during meiosis prevent normal meiotic progression and reduce grain number in hexaploid wheat (*Triticum aestivum* L.). *Theor Appl Genet* **130**: 1785–1800.
- Echlin, P.** (1971). The Role of the Tapetum During Microsporogenesis of Angiosperms. In *Pollen*, J. Heslop-harrison, ed (Butterworth-Heinemann), pp. 41–61.
- Ekberg, I. and Eriksson, G.** (1965). Demonstration of meiosis and pollen mitosis by photomicrographs and the distribution of meiotic stages in barley spikes. *Hereditas* **53**: 127–136.
- Enguita-Marruedo, A., Cappellen, W.A.V., Hoogerbrugge, J.W., Carofoglio, F., Wassenaar, E., Slotman, J.A., Houtsmuller, A., and Baarends, W.M.** (2018). Live cell analyses of synaptonemal complex dynamics and chromosome movements in cultured mouse testis tubules and embryonic ovaries. *Chromosoma*: 1–19.
- d’Erfurth, I., Cromer, L., Jolivet, S., Girard, C., Horlow, C., Sun, Y., To, J.P.C., Berchowitz, L.E., Copenhaver, G.P., and Mercier, R.** (2010). The CYCLIN-A CYCA1;2/TAM Is Required for the Meiosis I to Meiosis II Transition and Cooperates with OSD1 for the Prophase to First Meiotic Division Transition. *PLOS Genetics* **6**: e1000989.
- d’Erfurth, I., Jolivet, S., Froger, N., Catrice, O., Novatchkova, M., and Mercier, R.** (2009). Turning Meiosis into Mitosis. *PLOS Biology* **7**: e1000124.
- Finch, R.A. and Bennett, M.D.** (1972). The Duration of Meiosis in Diploid and Autotetraploid Barley. *Can. J. Genet. Cytol.* **14**: 507–515.

- Gavet, O. and Pines, J.** (2010). Progressive Activation of CyclinB1-Cdk1 Coordinates Entry to Mitosis. *Developmental Cell* **18**: 533–543.
- Gigant, E., Stefanutti, M., Laband, K., Gluszek-Kustusz, A., Edwards, F., Lacroix, B., Maton, G., Canman, J.C., Welburn, J.P.I., and Dumont, J.** (2017). Inhibition of ectopic microtubule assembly by the kinesin-13 KLP-7 prevents chromosome segregation and cytokinesis defects in oocytes. *Development* **144**: 1674–1686.
- Golubovskaya, I.N., Harper, L.C., Pawlowski, W.P., Schichnes, D., and Cande, W.Z.** (2002). The *pam1* Gene Is Required for Meiotic Bouquet Formation and Efficient Homologous Synapsis in Maize (*Zea mays* L.). *Genetics* **162**: 1979–1993.
- Grandont, L., Jenczewski, E., and Lloyd, A.** (2013). Meiosis and Its Deviations in Polyploid Plants. *CGR* **140**: 171–184.
- Gratzner, H.G.** (1982). Monoclonal antibody to 5-bromo- and 5-iododeoxyuridine: A new reagent for detection of DNA replication. *Science* **218**: 474–475.
- Grelon, M.** (2001). *AtSPO11-1* is necessary for efficient meiotic recombination in plants. *The EMBO Journal* **20**: 589–600.
- Gruel, J., Landrein, B., Tarr, P., Schuster, C., Refahi, Y., Sampathkumar, A., Hamant, O., Meyerowitz, E.M., and Jönsson, H.** (2016). An epidermis-driven mechanism positions and scales stem cell niches in plants. *Science Advances* **2**: e1500989.
- Hamant, O., Das, P., and Burian, A.** (2014). Time-Lapse Imaging of Developing Meristems Using Confocal Laser Scanning Microscope. In *Plant Cell Morphogenesis, Methods in Molecular Biology*. (Humana Press, Totowa, NJ), pp. 111–119.
- Hamant, O., Ma, H., and Cande, W.Z.** (2006). Genetics of Meiotic Prophase I in Plants. *Annual Review of Plant Biology* **57**: 267–302.

-
- Hand, M.L. and Koltunow, A.M.G.** (2014). The Genetic Control of Apomixis: Asexual Seed Formation. *Genetics* **197**: 441–450.
- Henderson, K.A. and Keeney, S.** (2004). Tying synaptonemal complex initiation to the formation and programmed repair of DNA double-strand breaks. *PNAS* **101**: 4519–4524.
- Heslop-Harrison, J.** (1966). Cytoplasmic Connexions between Angiosperm Meicytes. *Ann Bot* **30**: 221–222.
- Higgins, D.M., Nannas, N.J., and Dawe, R.K.** (2016). The Maize Divergent spindle-1 (dv1) Gene Encodes a Kinesin-14A Motor Protein Required for Meiotic Spindle Pole Organization. *Front. Plant Sci.* **7**.
- Higgins, J.D., Armstrong, S.J., Franklin, F.C.H., and Jones, G.H.** (2004). The Arabidopsis MutS homolog AtMSH4 functions at an early step in recombination: evidence for two classes of recombination in Arabidopsis. *Genes Dev.* **18**: 2557–2570.
- Higgins, J.D., Perry, R.M., Barakate, A., Ramsay, L., Waugh, R., Halpin, C., Armstrong, S.J., and Franklin, F.C.H.** (2012). Spatiotemporal Asymmetry of the Meiotic Program Underlies the Predominantly Distal Distribution of Meiotic Crossovers in Barley. *The Plant Cell* **24**: 4096–4109.
- Higgins, J.D., Wright, K.M., Bomblies, K., and Franklin, C.** (2014). Cytological techniques to analyze meiosis in *Arabidopsis arenosa* for investigating adaptation to polyploidy. *Front. Plant Sci* **4**: 546.
- Holubcová, Z., Howard, G., and Schuh, M.** (2013). Vesicles modulate an actin network for asymmetric spindle positioning. *Nature Cell Biology* **15**: 937.
- Hurel, A., Phillips, D., Vrielynck, N., Mézard, C., Grelon, M., and Christophorou, N.** (2018). A cytological approach to studying meiotic recombination and chromosome dynamics in *Arabidopsis thaliana* male meicytes in three dimensions. *The Plant Journal* **95**: 385–396.

- Ingouff, M., Selles, B., Michaud, C., Vu, T.M., Berger, F., Schorn, A.J., Autran, D., Durme, M.V., Nowack, M.K., Martienssen, R.A., and Grimanelli, D.** (2017). Live-cell analysis of DNA methylation during sexual reproduction in *Arabidopsis* reveals context and sex-specific dynamics controlled by noncanonical RdDM. *Genes Dev.* **31**: 72–83.
- Ishida, T., Kaneko, Y., Iwano, M., and Hashimoto, T.** (2007). Helical microtubule arrays in a collection of twisting tubulin mutants of *Arabidopsis thaliana*. *Proc Natl Acad Sci U S A* **104**: 8544–8549.
- Ito, M. and Stern, H.** (1967). Studies of meiosis in vitro: I. In vitro culture of meiotic cells. *Developmental Biology* **16**: 36–53.
- Iwata, E., Ikeda, S., Matsunaga, S., Kurata, M., Yoshioka, Y., Criqui, M.-C., Genschik, P., and Ito, M.** (2011). GIGAS CELL1, a Novel Negative Regulator of the Anaphase-Promoting Complex/Cyclosome, Is Required for Proper Mitotic Progression and Cell Fate Determination in *Arabidopsis*. *The Plant Cell* **23**: 4382–4393.
- Izhar, S. and Frankel, R.** (1973). Duration of Meiosis in *Petunia* Anthers in Vivo and in Floral Bud Culture1. *Acta Botanica Neerlandica* **22**: 14–22.
- Jackson, N., Sanchez-Moran, E., Buckling, E., Armstrong, S.J., Jones, G.H., and Franklin, F.C.H.** (2006). Reduced meiotic crossovers and delayed prophase I progression in *AtMLH3*-deficient *Arabidopsis*. *The EMBO Journal* **25**: 1315–1323.
- Jakoby, M. and Schnittger, A.** (2004). Cell cycle and differentiation. *Current Opinion in Plant Biology* **7**: 661–669.
- Jenczewski, E. and Alix, K.** (2004). From Diploids to Allopolyploids: The Emergence of Efficient Pairing Control Genes in Plants. *Critical Reviews in Plant Sciences* **23**: 21–45.

-
- Jiao, Y., Li, J., Tang, H., and Paterson, A.H.** (2014). Integrated Syntenic and Phylogenomic Analyses Reveal an Ancient Genome Duplication in Monocots. *The Plant Cell* **26**: 2792–2802.
- Kainmueller, D., Jug, F., Rother, C., and Myers, G.** (2014). Active Graph Matching for Automatic Joint Segmentation and Annotation of *C. elegans*. In *Medical Image Computing and Computer-Assisted Intervention – MICCAI 2014*, P. Golland, N. Hata, C. Barillot, J. Hornegger, and R. Howe, eds (Springer International Publishing: Cham), pp. 81–88.
- Katis, V.L., Lipp, J.J., Imre, R., Bogdanova, A., Okaz, E., Habermann, B., Mechtler, K., Nasmyth, K., and Zachariae, W.** (2010). Rec8 Phosphorylation by Casein Kinase 1 and Cdc7-Dbf4 Kinase Regulates Cohesin Cleavage by Separase during Meiosis. *Dev Cell* **18**: 397–409.
- Kitajima, T.S., Ohsugi, M., and Ellenberg, J.** (2011). Complete Kinetochore Tracking Reveals Error-Prone Homologous Chromosome Biorientation in Mammalian Oocytes. *Cell* **146**: 568–581.
- Klutstein, M., Fennell, A., Fernández-Álvarez, A., and Cooper, J.P.** (2015). The telomere bouquet regulates meiotic centromere assembly. *Nat Cell Biol* **17**: 458–469.
- Komaki, S. and Schnittger, A.** (2017). The Spindle Assembly Checkpoint in Arabidopsis Is Rapidly Shut Off during Severe Stress. *Developmental Cell* **43**: 172-185.e5.
- Komis, G., Novák, D., Ovečka, M., Šamajová, O., and Šamaj, J.** (2018). Advances in Imaging Plant Cell Dynamics. *Plant Physiology* **176**: 80–93.
- Lambing, C., Franklin, F.C.H., and Wang, C.-J.R.** (2017). Understanding and Manipulating Meiotic Recombination in Plants[OPEN]. *Plant Physiol* **173**: 1530–1542.

- Lambing, C. and Heckmann, S.** (2018). Tackling Plant Meiosis: From Model Research to Crop Improvement., Tackling Plant Meiosis: From Model Research to Crop Improvement. *Front Plant Sci* **9**: 829–829.
- Lee, C.-Y., Conrad, M.N., and Dresser, M.E.** (2012). Meiotic Chromosome Pairing Is Promoted by Telomere-Led Chromosome Movements Independent of Bouquet Formation. *PLOS Genetics* **8**: e1002730.
- Lee, C.-Y., Horn, H.F., Stewart, C.L., Burke, B., Bolcun-Filas, E., Schimenti, J.C., Dresser, M.E., and Pezza, R.J.** (2015). Mechanism and regulation of rapid telomere prophase movements in mouse meiotic chromosomes. *Cell Rep* **11**: 551–563.
- Leflon, M., Grandont, L., Eber, F., Huteau, V., Coriton, O., Chelysheva, L., Jenczewski, E., and Chèvre, A.-M.** (2010). Crossovers Get a Boost in Brassica Allotriploid and Allotetraploid Hybrids[W]. *Plant Cell* **22**: 2253–2264.
- Leyk, S.** (2016). CRISPR/Cas9 vermittelte Mutation des meiotischen Gens REC8 in *Arabidopsis thaliana* und Generierung eines REC8-mNeon Konstrukts.
- Lindgren, D., Eriksson, G., and Ekberg, I.** (1969). The Relative Duration of the Meiotic Stages in Pollen Mother Cells of Barley. *Hereditas* **63**: 205–212.
- Liu, T.-L. et al.** (2018). Observing the cell in its native state: Imaging subcellular dynamics in multicellular organisms. *Science* **360**: eaaq1392.
- Llères, D., Bailly, A.P., Perrin, A., Norman, D.G., Xirodimas, D.P., and Feil, R.** (2017). Quantitative FLIM-FRET Microscopy to Monitor Nanoscale Chromatin Compaction In Vivo Reveals Structural Roles of Condensin Complexes. *Cell Reports* **18**: 1791–1803.
- Loidl, J.** (2016). Conservation and Variability of Meiosis Across the Eukaryotes. *Annual Review of Genetics* **50**: 293–316.
- Luo, Q., Li, Y., Shen, Y., and Cheng, Z.** (2014). Ten Years of Gene Discovery for Meiotic Event Control in Rice. *Journal of Genetics and Genomics* **41**: 125–137.

-
- Ma, H.** (2006). A Molecular Portrait of Arabidopsis Meiosis. *Arabidopsis Book* **4**.
- Magnard, J.-L., Yang, M., Chen, Y.-C.S., Leary, M., and McCormick, S.** (2001). The Arabidopsis Gene Tardy Asynchronous Meiosis Is Required for the Normal Pace and Synchrony of Cell Division during Male Meiosis. *Plant Physiol* **127**: 1157–1166.
- Martinez-Garcia, M., Schubert, V., Osman, K., Darbyshire, A., Sanchez-Moran, E., and Franklin, F.C.H.** (2018). TOPll and chromosome movement help remove interlocks between entangled chromosomes during meiosis. *J Cell Biol*: jcb.201803019.
- Martinez-Perez, E., Shaw, P.J., and Moore, G.** (2000). Polyploidy Induces Centromere Association. *The Journal of Cell Biology* **148**: 233–238.
- Mastop, M., Bindels, D.S., Shaner, N.C., Postma, M., Gadella, T.W.J., and Goedhart, J.** (2017). Characterization of a spectrally diverse set of fluorescent proteins as FRET acceptors for mTurquoise2. *Scientific Reports* **7**: 11999.
- Matuszewski, D.J., Wählby, C., Krona, C., Nelander, S., and Sintorn, I.-M.** (2018). Image-Based Detection of Patient-Specific Drug-Induced Cell-Cycle Effects in Glioblastoma. *SLAS DISCOVERY: Advancing Life Sciences R&D* **23**: 1030–1039.
- McKim, K.S., Green-Marroquin, B.L., Sekelsky, J.J., Chin, G., Steinberg, C., Khodosh, R., and Hawley, R.S.** (1998). Meiotic Synapsis in the Absence of Recombination. *Science* **279**: 876–878.
- Meinke, D. and Koornneef, M.** (1997). Community standards for Arabidopsis gene. *The Plant Journal* **2**: 247–253.
- Mercier, R., Mézard, C., Jenczewski, E., Macaisne, N., and Grelon, M.** (2015). The Molecular Biology of Meiosis in Plants. *Annual Review of Plant Biology* **66**: 297–327.
- Mogessie, B. and Schuh, M.** (2017). Actin protects mammalian eggs against chromosome segregation errors. *Science* **357**: eaal1647.

- NAKAGAWA, T. et al.** (2007). Improved Gateway Binary Vectors: High-Performance Vectors for Creation of Fusion Constructs in Transgenic Analysis of Plants. *Bioscience, Biotechnology, and Biochemistry* **71**: 2095–2100.
- Nannas, N.J., Higgins, D.M., and Dawe, R.K.** (2016). Anaphase asymmetry and dynamic repositioning of the division plane during maize meiosis. *J Cell Sci* **129**: 4014–4024.
- Nasmyth, K. and Haering, C.H.** (2009). Cohesin: Its Roles and Mechanisms. *Annual Review of Genetics* **43**: 525–558.
- Ovečka, M., Wangenheim, D. von, Tomančák, P., Šamajová, O., Komis, G., and Šamaj, J.** (2018). Multiscale imaging of plant development by light-sheet fluorescence microscopy. *Nature Plants* **4**: 639.
- Pacini, E. and Cresti, M.** (1978). Ultrastructural characteristics of the tapetum and microspore mother cells in *Lycopersicon peruvianum* during meiotic prophase. *Bulletin de la Société Botanique de France. Actualités Botaniques* **125**: 121–128.
- Padmanabhan, M. and Dinesh-Kumar, S.P.** (2009). Virus-Induced Gene Silencing as a Tool for Delivery of dsRNA into Plants. *Cold Spring Harb Protoc* **2009**: pdb.prot5139.
- Pecinka, A., Fang, W., Rehmsmeier, M., Levy, A.A., and Mittelsten Scheid, O.** (2011). Polyploidization increases meiotic recombination frequency in *Arabidopsis*. *BMC Biology* **9**: 24.
- Peer, Y.V. de, Mizrachi, E., and Marchal, K.** (2017). The evolutionary significance of polyploidy. *Nature Reviews Genetics* **18**: 411.
- Peirson, B.N., Bowling, S.E., and Makaroff, C.A.** (1997). A defect in synapsis causes male sterility in a T-DNA-tagged *Arabidopsis thaliana* mutant. *The Plant Journal* **11**: 659–669.

-
- Pelé, A., Rousseau-Gueutin, M., and Chèvre, A.-M.** (2018). Speciation Success of Polyploid Plants Closely Relates to the Regulation of Meiotic Recombination. *Front. Plant Sci.* **9**.
- Peters, J.-M., Tedeschi, A., and Schmitz, J.** (2008). The cohesin complex and its roles in chromosome biology. *Genes Dev.* **22**: 3089–3114.
- Peterson, R., Slovin, J.P., and Chen, C.** (2010). A simplified method for differential staining of aborted and non-aborted pollen grains. *International Journal of Plant Biology* **1**: 13.
- Ramsey, J. and Schemske, D.W.** (2002). Neopolyploidy in Flowering Plants. *Annual Review of Ecology and Systematics* **33**: 589–639.
- Rog, O. and Dernburg, A.F.** (2015). Direct Visualization Reveals Kinetics of Meiotic Chromosome Synapsis. *Cell Reports* **10**: 1639–1645.
- Ross, K.J., Fransz, P., and Jones, G.H.** (1996). A light microscopic atlas of meiosis in *Arabidopsis thaliana*. *Chromosome Res* **4**: 507–516.
- Salic, A. and Mitchison, T.J.** (2008). A chemical method for fast and sensitive detection of DNA synthesis in vivo. *PNAS* **105**: 2415–2420.
- Sanchez-Moran, E., Santos, J.-L., Jones, G.H., and Franklin, F.C.H.** (2007). ASY1 mediates AtDMC1-dependent interhomolog recombination during meiosis in *Arabidopsis*. *Genes Dev.* **21**: 2220–2233.
- Sattler, M.C., Carvalho, C.R., and Clarindo, W.R.** (2016). The polyploidy and its key role in plant breeding. *Planta* **243**: 281–296.
- Schmidt, A., Schmid, M.W., and Grossniklaus, U.** (2015). Plant germline formation: common concepts and developmental flexibility in sexual and asexual reproduction. *Development* **142**: 229–241.
- Schubert, V., Weißleder, A., Ali, H., Fuchs, J., Lermontova, I., Meister, A., and Schubert, I.** (2009). Cohesin gene defects may impair sister chromatid

- alignment and genome stability in *Arabidopsis thaliana*. *Chromosoma* **118**: 591–605.
- Schuh, M. and Ellenberg, J.** (2007). Self-Organization of MTOCs Replaces Centrosome Function during Acentrosomal Spindle Assembly in Live Mouse Oocytes. *Cell* **130**: 484–498.
- Shaner, N.C., Lambert, G.G., Chamma, A., Ni, Y., Cranfill, P.J., Baird, M.A., Sell, B.R., Allen, J.R., Day, R.N., Israelsson, M., Davidson, M.W., and Wang, J.** (2013). A bright monomeric green fluorescent protein derived from *Branchiostoma lanceolatum*. *Nature Methods* **10**: 407–409.
- Sheehan, M.J. and Pawlowski, W.P.** (2009). Live imaging of rapid chromosome movements in meiotic prophase I in maize. *PNAS* **106**: 20989–20994.
- Shibuya, H., Morimoto, A., and Watanabe, Y.** (2014). The Dissection of Meiotic Chromosome Movement in Mice Using an In Vivo Electroporation Technique. *PLoS Genet* **10**.
- Smyth, D.R., Bowman, J.L., and Meyerowitz, E.M.** (1990). Early flower development in *Arabidopsis*. *Plant Cell* **2**: 755–767.
- Soltis, D.E., Soltis, P.S., Schemske, D.W., Hancock, J.F., Thompson, J.N., Husband, B.C., and Judd, W.S.** (2007). Autopolyploidy in angiosperms: have we grossly underestimated the number of species?
- Somerville, C. and Koornneef, M.** (2002). A fortunate choice: the history of *Arabidopsis* as a model plant. *Nature Reviews Genetics* **3**: 883–889.
- Stefani, A. and Colonna, N.** (1996). The Influence of Temperature on Meiosis and Microspores Development in *Dasypyrum villosum* (L.) P. Candargy. *CYTOLOGIA* **61**: 277–283.
- Stronghill, P.E., Azimi, W., and Hasenkampf, C.A.** (2014). A novel method to follow meiotic progression in *Arabidopsis* using confocal microscopy and 5-ethynyl-2'-deoxyuridine labeling. *Plant Methods* **10**: 33.

-
- Tomita, K. and Cooper, J.P.** (2007). The Telomere Bouquet Controls the Meiotic Spindle. *Cell* **130**: 113–126.
- Ünal, M., Vardar, F., and Aytürk, Ö.** (2013). Callose in Plant Sexual Reproduction. *Current Progress in Biological Research*.
- Wang, Y. and Copenhaver, G.P.** (2018). Meiotic Recombination: Mixing It Up in Plants. *Annual Review of Plant Biology* **69**: 577–609.
- Wang, Y., Jha, A.K., Chen, R., Doonan, J.H., and Yang, M.** (2010). Polyploidy-associated genomic instability in *Arabidopsis thaliana*. *Genesis* **48**: 254–263.
- Wang, Y., Magnard, J.-L., McCormick, S., and Yang, M.** (2004a). Progression through Meiosis I and Meiosis II in *Arabidopsis* Anthers Is Regulated by an A-Type Cyclin Predominately Expressed in Prophase I. *Plant Physiol* **136**: 4127–4135.
- Wang, Y., Wu, H., Liang, G., and Yang, M.** (2004b). Defects in nucleolar migration and synapsis in male prophase I in the *ask1-1* mutant of *Arabidopsis*. *Sex Plant Reprod* **16**: 273–282.
- Wijnker, E. and Schnittger, A.** (2013). Control of the meiotic cell division program in plants. *Plant Reprod* **26**: 143–158.
- Wilson, J.Y.** (1959). Duration of meiosis in relation to temperature. *Heredity* **13**: 263–267.
- Wynne, D.J., Rog, O., Carlton, P.M., and Dernburg, A.F.** (2012). Dynein-dependent processive chromosome motions promote homologous pairing in *C. elegans* meiosis. *J Cell Biol* **196**: 47–64.
- Yang, J., Tian, L., Sun, M.-X., Huang, X.-Y., Zhu, J., Guan, Y.-F., Jia, Q.-S., and Yang, Z.-N.** (2013). AUXIN RESPONSE FACTOR17 Is Essential for Pollen Wall Pattern Formation in *Arabidopsis*. *Plant Physiology* **162**: 720–731.
- Yang, X., Timofejeva, L., Ma, H., and Makaroff, C.A.** (2006). The *Arabidopsis* SKP1 homolog ASK1 controls meiotic chromosome remodeling and release of

- chromatin from the nuclear membrane and nucleolus. *Journal of Cell Science* **119**: 3754–3763.
- Yant, L., Hollister, J.D., Wright, K.M., Arnold, B.J., Higgins, J.D., Franklin, F.C.H., and Bomblies, K.** (2013). Meiotic Adaptation to Genome Duplication in *Arabidopsis arenosa*. *Current Biology* **23**: 2151–2156.
- Yao, X., Tian, L., Yang, J., Zhao, Y.-N., Zhu, Y.-X., Dai, X., Zhao, Y., and Yang, Z.-N.** (2018). Auxin production in diploid microsporocytes is necessary and sufficient for early stages of pollen development. *PLOS Genetics* **14**: e1007397.
- Yu, H., Wang, M., Tang, D., Wang, K., Chen, F., Gong, Z., Gu, M., and Cheng, Z.** (2010). OsSPO11-1 is essential for both homologous chromosome pairing and crossover formation in rice. *Chromosoma* **119**: 625–636.
- Yu, H.-G., Hiatt, E.N., Chan, A., Sweeney, M., and Dawe, R.K.** (1997). Neocentromere-mediated Chromosome Movement in Maize. *J Cell Biol* **139**: 831–840.
- Yu, J. et al.** (2005). The Genomes of *Oryza sativa*: A History of Duplications. *PLOS Biology* **3**: e38.
- Yu, Z., Haage, K., Streit, V.E., Gierl, A., and Ruiz, R.A.T.** (2009). A large number of tetraploid *Arabidopsis thaliana* lines, generated by a rapid strategy, reveal high stability of neo-tetraploids during consecutive generations. *Theor Appl Genet* **118**: 1107–1119.
- Yuan, G.** (2018). Control of centromeric cohesion during meiosis in *Arabidopsis*.
- Yuan, G., Ahootapeh, B.H., Komaki, S., Schnittger, A., Lillo, C., Storme, N.D., and Geelen, D.** (2018). PROTEIN PHOSPHATASE 2A B'α and β Maintain Centromeric Sister Chromatid Cohesion during Meiosis in *Arabidopsis*. *Plant Physiology* **178**: 317–328.

-
- Zamariola, L., Storme, N.D., Tiang, C., Armstrong, S.J., Franklin, F.C.H., and Geelen, D.** (2013). SGO1 but not SGO2 is required for maintenance of centromere cohesion in *Arabidopsis thaliana* meiosis. *Plant Reprod* **26**: 197–208.
- Zenzes, M.T., Bielecki, R., Casper, R.F., and Leibo, S.P.** (2001). Effects of chilling to 0°C on the morphology of meiotic spindles in human metaphase II oocytes. *Fertility and Sterility* **75**: 769–777.
- Zhang, C., Shen, Y., Tang, D., Shi, W., Zhang, D., Du, G., Zhou, Y., Liang, G., Li, Y., and Cheng, Z.** (2018). The zinc finger protein DCM1 is required for male meiotic cytokinesis by preserving callose in rice. *PLOS Genetics* **14**: e1007769.
- Zhao, X. et al.** (2017). RETINOBLASTOMA RELATED1 mediates germline entry in *Arabidopsis*. *Science* **356**: eaaf6532.
- Zhao, X., Harashima, H., Dissmeyer, N., Pusch, S., Weimer, A.K., Bramsiepe, J., Bouyer, D., Rademacher, S., Nowack, M.K., Novak, B., Sprunck, S., and Schnittger, A.** (2012). A General G1/S-Phase Cell-Cycle Control Module in the Flowering Plant *Arabidopsis thaliana*. *PLoS Genet* **8**: e1002847.
- Zhou, A. and Pawlowski, W.P.** (2014). Regulation of meiotic gene expression in plants. *Front Plant Sci* **5**.
- Zielinski, M.L. and Mittelsten Scheid, O.** (2012). Meiosis in polyploid plants. In *Polyploid and genome evolution* (Springer: Berlin, Heidelberg), pp. 33–55.

Annex 1: Observed cellular states

STATES OF CELL FEATURES					Count	Frequency in %	Neighbor. score	Landmark
Cell shape	Nucleus Position	Nucleolus Position	Rec8/ Chromatin	Mt Array				
1	1	1	1	1	844	7.82714	-0.17440	START
1	1	1	2	1	9	0.08346	-0.54879	
1	1	2	2	1	2280	21.14439	3.37785	A1
1	1	2	2	2	162	1.50236	-0.05031	
1	1	2	3	1	32	0.29676	-0.33961	
1	1	2	3	2	20	0.18548	-0.34049	
1	1	3	2	1	65	0.60280	-0.22316	
1	1	3	2	2	34	0.31531	-0.25820	
1	1	3	3	1	184	1.70639	-0.04491	
1	1	3	3	2	232	2.15153	1.12512	A2
1	1	3	3	3	1	0.00927	-0.43239	
1	2	2	2	1	6	0.05564	-0.30950	
1	2	2	2	2	3	0.02782	-0.30187	
1	2	3	2	1	7	0.06492	-0.30881	
1	2	3	2	2	13	0.12056	-0.41522	
1	2	3	2	3	1	0.00927	-0.34990	
1	2	3	3	1	17	0.15766	-0.49114	
1	2	3	3	2	48	0.44515	-0.26616	
1	2	3	3	3	36	0.33386	-0.51894	
1	2	3	3	4	1	0.00927	-0.54020	
2	1	2	2	1	1	0.00927	-0.31383	
2	1	2	2	2	2	0.01855	-0.30747	
2	1	3	2	1	1	0.00927	-0.30969	
2	1	3	2	2	9	0.08346	-0.42838	
2	1	3	3	1	1	0.00927	-0.56276	
2	1	3	3	2	4	0.03710	-0.44938	
2	2	2	2	2	1	0.00927	-0.39582	
2	2	2	3	2	5	0.04637	-0.42461	
2	2	3	2	1	3	0.02782	-0.33986	
2	2	3	2	2	14	0.12983	-0.31077	
2	2	3	2	3	14	0.12983	-0.43030	
2	2	3	3	1	28	0.25967	-0.25540	

Annex 1: Observed cellular states

STATES OF CELL FEATURES					Count	Frequency in %	Neighbor. score	Landmark
Cell shape	Nucleus Position	Nucleolus Position	Rec8/ Chromatin	Mt Array				
2	2	3	3	2	497	4.60911	1.31687	A3
2	2	3	3	3	1069	9.91375	3.24299	A4
2	2	3	3	4	64	0.59353	-0.58958	
2	2	3	4	2	17	0.15766	-0.60222	
2	2	3	4	3	510	4.72967	0.39915	
2	2	3	4	4	327	3.03255	0.11708	
3	2	3	3	3	21	0.19475	-0.78509	
3	2	3	3	4	51	0.47297	-0.54994	
3	2	3	4	3	6	0.05564	-0.73009	
3	2	3	4	4	953	8.83799	3.04585	A5
3	2	3	4	5	20	0.18548	-0.46757	
3	2	3	5	4	39	0.36168	-0.35569	
3	2	3	5	5	12	0.1112863	-0.395371	
3	2	4	5	4	10	0.0927386	-0.4094074	
3	2	4	5	5	5	0.0463693	-0.71537	
3	2	4	6	5	1	0.0092739	-0.5929813	
3	3	3	4	4	48	0.4451451	-0.3309423	
3	3	3	4	5	128	1.1870537	0.0313036	
3	3	3	5	4	1	0.0092739	-0.4912063	
3	3	3	5	5	127	1.1777798	1.328134	A6
3	3	3	5	6	1	0.0092739	-0.8595962	
3	3	3	6	5	23	0.2132987	-0.443621	
3	3	4	4	5	8	0.0741909	-0.9155878	
3	3	4	5	5	139	1.2890661	0.439639	
3	3	4	5	6	2	0.0185477	-0.8609494	
3	3	4	6	5	196	1.817676	0.6060751	
3	3	4	6	6	26	0.2411203	-0.4364902	
3	4	4	7	7	1	0.0092739	-0.548784	
3	4	4	7	8	6	0.0556431	-0.2609694	
3	4	4	8	9	1	0.0092739	-0.7267524	
3	4	4	8	10	2	0.0185477	-0.5691419	
3	4	4	8	11	1	0.0092739	-0.4254582	

Annex 1: Observed cellular states

STATES OF CELL FEATURES					Count	Frequency in %	Neighbor. score	Landmark
Cell shape	Nucleus Position	Nucleolus Position	Rec8/ Chromatin	Mt Array				
3	5	4	8	10	1	0.0092739	-0.4030031	
3	5	4	8	11	1	0.0092739	-0.4149197	
3	6	4	8	13	3	0.0278216	-0.4461842	
4	3	3	4	4	6	0.0556431	-0.5027017	
4	3	3	4	5	35	0.324585	-0.3621489	
4	3	3	5	5	82	0.7604563	0.0257596	
4	3	3	5	6	1	0.0092739	-0.810993	
4	3	3	6	5	6	0.0556431	-0.6854284	
4	3	3	6	6	9	0.0834647	-0.4090456	
4	3	3	6	7	1	0.0092739	-0.4955057	
4	3	4	5	5	68	0.6306223	-0.2313493	
4	3	4	6	5	539	4.9986089	2.7591102	A7
4	3	4	6	6	115	1.0664936	0.2150927	
4	3	4	6	7	10	0.0927386	-0.3016266	
4	3	4	7	7	4	0.0370954	-0.5739789	
4	4	4	6	8	2	0.0185477	-0.5099894	
4	4	4	7	7	6	0.0556431	-0.3319022	
4	4	4	7	8	75	0.6955393	2.4446814	A8
4	4	4	7	9	1	0.0092739	-0.5859199	
4	4	4	8	9	13	0.1205601	-0.1458061	
4	4	4	8	10	18	0.1669294	-0.1164003	
4	4	4	8	11	5	0.0463693	-0.4135118	
4	5	4	8	10	8	0.0741909	-0.3092366	
4	5	4	8	11	203	1.882593	2.812313	A9
4	5	4	8	12	31	0.2874896	-0.2456889	
4	5	4	8	13	3	0.0278216	-0.4703186	
4	6	4	8	11	4	0.0370954	-0.4719901	
4	6	4	8	12	3	0.0278216	-0.5521145	
4	6	4	8	13	158	1.4652694	2.3926466	A10
4	6	4	8	14	11	0.1020124	-0.4474814	
4	7	4	8	13	7	0.064917	-0.4635346	
4	7	4	8	14	73	0.6769916	-0.3495561	

Annex 1: Observed cellular states

STATES OF CELL FEATURES					Count	Frequency in %	Neighbor. score	Landmark
Cell shape	Nucleus Position	Nucleolus Position	Rec8/ Chromatin	Mt Array				
5	6	4	8	13	1	0.0092739	-0.4792641	
5	7	4	8	14	724	6.7142725	2.4389252	A11
5	7	4	8	15	46	0.4265974	-0.4884569	
6	7	4	8	14	1	0.0092739	-0.6556153	
6	7	4	8	15	119	1.103589	-0.3063485	END

Annex 3 Output of the single cell analysis for landmark duration in KINGBIRD_2X

sample	Landmark												
	0	1	2	3	4	5	6	7	8	9	10	11	12
FLOWER01_2X_SC-cell2									40	45			
FLOWER01_2X_SC-cell5									45	45			
FLOWER01_2X_SC-cell6									45				
FLOWER02_2X_SC-cell1										45	40	120	
FLOWER02_2X_SC-cell3											40	135	
FLOWER03_2x_L_SC-cell10							160	230	50	70	30		
FLOWER03_2x_L_SC-cell11					110								
FLOWER03_2x_L_SC-cell12					30	330					30		
FLOWER03_2x_L_SC-cell14					110								
FLOWER03_2x_L_SC-cell15					200	150	100			60	40		
FLOWER03_2x_L_SC-cell2					160								
FLOWER03_2x_L_SC-cell3					110								
FLOWER03_2x_L_SC-cell4										60	40		
FLOWER03_2x_L_SC-cell5					110								
FLOWER03_2x_L_SC-cell6					110								
FLOWER03_2x_L_SC-cell7							110	190	40				
FLOWER03_2x_L_SC-cell8							120	190	40	70	30		
FLOWER03_2x_L_SC-cell9							130	170					
FLOWER03_2x_R_SC-cell1							70					30	
FLOWER03_2x_R_SC-cell10										50	50		
FLOWER03_2x_R_SC-cell2							80	270	40	50	30		
FLOWER03_2x_R_SC-cell3							240				40		
FLOWER03_2x_R_SC-cell4							200	240			30		
FLOWER03_2x_R_SC-cell5							190	260					
FLOWER03_2x_R_SC-cell6							210				30		
FLOWER03_2x_R_SC-cell7				100	90								
FLOWER03_2x_R_SC-cell8							230			60	40		
FLOWER03_2x_R_SC-cell9											40		
FLOWER12_2X_R_SC-cell14		725			220								
FLOWER12_2X_R_SC-cell15					180								
FLOWER12_2X_R_SC-cell16					200								
FLOWER12_2X_R_SC-cell19					170								
FLOWER12_2X_R_SC-cell20					210								
FLOWER12_2X_R_SC-cell3					280								
FLOWER12_2X_R_SC-cell7		675											
FLOWER13b_2X_U_SC-cell1					107								
FLOWER13b_2X_U_SC-cell10					107								
FLOWER13b_2X_U_SC-cell11					167								
FLOWER13b_2X_U_SC-cell2					137								
FLOWER13b_2X_U_SC-cell4					157								
FLOWER13b_2X_U_SC-cell5				40	117								
FLOWER13b_2X_U_SC-cell8					167								
FLOWER14_2X_L_SC-cell1				190	120								
FLOWER14_2X_L_SC-cell10				300	210								
FLOWER14_2X_L_SC-cell11				130	280								
FLOWER14_2X_L_SC-cell12			130	50	240								
FLOWER14_2X_L_SC-cell2				170	380								
FLOWER14_2X_L_SC-cell3					330								
FLOWER14_2X_L_SC-cell4			80	180	340								
FLOWER14_2X_L_SC-cell5			190	300									
FLOWER14_2X_L_SC-cell6			70	230									
FLOWER14_2X_L_SC-cell7			70	450									
FLOWER14_2X_L_SC-cell8			100	370									
FLOWER14_2X_L_SC-cell9			160	340									
FLOWER14_2X_U_SC-cell11			50	130	391								
FLOWER14_2X_U_SC-cell15				170									
FLOWER14_2X_U_SC-cell17			60	170	281								
FLOWER14_2X_U_SC-cell18			30	160	291								
FLOWER14_2X_U_SC-cell3			80	110									
FLOWER14_2X_U_SC-cell4		575	90	70	371								
FLOWER14_2X_U_SC-cell6			70	140	291								
FLOWER17_2X_L_SC-cell1			110	260									
FLOWER17_2X_L_SC-cell14			70	300									
FLOWER17_2X_L_SC-cell16			70	300									
FLOWER17_2X_L_SC-cell2				210									
FLOWER17_2X_R_SC-cell11			270										
FLOWER17_2X_R_SC-cell12				180									
FLOWER17_2X_R_SC-cell13			50										
FLOWER17_2X_R_SC-cell17							165						
FLOWER17_2X_R_SC-cell18							255						
FLOWER17_2X_R_SC-cell2			130	120									
FLOWER17_2X_R_SC-cell3			210	200			105						
FLOWER17_2X_R_SC-cell6				120			135						
FLOWER22_2X_R_SC-cell1							120						
FLOWER22_2X_R_SC-cell10								100					
FLOWER22_2X_R_SC-cell12							260						
FLOWER22_2X_R_SC-cell13								550.5	100				
FLOWER22_2X_R_SC-cell15									100				
FLOWER22_2X_R_SC-cell2									100				
FLOWER22_2X_R_SC-cell3									100				
FLOWER22_2X_R_SC-cell5							180	510.5	100				
FLOWER22_2X_R_SC-cell6									100				
FLOWER22_2X_R_SC-cell7									100				
FLOWER22_2X_R_SC-cell9									100				
FLOWER22_2x_L_SC-cell1						778							
FLOWER22_2x_L_SC-cell10							250						
FLOWER22_2x_L_SC-cell11							140						
FLOWER22_2x_L_SC-cell2						798							
FLOWER22_2x_L_SC-cell3							260						
FLOWER22_2x_L_SC-cell7						818							
FLOWER22_2x_L_SC-cell9							110						
FLOWER24_2X_R_SC-cell12									178				
FLOWER24_2X_R_SC-cell14									168				
FLOWER24_2X_R_SC-cell15									128				

Annex 3 Output of the single cell analysis for landmark duration in KINGBIRD_2X

sample	Landmark												
	0	1	2	3	4	5	6	7	8	9	10	11	12
FLOWER24_2X_R_SC-cell2								138					
FLOWER24_2X_R_SC-cell9								188					
FLOWER24_2x_L_SC-cell5								198					
FLOWER27_2X_SC-cell11												39	
FLOWER27_2X_SC-cell13										63		33	
FLOWER27_2X_SC-cell14												36	
FLOWER27_2X_SC-cell16										60		30	
FLOWER27_2X_SC-cell17										60		33	
FLOWER27_2X_SC-cell2												39	
FLOWER27_2X_SC-cell6												30	
FLOWER27_2X_SC-cell8												33	
FLOWER27_2X_SC-cell9												39	
flower29_2x_L_SC-cell-1								80					240
flower29_2x_L_SC-cell0												50	230
flower29_2x_L_SC-cell1		550	60	210	80	377	160						
flower29_2x_L_SC-cell10		470	120	120	140	257	320	150	60	50		50	
flower29_2x_L_SC-cell12		440	50	190	210	317	230	170	30	70		50	
flower29_2x_L_SC-cell14		420	110			317	270	150				40	
flower29_2x_L_SC-cell15		410	110	180			190	230				40	
flower29_2x_L_SC-cell17						367	300	50	30	70		40	
flower29_2x_L_SC-cell18		570	80	110	200	347	220	170	40	60		40	
flower29_2x_L_SC-cell19			180	50	190	387	160	190	30	70		40	
flower29_2x_L_SC-cell2		490	20	170	190	317						50	
flower29_2x_L_SC-cell20		550	120	80	160	357	200	190	30	70		40	
flower29_2x_L_SC-cell3		510	60	140	150	457	140						
flower29_2x_L_SC-cell4					170	297						40	
flower29_2x_L_SC-cell5					210	267							
flower29_2x_L_SC-cell6							360					50	
flower29_2x_L_SC-cell7						357	250	130	30	70		50	
flower29_2x_L_SC-cell8									30	70		50	
flower29_2x_L_SC-cell9						237	360	130	40	60		50	
flower29_2x_R_SC-cell1									40	40		60	
flower29_2x_R_SC-cell11		500											
flower29_2x_R_SC-cell13				190									
flower29_2x_R_SC-cell17		460	50	150									
flower29_2x_R_SC-cell18		430	70	110									
flower29_2x_R_SC-cell19		510	120	180									
flower29_2x_R_SC-cell2							180			40		60	
flower29_2x_R_SC-cell3		330	30	90									
flower29_2x_R_SC-cell4									40	40		60	
flower29_2x_R_SC-cell5									40	40		60	
flower29_2x_R_SC-cell7									40	40		60	
flower29_2x_R_SC-cell9									40	40		60	
AVERAGE		478.666667	93.4857143	177.113636	185.733333	376.85	188.578947	194.666667	55.7419355	54.3793103	41.3478261	147.2	//
ST.DEV //		151.906318	56.4172332	94.3105252	86.8102424	204.713478	79.6918496	113.192399	29.939904	14.4776029	10.7315058	93.4168079	//
COUNTS		0	18	35	44	45	20	38	27	31	29	46	5
													0

Annex 4 Output of the single cell analysis for landmark duration in KINGBIRD_4X

sample	Landmark												
	0	1	2	3	4	5	6	7	8	9	10	11	12
FLOWER01_4X_L_SC-cell12							372	450					
FLOWER01_4X_L_SC-cell13					150	634	486	300					
FLOWER01_4X_L_SC-cell14						568	442	380					
FLOWER01_4X_L_SC-cell15			120										
FLOWER01_4X_L_SC-cell16				170	250			430	100				
FLOWER01_4X_L_SC-cell17													
FLOWER01_4X_L_SC-cell18								230	80				
FLOWER01_4X_L_SC-cell3							230	350	150				
FLOWER01_4X_L_SC-cell4							382	370	150				
FLOWER01_4X_L_SC-cell5		70	140	290									
FLOWER01_4X_L_SC-cell6		78						410	150				
FLOWER01_4X_L_SC-cell7		80		210			370						
FLOWER01_4X_L_SC-cell8													
FLOWER01_4X_L_SC-cell9				120	240			430					
FLOWER01_4x_R_SC-cell11												80	
FLOWER01_4x_R_SC-cell12				220			320	330	100	120	70		
FLOWER01_4x_R_SC-cell13				120			310	340	110	120	70		
FLOWER01_4x_R_SC-cell14					220					130	90		
FLOWER01_4x_R_SC-cell15							302	300	100	130	70		
FLOWER01_4x_R_SC-cell16								360	90	130	90		
FLOWER01_4x_R_SC-cell18		30	100				250	350	90	140	80		
FLOWER01_4x_R_SC-cell4							153	479	110	110	80		
FLOWER01_4x_R_SC-cell9		60	70	470				453	110	120	90		
FLOWER03_4X_L_SC-cell1		120	168										
FLOWER03_4X_L_SC-cell10		96	180										
FLOWER03_4X_L_SC-cell11		48	228	156									
FLOWER03_4X_L_SC-cell12		72	156	156									
FLOWER03_4X_L_SC-cell18		132	204										
FLOWER03_4X_L_SC-cell19				180									
FLOWER03_4X_L_SC-cell3		48											
FLOWER03_4X_L_SC-cell4				156									
FLOWER03_4X_L_SC-cell5		72	204										
FLOWER03_4X_L_SC-cell8		96	240										
FLOWER03_4X_R_SC-cell10		120	96										
FLOWER03_4X_R_SC-cell13		48	192										
FLOWER03_4X_R_SC-cell15		84	264										
FLOWER03_4X_R_SC-cell18		60	228										
FLOWER03_4X_R_SC-cell3		48	168										
FLOWER03_4X_R_SC-cell4				168									
FLOWER03_4X_R_SC-cell5					168								
FLOWER03_4X_R_SC-cell9		60	204										
FLOWER04_4X_L_SC-cell11		120	180		324								
FLOWER04_4X_L_SC-cell12					156								
FLOWER04_4X_L_SC-cell14													
FLOWER04_4X_L_SC-cell3													
FLOWER04_4X_L_SC-cell6		71	108		336								
FLOWER04_4X_L_SC-cell7		83	120		336								
FLOWER04_4X_L_SC-cell8													
FLOWER04_4X_L_SC-cell9				144	240								
FLOWER04_4X_R_SC-cell12				204	228								
FLOWER04_4X_R_SC-cell14		59	156		336								
FLOWER04_4X_R_SC-cell15				156	276								
FLOWER04_4X_R_SC-cell16				143	132	276							
FLOWER04_4X_R_SC-cell5		120	156		120								
FLOWER04_4X_R_SC-cell7		239	264		276								
FLOWER04_4X_R_SC-cell9		83	192		264								
FLOWER04_4X_R_SC-cell9		83	156		396								
FLOWER08_4X_L_SC-cell10							210	90					286
FLOWER08_4X_L_SC-cell12							230	50					
FLOWER08_4X_L_SC-cell13													376
FLOWER08_4X_L_SC-cell14													351
FLOWER08_4X_L_SC-cell15													321
FLOWER08_4X_L_SC-cell2							170	150					
FLOWER08_4X_L_SC-cell4													266
FLOWER08_4X_L_SC-cell6							200	110					
FLOWER08_4X_L_SC-cell7													283.5
FLOWER08_4X_L_SC-cell8							180	170					306
FLOWER08_4X_L_SC-cell9													266
FLOWER08_4X_R_SC-cell10							140						
FLOWER08_4X_R_SC-cell12							140						
FLOWER08_4X_R_SC-cell14							150						
FLOWER08_4X_R_SC-cell15							200						
FLOWER08_4X_R_SC-cell16							210						
FLOWER08_4X_R_SC-cell4							230						
FLOWER08_4X_R_SC-cell8							150						
FLOWER10_4X_L_SC-cell1							250	250					
FLOWER10_4X_L_SC-cell10							360	100					
FLOWER10_4X_L_SC-cell2							200	290					
FLOWER10_4X_L_SC-cell2.5												53	
FLOWER10_4X_L_SC-cell3												44	
FLOWER10_4X_L_SC-cell3.5							190	210				53	
FLOWER10_4X_L_SC-cell4							290	140				53	
FLOWER10_4X_L_SC-cell5							488	150					
FLOWER10_4X_L_SC-cell7							360	130					
FLOWER10_4X_L_SC-cell8							350	130					
FLOWER10_4X_L_SC-cell9							380	140					
FLOWER10_4X_R_SC-cell1							250	80	60	80	40		
FLOWER10_4X_R_SC-cell10							200	160	70	110			
FLOWER10_4X_R_SC-cell11													
FLOWER10_4X_R_SC-cell12							180	140	70	110			
FLOWER10_4X_R_SC-cell13								250	60				
FLOWER10_4X_R_SC-cell14								270	60	110			
FLOWER10_4X_R_SC-cell16							200						
FLOWER10_4X_R_SC-cell17												60	321
FLOWER10_4X_R_SC-cell18								130	60	90	60		

Annex 4 Output of the single cell analysis for landmark duration in KINGBIRD_4X

sample	Landmark												
	0	1	2	3	4	5	6	7	8	9	10	11	12
FLOWER10_4X_R_SC-cell19									60	90	60		
FLOWER10_4X_R_SC-cell2							260	130	60	80	40	227	
FLOWER10_4X_R_SC-cell3							293	150	60	80	40	227	
FLOWER10_4X_R_SC-cell4								130	70	90	40	217	
FLOWER10_4X_R_SC-cell5											50	285	
FLOWER10_4X_R_SC-cell6								110	60	110			
FLOWER10_4X_R_SC-cell7							220	120	70	100			
FLOWER10_4X_R_SC-cell8							260	140	70	100			
FLOWER10_4X_R_SC-cell9							180	190	70	110			
FLOWER11_4X_L_SC-cell1											40	365	
FLOWER11_4X_L_SC-cell2											65		
FLOWER11_4X_L_SC-cell3											65		
FLOWER11_4X_L_SC-cell4											65		
FLOWER11_4X_L_SC-cell6												580	
FLOWER11_4X_L_SC-cell7											65	470	
FLOWER11_4X_L_SC-cell9											250		
FLOWER11_4X_R_SC-cell1											40	255	
FLOWER11_4X_R_SC-cell2											40	275	
FLOWER11_4X_R_SC-cell3										100	55	390	
FLOWER11_4X_R_SC-cell4											45	380	
FLOWER11_4X_R_SC-cell5											45	550	
FLOWER11_4X_R_SC-cell6											45	650	
FLOWER13_4X_L_SC-cell1							60	280	50	60	30		
FLOWER13_4X_L_SC-cell10							130	90	60	70	40		
FLOWER13_4X_L_SC-cell11							120	120	50	80	40		
FLOWER13_4X_L_SC-cell12							120	120	60	70	40		
FLOWER13_4X_L_SC-cell13												30	
FLOWER13_4X_L_SC-cell14						325	100	130	50	80	40		
FLOWER13_4X_L_SC-cell15						165	210	160	50	90	30		
FLOWER13_4X_L_SC-cell17												50	
FLOWER13_4X_L_SC-cell18						185	320	40	50	100	40		
FLOWER13_4X_L_SC-cell19						275	220	100	50	100	40		
FLOWER13_4X_L_SC-cell2									50	60	30		
FLOWER13_4X_L_SC-cell20								70	40	100	40		
FLOWER13_4X_L_SC-cell21						155	170	200	40				
FLOWER13_4X_L_SC-cell22						225	170	190	40	100	60		
FLOWER13_4X_L_SC-cell3							90	270	50	60	30		
FLOWER13_4X_L_SC-cell4												40	
FLOWER13_4X_L_SC-cell5							150	170	50	70	30		
FLOWER13_4X_L_SC-cell6							280	70	70	50	30		
FLOWER13_4X_L_SC-cell7							290	100					
FLOWER13_4X_L_SC-cell9							180	110	70	50	40		
FLOWER13_4X_R_SC-cell1							200						
FLOWER13_4X_R_SC-cell2							200						
FLOWER14_4X_L_SC-cell1									60	70	30		
FLOWER14_4X_L_SC-cell11									40	80	40		
FLOWER14_4X_L_SC-cell12							220	180	40	80	40		
FLOWER14_4X_L_SC-cell2										70	30		
FLOWER14_4X_L_SC-cell3								180				30	
FLOWER14_4X_L_SC-cell4							210	150	50	70	40		
FLOWER14_4X_L_SC-cell5							280	160	40	80	30		
FLOWER14_4X_L_SC-cell6							220	100	60	80	30		
FLOWER14_4X_L_SC-cell7							80	220	50	80	30		
FLOWER14_4X_L_SC-cell8							190	180	50	80	40		
FLOWER14_4X_L_SC-cell9							220	170	50	80	40		
FLOWER14_4X_R_SC-cell1							190	230	50	80	30		
FLOWER14_4X_R_SC-cell12							240	100	40	80	40		
FLOWER14_4X_R_SC-cell13							220	110	40	80	40		
FLOWER14_4X_R_SC-cell15										90	30		
FLOWER14_4X_R_SC-cell16							280	160	40	80	40		
FLOWER14_4X_R_SC-cell17								220	40	80	40		
FLOWER14_4X_R_SC-cell18												30	
FLOWER14_4X_R_SC-cell19							210	190	30	80	40		
FLOWER14_4X_R_SC-cell2							220						
FLOWER14_4X_R_SC-cell20										80	40		
FLOWER14_4X_R_SC-cell3							190	180	50	80	20		
FLOWER14_4X_R_SC-cell5												40	
FLOWER14_4X_R_SC-cell6													30
FLOWER14_4X_R_SC-cell8							310	150	50	80	40		
FLOWER14_4X_R_SC-cell9							260	110	50	80	30		
FLOWER19_4X_L_SC-cell1		1115											
FLOWER19_4X_L_SC-cell12		1370											
FLOWER19_4X_L_SC-cell2		1130											
FLOWER19_4X_L_SC-cell8		960											
FLOWER20_4X_L_SC-cell1			60				189	250					
FLOWER20_4X_L_SC-cell10			140				569	190					
FLOWER20_4X_L_SC-cell11								150					
FLOWER20_4X_L_SC-cell12				250									
FLOWER20_4X_L_SC-cell13			70						210				
FLOWER20_4X_L_SC-cell14			70				469	200					
FLOWER20_4X_L_SC-cell15			30										
FLOWER20_4X_L_SC-cell16			60										
FLOWER20_4X_L_SC-cell17									170				
FLOWER20_4X_L_SC-cell3			70	170					260				
FLOWER20_4X_L_SC-cell4							284	200					
FLOWER20_4X_L_SC-cell5			140						290				
FLOWER20_4X_L_SC-cell6			70	160									
FLOWER20_4X_L_SC-cell8			100	150					150				
FLOWER20_4X_L_SC-cell9			70						180				
FLOWER24_4X_L_SC-cell10						758							
FLOWER24_4X_L_SC-cell14						778							
FLOWER24_4X_L_SC-cell15						798							
FLOWER24_4X_L_SC-cell16						828							
FLOWER24_4X_L_SC-cell4						668							

Annex 4 Output of the single cell analysis for landmark duration in KINGBIRD_4X

sample	Landmark												
	0	1	2	3	4	5	6	7	8	9	10	11	12
FLOWER24_4X_L_SC-cell8						568							
FLOWER24_4X_L_SC-cell9						678							
FLOWER25_4X_L_SC-cell11			40	378	260								
FLOWER25_4X_L_SC-cell13				288	390								
FLOWER25_4X_L_SC-cell14			60										
FLOWER25_4X_L_SC-cell15					150								
FLOWER25_4X_L_SC-cell2			110										
FLOWER25_4X_L_SC-cell4			40	408	310								
FLOWER25_4X_L_SC-cell8			50										
FLOWER25_4X_L_SC-cell9					260								
FLOWER25_4X_R_SC-cell10			30	228	320								
FLOWER25_4X_R_SC-cell11			278										
FLOWER25_4X_R_SC-cell13					280								
FLOWER25_4X_R_SC-cell3			100	260									
FLOWER25_4X_R_SC-cell4			50	310									
FLOWER25_4X_R_SC-cell5			50	200	300								
FLOWER25_4X_R_SC-cell8			208	240	220								
FLOWER25_4X_R_SC-cell9				260	210	190							
FLOWER26_4X_L_SC-cell1						410							
FLOWER26_4X_L_SC-cell2						390							
FLOWER26_4X_L_SC-cell4							340						
FLOWER26_4X_L_SC-cell6						360							
FLOWER26_4X_R_SC-cell1						330	210						
FLOWER26_4X_R_SC-cell2						370	170						
FLOWER26_4X_R_SC-cell3						390	140						
FLOWER26_4X_R_SC-cell4						390							
FLOWER26_4X_R_SC-cell5						460							
FLOWER26_4X_R_SC-cell6						310	290						
FLOWER27_4X_L_SC-cell1								258					
FLOWER27_4X_L_SC-cell2								238					
FLOWER27_4X_L_SC-cell5								248					
FLOWER27_4X_R_SC-cell10								158					
FLOWER27_4X_R_SC-cell12								188					
FLOWER27_4X_R_SC-cell14								208					
FLOWER27_4X_R_SC-cell15								138					
FLOWER27_4X_R_SC-cell5								138					
FLOWER27_4X_R_SC-cell9								178					
FLOWER29_4X_L_SC-cell1											40	230	
FLOWER29_4X_L_SC-cell2									80	110	50	240	
FLOWER29_4X_L_SC-cell3											70	240	
FLOWER29_4X_L_SC-cell4											50	220	
FLOWER29_4X_L_SC-cell5										110	40	240	
FLOWER29_4X_L_SC-cell6											60	230	
FLOWER29_4X_L_SC-cell8											110	230	
FLOWER29_4X_R_SC-cell1										70	40	250	
FLOWER29_4X_R_SC-cell2										60	40	230	
FLOWER29_4X_R_SC-cell3											40	270	
FLOWER29_4X_R_SC-cell4										60	40	290	
FLOWER29_4X_R_SC-cell5										70	30	280	
FLOWER29_4X_R_SC-cell6											30	250	
AVERAGE //		762.833333	83.8301887	185.529412	250.888889	415.481481	234.835294	194.222222	63.4285714	85.7272727	47.7252747	293.77027 //	
ST.DEV //		604.506217	51.4290908	75.4181286	99.2041986	236.600665	101.764065	100.315783	28.7557648	24.468847	27.7673133	123.864655 //	
COUNTS		2	6	53	51	36	27	85	99	63	66	91	37

Annex 5. Summary of data analysed and sample size used for this study

NUMBER OF SAMPLES PER LANDMARK EXTRACTION

	<i>KINGBIRD_2X</i>
flower	21
anther	35
cell	169

NUMBER OF SAMPLES PER TIME COURSE

	<i>KINGBIRD_2X</i>	<i>KINGBIRD_4X</i>
flower	11	15
anther	17	27
cell	137	239

TIMECOURSE_info on movies

<i>KINGBIRD_2X</i>			
flower/anther	observed meiocytes	overall time (m)	n°of movies
1	3	275	1
2	2	275	1
3/L	13	1140	2
3/R	10	1140	2
12/R	7	1546	3
13b/U	7	1338	3
14/L	12	1546	3
14/U	7	1546	3
17/L	4	2211	4
17/R	8	2211	4
22/L	7	1683.5	4
22/R	11	1683.5	4
24/L	1	300	3
24/R	5	300	3
27	9	159	1
29/L	19	2771	3
29/R	12	2771	3
11/17	137		47

Annex 5. Summary of data analysed and sample size used for this study

KINGBIRD 4X			
flower/anther	n° of cells for SC analysis	overall time (m)	n° of movies
1/L	14	2633	8
1/R	9	2633	8
3/L	10	1169	3
3/R	8	1169	3
4/L	8	1169	3
4/R	7	1169	3
8/L	11	1300	4
8/R	7	1300	4
10/L	11	1117	6
10/R	18	1117	6
11/L	7	1075	2
11/R	6	1075	2
1/3L	20	1075	2
13/R	2	1075	2
14/L	11	1075	2
14/R	15	1075	2
19/L	4	1542	3
20/L	15	2211	4
24/L	7	1098	2
25/L	8	1098	2
25/R	8	1098	2
26/L	4	1098	2
26/R	6	1098	2
27/L	3	300	3
27/R	6	300	3
29/L	7	1193	4
29/R	6	1193	4
15/27	238		91

	MAX TIME OF SAMPLE OBSERVATION (m)	MAX DURATION OF SINGLE MOVIE (m)
KINGBIRD_2X	2771	1130
KINGBIRD_4X	2633	960

Annex 6 Duration of meiosis in diploid and tetraploid *KINGBIRD* lines

Landmark	<i>KINGBIRD_2X</i>			<i>KINGBIRD_4X</i>		
	Counts	Average duration (min)	St.Dev	Counts	Average duration (min)	St.Dev
START	0	//	//	0	//	//
A1	17	506.76	97.05	4	1143.75	169.28
A2	34	96.18	54.94	51	87.04	49.72
A3	43	181.16	91.47	49	192.98	66.93
A4	44	189.86	83.22	34	265.41	80.79
A5	17	396.42	190.13	25	448.32	213.26
A6	37	193.51	74.67	83	240.35	96.44
A7	26	201.88	108.91	97	198.08	97.61
A8	30	57.33	29.09	61	65.25	27.36
A9	28	56.00	11.76	64	88.13	20.62
A10	45	42.04	9.74	89	48.57	27.49
A11	4	181.25	62.50	35	309.93	106.17
END	0	//	//	0	//	//

Annex 7 Statistical comparison between the duration of meiosis in KINGBIRD 2X and 4X

Landmark	Significance		Duration KINGBIRD 2X								Duration KINGBIRD 4X							
	Mann-Whitney U statistic	p-value	n	mean	std	min	q1	median	q3	max	n	mean	std	min	q1	median	q3	max
A1	0.000	0.371	3	583.095	113.075	474.286	524.643	575.000	637.500	700.000	1	1143.750		1143.750	1143.750	1143.750	1143.750	1143.750
A2	11.000	0.371	3	101.685	24.735	84.286	87.527	90.769	110.385	130.000	5	87.089	15.221	73.000	78.857	80.000	92.364	111.222
A3	8.000	0.403	5	140.393	73.444	40.000	100.000	140.714	210.000	211.250	5	193.156	54.761	143.750	164.000	182.500	189.750	285.778
A4	7.000	0.334	6	188.650	62.925	114.444	145.250	190.000	210.000	290.455	4	245.400	57.195	160.000	242.500	270.000	272.900	281.600
A5	9.000	0.766	3	456.905	299.012	240.000	286.357	332.714	565.357	798.000	5	423.340	234.384	190.000	221.667	378.889	601.000	725.143
A6	6.000	0.156	4	186.369	37.762	153.333	162.083	176.786	201.071	238.571	7	255.982	74.927	177.059	202.708	230.000	300.826	377.750
A7	19.000	0.395	4	266.838	178.461	149.091	162.023	193.881	298.696	530.500	7	192.610	85.182	114.000	149.158	164.118	199.606	372.625
A8	4.000	0.178	4	55.744	29.631	37.143	41.161	42.917	57.500	100.000	5	70.788	26.291	46.111	51.875	64.286	80.000	111.667
A9	0.000	0.008	5	53.267	7.844	45.000	45.000	55.333	60.000	61.000	6	92.828	18.659	76.000	79.286	88.462	99.231	125.000
A10	7.000	0.337	4	39.894	6.841	34.667	35.205	37.692	42.381	49.524	6	53.260	17.628	34.800	40.641	49.324	63.604	80.000
A11	0.000	0.105	2	181.250	76.014	127.500	154.375	181.250	208.125	235.000	4	310.873	86.965	246.154	253.088	281.169	338.953	435.000

Annex 8 List of reporters screened for meiotic expression and and scheme of crosses

construct	background	origin	characteristics																																																																																																				
Constitutively expressed genes																																																																																																							
PRO35S::H2B-YFP	Col0, WT	Graumann K., OBU, Oxford, UK	no signal in meiocytes																																																																																																				
PROCENH3::CENH3::GFP	Col0, WT	Schnittger lab, UHH, Hamburg	signal disappears at late meiotic stages																																																																																																				
PROCENH3::GFP::CENH3	Col0, <i>cenh3</i> -/-	Ravi M., IISER, Thiruvananthapuram, IN	good signal in meiocytes																																																																																																				
HTA1::RFP	Col0, WT	Berger F., GMI, Vien, AT	good signal in meiocytes																																																																																																				
	Col0, SAIL_807_B08 (<i>rec8</i>) +/-	crossed by Prusicki M., UHH, Hamburg, DE	fuzzy signal in meiocytes																																																																																																				
HTA2::RFP	Col0, WT	Berger F., GMI, Vien, AT	fuzzy signal in meiocytes																																																																																																				
HTA10::RFP	Col0, WT	Berger F., GMI, Vien, AT	fuzzy signal in meiocytes																																																																																																				
HTA13::RFP	Col0, WT	Berger F., GMI, Vien, AT	fuzzy signal in meiocytes																																																																																																				
H2A.X::3::RFP	Col0, WT	Berger F., GMI, Vien, AT	fuzzy signal in meiocytes																																																																																																				
H2A.X::5::RFP	Col0, WT	Berger F., GMI, Vien, AT	good signal in meiocytes																																																																																																				
	Col0, SAIL_807_B08 (<i>rec8</i>) +/-	crossed by Prusicki M., UHH, Hamburg, DE	to be checked																																																																																																				
PROSUN1::SUN1::GFP	Col0, WT	Oda Y., NIG, Mishima, JP	good signal in meiocytes																																																																																																				
PRORPSSA::TagRFP::TUB4	Col0, WT	Ishida T., Kumamoto University, Kumamoto, JP	good signal in meiocytes																																																																																																				
PRORPSSA::TagRFP::TUA5	Col0, WT	Komaki S., UHH, Hamburg, DE	good signal in meiocytes																																																																																																				
Cell cycle related genes																																																																																																							
RAD51::GFP	Col0, <i>atrads1-1</i> -/-	White C., GreD, Clermont-Ferrand, FR	no rescue in somatic cells																																																																																																				
Meiotic specific genes																																																																																																							
PROREC8::REC8::mEGFP	Col0, SAIL_807_B08 (<i>rec8</i>) +/- and -/-	Komaki S., UHH, Hamburg, DE	good signal and rescue (line3)																																																																																																				
PROREC8::REC8::RFP	Col0, SAIL_807_B08 (<i>rec8</i>) +/- and -/-		less intense than REC8-GFP, after pachytene is more difficult to detect																																																																																																				
PROREC8::REC8::mNeonGreen	Col0, SAIL_807_B08 (<i>rec8</i>) +/- and -/-	Prusicki M., UHH, Hamburg, DE	good signal in meiocytes, but no rescue of sterility																																																																																																				
	Col0, WT		good signal in meiocytes																																																																																																				
KINGBIRDS																																																																																																							
KINGBIRD	Col0, SAIL_807_B08 (<i>rec8</i>) +/- and -/-	crossed by Prusicki M., UHH, Hamburg, DE	good signal in meiocytes																																																																																																				
	Col0, tetraploid	Prusicki M., UHH, Hamburg, DE	good signal in meiocytes																																																																																																				
	Col0, Salk_041462 (<i>mlh3</i> +/-)	crossed by Prusicki M., UHH, Hamburg, DE	good signal in meiocytes																																																																																																				
	Salk_015849 (<i>mlh3</i> +/-)	crossed by Prusicki M., UHH, Hamburg, DE	good signal in meiocytes																																																																																																				
KINGBIRD2	Col0, WT	Komaki S., UHH, Hamburg, DE	good signal in meiocytes																																																																																																				
	Col0, SAIL_505_C06 (<i>tam1-2</i>) +/-	transformation by Prusicki M., UHH, Hamburg, DE	good signal in meiocytes																																																																																																				
	Col0, <i>knp4.6.7</i> -/-	transformation by Prusicki M., UHH, Hamburg, DE	good signal in meiocytes																																																																																																				
	Col0, <i>knp3.4.6.7</i> -/-	transformation by Prusicki M., UHH, Hamburg, DE	good signal in meiocytes																																																																																																				
	Col0, Salk_015849 (<i>mlh3</i>) +/-	transformation by Prusicki M., UHH, Hamburg, DE	good signal in meiocytes																																																																																																				
	Col0, Salk_041462 (<i>mlh3</i>) +/-	transformation by Prusicki M., UHH, Hamburg, DE	good signal in meiocytes																																																																																																				
<table border="1"> <thead> <tr> <th></th> <th>GFP::CENH3</th> <th>TagRFP::CENH3</th> <th>HTA1::RFP</th> <th>H2A.X::5::RFP</th> <th>TagRFP::TUB4</th> <th>SUN1::GFP</th> <th>RBR1::mCherry</th> <th>REC8::RFP</th> <th>REC8::GFP</th> </tr> </thead> <tbody> <tr> <td>male</td> <td></td> <td></td> <td></td> <td></td> <td></td> <td></td> <td></td> <td></td> <td></td> </tr> <tr> <td>female</td> <td></td> <td></td> <td></td> <td></td> <td></td> <td></td> <td></td> <td></td> <td></td> </tr> <tr> <td>GFP::CENH3</td> <td></td> <td></td> <td>✓</td> <td></td> <td></td> <td></td> <td></td> <td>✓</td> <td></td> </tr> <tr> <td>TagRFP::CENH3</td> <td></td> <td></td> <td></td> <td></td> <td></td> <td>✓</td> <td></td> <td></td> <td>✓</td> </tr> <tr> <td>TagRFP::TUB4</td> <td></td> <td></td> <td></td> <td></td> <td></td> <td>✓</td> <td></td> <td></td> <td></td> </tr> <tr> <td>TagRFP::TUA5</td> <td>✓</td> <td></td> <td></td> <td></td> <td></td> <td></td> <td></td> <td></td> <td></td> </tr> <tr> <td>SUN1::GFP</td> <td></td> <td>✓</td> <td></td> <td></td> <td></td> <td></td> <td>✓</td> <td></td> <td></td> </tr> <tr> <td>RAD51::GFP</td> <td></td> <td>✓</td> <td></td> <td></td> <td></td> <td></td> <td></td> <td>✓</td> <td></td> </tr> <tr> <td>REC8::GFP</td> <td></td> <td></td> <td></td> <td>✓</td> <td></td> <td></td> <td></td> <td></td> <td></td> </tr> </tbody> </table>					GFP::CENH3	TagRFP::CENH3	HTA1::RFP	H2A.X::5::RFP	TagRFP::TUB4	SUN1::GFP	RBR1::mCherry	REC8::RFP	REC8::GFP	male										female										GFP::CENH3			✓					✓		TagRFP::CENH3						✓			✓	TagRFP::TUB4						✓				TagRFP::TUA5	✓									SUN1::GFP		✓					✓			RAD51::GFP		✓						✓		REC8::GFP				✓					
	GFP::CENH3	TagRFP::CENH3	HTA1::RFP	H2A.X::5::RFP	TagRFP::TUB4	SUN1::GFP	RBR1::mCherry	REC8::RFP	REC8::GFP																																																																																														
male																																																																																																							
female																																																																																																							
GFP::CENH3			✓					✓																																																																																															
TagRFP::CENH3						✓			✓																																																																																														
TagRFP::TUB4						✓																																																																																																	
TagRFP::TUA5	✓																																																																																																						
SUN1::GFP		✓					✓																																																																																																
RAD51::GFP		✓						✓																																																																																															
REC8::GFP				✓																																																																																																			

Annex 9 Buffers and media used in this study

0.5X MS			1 l
MS Basal powder	0.2%		2.2 g
Sucrose	1%		10 g
Millipore water	up to volume		1 l
Agar (for solid medium)	1%		10 g

pH 5.8 (adjusted with KOH)

ACM			1l
0.5 X MS (liquid) pH5.8	up to volume		1l
Agarose	0.8%		8 g
Vitamin mix	1X		1 ml

Vitamin mix (Stock 1000X):

Myoinositol	10%		5 g
Nicotinic acid	0.01%		0.05 g
Pyridoxine-HCl	0.01%		0.05 g
Thiaminie-HCl	0.1%		0.5 g
Glycine	0.2%		0.1 g
Millipore water (autoclaved)	up to volume		50 ml

Magic Buffer			1 l
Tris HCl (pH7.5)	50 mM		50 ml
NaCl	300 mM		60 ml
Sucrose	300 mM		100 g
Millipore water	up to volume		890 ml

LB			1 l
Tryptone	1%		10 g
Yeast Extract	0.5%		5 g
NaCl	0.5%		5 g
Millipore water	up to volume		1 l
Agar (for solid medium)	0.8%		8 g

VIGS

YEB			1 l
Bacto beef extract	0.5%		5 g
Bacto yeast extract	0.1%		1 g
Bacto peptone	0.5%		5 g
Sucrose	0.5%		5 g
MgSO4	2mM		0.492 g
Millipore water	up to volume		1 l

pH 7.2

Annex 9 Buffers and media used in this study

Induction medium		1l
K ₂ HPO ₄	1.05%	10.5 g
KH ₂ PO ₄	0.45%	4.5 g
(NH ₄) ₂ SO ₄	0.1%	1 g
NaCitrate	0.05%	0.5 g
MgSO ₄	1mM	0.246 g
Glucose	0.1%	1 g
Fructose	0.1%	1 g
Glycerol	0.4%	4 ml
MES	10 mM	1.95 g
Millipore water	up to volume	1 l

pH 5.6 (adjusted with HCl)

Acetosyringone (after autoclaving) 50 µg/ml

Infiltration medium		125 ml
MES	0.2%	244 mg
MS	0.2%	255 mg
Millipore water	up to volume	125 ml

CELL SPREAD

Citrate buffer		100 ml
0.1M Sodium Citrate	4.45%	4.45 ml
0.1 M Citric Acid	5.55%	5.55 ml
Millipore water	up to volume	90 ml

pH 4.5

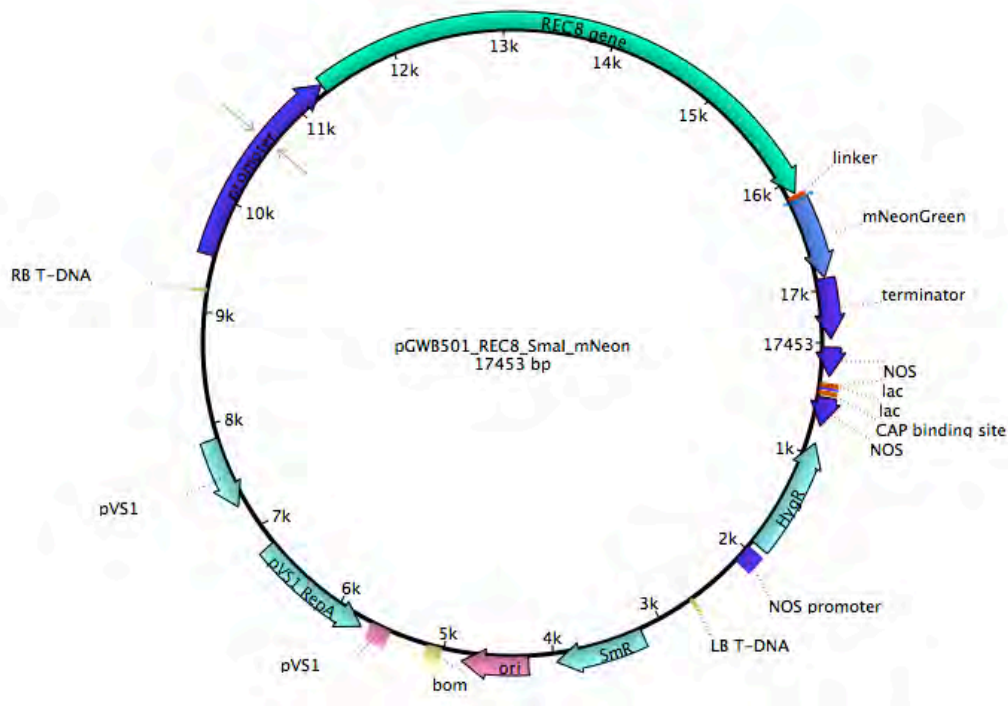
Enzyme mix		10 ml
Cellulase	1.5%	0.150 g
Pectolyase	1.5%	0.150 g
Cytohelicase	1.5%	0.150 g
0.01 M Citrate buffer	up to volume	10 ml

Petereson staining		100 ml
95% alcohol	10%	10 ml
Malachite green	0.001%	1 ml (1% in 95%alcohol)
glycerol	25%	25 ml
Acid fuchsin	0.005%	5 ml (1% in water)
Orange G	0.0005%	0.5 ml (1% in water)
Acetic acid	4%	4 ml
Millipore water	up to volume	

Annex 10. Primers used in this study

Purpose	Primer name	Sequence (5'-3')
Genotyping		
<i>rec8</i> T_DNA	SAIL_LB3	TAGCATCTGAATTTTCATAACCAATCTCGATACAC
	SAIL_807_B08-RP	GGGGGAAAAGAGAAAGGTTTC
<i>rec8</i> WT allele	SAIL_807_B08-LP	CTCATATTCACGGTGTCTCC
	SAIL_807_B08-RP	GGGGGAAAAGAGAAAGGTTTC
<i>rec8</i> WT allele in <i>REC8:GFP/REC8:mNEON</i>	SAIL_807_B08-RP	GGGGGAAAAGAGAAAGGTTTC
	TL-gREC8-R	GAACGGAGAAGGGTAAGGCTCTTGAGTC
<i>tam 1-2</i> T_DNA	SAIL_LB3	TAGCATCTGAATTTTCATAACCAATCTCGATACAC
	N874380L	CAGAAATCCTCCACTTGCG
<i>tam1-2</i> WT allele	N874380L	CAGAAATCCTCCACTTGCG
	N874380U	GACTTGATGGATCCACAGC
<i>mlh3-1</i> T_DNA	SALK_LB1.3	ATTTTGCCGATTTTCGGAAC
	RP_SALK_015849	GCCTAGGAATGTCAAAGGGAC
<i>mlh3-1</i> WT allele	RP_SALK_015849	GCCTAGGAATGTCAAAGGGAC
	LP_SALK_015849	GTAGCCCCAAGAAAGTTTTGG
<i>mlh3-2</i> T_DNA	SALK_LB1.3	ATTTTGCCGATTTTCGGAAC
	RP_SALK_041465	AGTATAGCAACCTGGGAAGGC
<i>mlh3-2</i> WT allele	RP_SALK_041465	AGTATAGCAACCTGGGAAGGC
	LP_SALK041465	TGACATTAAAGGTAAGTACTGCCGG
<i>krp3</i> T_DNA	KRP3 T_DNA	AACGTCCGCAATGTGTTATTAAGTTGTC
	KRP3_F1	TCAAACCAAACCAAACATCC
<i>krp3</i> WT allele	KRP3_F1	TCAAACCAAACCAAACATCC
	KRP3_R1	CATGTGTACTTCATTGCAGAG
<i>krp4</i> T_DNA	SAIL_LB3	TAGCATCTGAATTTTCATAACCAATCTCGATACAC
	KRP4_F1	TGGGTTTGTTTATGTCAAAGC
<i>krp4</i> WT allele	KRP4_F1	TGGGTTTGTTTATGTCAAAGC
	KRP4_R1	TTCCAAGTTAGACGTGTTTG
<i>krp6</i> T_DNA	SAIL_LB3	TAGCATCTGAATTTTCATAACCAATCTCGATACAC
	KRP6_RP	ATTCATCACCGACTCTCATG
<i>krp6</i> WT allele	KRP6_LP3	ATTCATCACCGACTCTCATG
	KRP6_RP	TCACTCACTGGACTCGTCTC
<i>krp7</i> T_DNA	KRP7 T_DNA	ATATTGACCATCATACTCATTGC
	KRP7_R2	AAGTCATCAAGCTCTGCCTG
<i>krp7</i> WT allele	KRP7_F1	CTTCATTTTCAGATCTGGAGGTG
	KRP7_R2	AAGTCATCAAGCTCTGCCTG
Cloning of PRO_{REC8}:REC8:mNEONGreen		
amplification of mNG	SmaI-mNeon-F	GGGGGAGTACCGCCCCGTCCG
	SmaI-mNeon-R	GGGTCACTTGTAAGCTCGTCCA
Cloning of VIGS constructs		
OSD1 (cDNA)	OSD1_XbaI_F	CATCTAGACCCCAAGAAAGCTCTTTCTC
	OSD1_EcoRI_R	CAGAATTCCTCAATATCTGGATTCACCGG
PDS (Burch-Smith <i>et al.</i> 2006)	PDS_XbaI_F	CGCTCTAGAAACTCTTAACCGTGCCATCGTCATTGAG
	PDS_EcoRI	CGCGAATTCTGCGGCGAATTTGCCTTATCAAACG

Annex 11. REC8-mNG construct and sequences



>mNeonGreen_gene_plant codon optimized

>711 bp

>MOLECULAR LINKER START CODON STOP CODON

GCAGCTATGTGCTGTTACGCGTTGTACAGGAGTACCGCCCGTCCGGTCTGCCGTCACCGAGATCAGCGGA
GAGTTCATGGTGTCCAAGGGCGAGGAGGACAACATGGCCAGCCTCCCCGCTACCCACGAGTTGCACATCTTCG
GATCTATTAACGGTGTGACTTCGATATGGTCGCCAGGGGACCGGCAACCCAAATGACGGATACGAAGAGCT
GAACCTCAAGTCCACTAAGGGGAGACCTCAATTCTCGCCTTGGATCTTGGTGCCGCACATCGGATACGGCTTCCA
TCAGTACCTCCCCTACCCAGACGGTATGAGCCCCTTCAGGCCGCTATGGTCGATGGGTCCGGCTACCAAGTGC
ACCGCACCATTGCAGTTTGAGGACGGAGCCTCACTGACAGTCAACTACAGATACACCTATGAGGGCTCCACATC
AAGGGGAGAGGCCAAGTGAAGGGCACGGGTTTCCAGCAGACGGCCCTGTTATGACCAACAGCCTCACCGCG
GCCGACTGGTGCCGTTCTAAGAAGACCTACCCGAACGATAAGACTATTATCTCCACCTTCAAATGGTCGTACACC
ACAGGGAACGAAAGCGCTACAGGAGCACCGCTAGGACCACGTACACCTTCGCCAAGCCAATGGCCGCTAATT
ACCTTAAGAACCAGCCCATGTACGTCTCCGCAAGACTGAGTTGAAGCACTCCAAGACCGAACTGAACTTCAAG
GAGTGGCAGAAGGCTTTCACCGACGTGATGGGCATGGACGAGCTTACAAGTGAACCCGGTCGACGAGTGGCAT
GCCG

>mNeonGreen_protein_plant codon optimized

>236 a.a. MW=26650.

>MOLECULAR LINKER

GVPPRPVLPVTEISGEFMVSKGEEDNMASLPATHELHIFGSINGVDFDMVGQGTGNPNPDGYEELNLKSTKGDLOFS
PWILVPHIGYGFHQYLPYPDGMSPFQAAMVDGSGYQVHRMTMQFEDGASLTVNYRYTYEGSHIKGEAQVKGTFPA
DGPVMTNSLTAADWCRSKKTYPNDKTIISTFKWSYTTGNGKRYRSTARTTYTFAKPMANLYKNQPMYVFRKTELK
HSKTELNFKEWQKAFTDVMGMDELYK*

Appendix

Index of Figures

Figure 1.1 Recombination pathways of <i>Arabidopsis thaliana</i>	2
Figure 1.2 Progression of male meiosis in <i>Arabidopsis thaliana</i>	7
Figure 1.3 Cohesin structure and cleavage during meiosis.....	10
Figure 1.4 Meiotic defects and adaptation in polyploids.....	13
Figure 3.1 Sample isolation and viability.....	29
Figure 3.2 Microscope set up.....	31
Figure 3.3 Expression pattern of $PRO_{REC8}:REC8:mEGFP$ and $PRO_{RPSA5}:TagRFP:TUB4$ in the <i>KINGBIRD</i> line.....	33
Figure 3.4 $PRO_{REC8}:REC8:GFP$, $PRO_{RPSA5}:TgRFP:TUB4$ and the <i>KINGBIRD</i> line have wild-type phenotype.....	35
Figure 3.5 Conformations of cellular features.....	38
Figure 3.6 Percentage of simultaneous exchanges of cellular features.....	40
Figure 3.7 Map of meiotic cellular states.....	42
Figure 3.8 Landmark scheme.....	43
Figure 3.9 Cellular states at the nuclear envelope breakdown	44
Figure 3.10 Generation of tetraploid of <i>KINGBIRD</i> reporter line	47
Figure 3.11 Progression of meiosis in <i>KINGBIRD</i> 4X anthers.....	48
Figure 3.12 Example of time course analysis procedure.....	50
Figure 3.13 Time course of male meiosis I anthers of <i>Arabidopsis thaliana</i>	52
Figure 3.14 Comparison between diploid and tetraploid time course.....	54
Figure 3.15 More reporters are available to study meiosis.....	57
Figure 3.16 $PRO_{REC8}:REC8:mNG$ performance.....	60
Figure 4.1 Possible changes of the landmark system.....	68

Index of Tables

Table 1.1 Duration of meiosis in monocots.....	19
Table 1.2 Duration of meiosis in dicots and gymnosperm.....	20

Index of Annexes

Annex 1 Observed cellular states.....	102
Annex 2 Results of Bootstrap analysis.....	106
Annex 3 Output for the single cell analysis for landmark duration in <i>KINGBIRD 2X</i>	108
Annex 4 Output for the single cell analysis for landmark duration in <i>KINGBIRD 4X</i>	110
Annex 5 Summary of data analyzed and sample size used for this study.....	113
Annex 6 Duration of meiosis in diploid and tetraploid <i>KINGBIRD</i> lines.....	115
Annex 7 Statistical comparison between the duration of meiosis in <i>KINGBIRD 2X</i> and <i>4X</i>	117
Annex 8 List of reporters screened for meiotic expression and scheme of crosses.....	118
Annex 9 Buffer and media used in this study.....	119
Annex 10 Primers used in this study.....	121
Annex 11 <i>REC8:mNG</i> vector map and mNG sequences.....	122

Index of Abbreviations

2D/4D	two/four Dimensions
2X/4X	Diploid/Tetraploid population
ACM	Apex Culture Medium
ASY1, ASY3	Asynaptic 1, Asynaptic 3
BrdU	5-bromo-2'-deoxyuridine
CDK	Cyclin Dependent Kinase
CENH3	Centromere Histon 3
CLSM	Confocal Laser Scanning Microscope
RISPR Cas9	Clustered Regularly Interspaced Short Palindromic Repeats
CYCB3	Cyclin B3
DAPI	4',6-diamidino-2-phenylindole
DNA	Deoxyribonucleic acid
DSB	Double Strand Break
EdU	5-Ethynyl-2'-deoxyuridine
EGFP/GFP	Enhanced Green Fluorescent Protein
F0, F1, F2...	Filial 0, 1, 2...
FLIM	Fluorescence Lifetime Imaging Microscopy
FRAP	Fluorescence Recovery After Photobleaching
FRET	Förster Resonance Energy Transfer
H2A	Histon 2A
H2B	Histon 2B
HTA10	Histon 2A
KRP	Kip Related Protein
LB	Lysogeny Broth/Left Border
MilliQ	millipore water
MLH1	MutL homolog 1
MLH3	MutL homolog 3
MMX	Mastermix
mNG	mNeonGreen
MS	Murashige and Skoog medium
MSH4	MutS Homolog 4
MSH5	MutS Homolog 5
MTs	Microtubules
NASC	Nottingham Arabidopsis Stock Center
NE	Nuclear Envelope
OSD1/GIG1	Omission of Second meiotic Division 1/GIGas cells 1
PDS	Phytoene DeSaturase
RAD21/SYN2,3 or 4	RAD21 cohesin complex component/Synaptic 2, 3, or 4
RAD51	Ricombinase A
RB	Right Border
RBR1	Ring Between Ring 1
REC8/SYN1/DIF1	Meiotic Recombination Protein 8/ Synaptic 1 /Determinate Inferile 1
RFP	Red Fluorescent Protein
RPS5A	Ribosomal Protein S5 A

Appendix

SAIL	Syngenta Arabidopsis Insertion Library
SAM	Shoot Apical Meristem
SDS	Solo DancerS
SUN1	Sad1 And UNC84 Domain-Containing protein 1
T0, T1, T2...	Transformant generation 0, 1, 2....
TAE	Tris base, acetic acid and EDTA Buffer
TagRFP	Tag Red Fluorescent Protein
TAM	Tard Asynchronous Meiosis
T-DNA	Transferred-DNA
TRV1, TRV2	Tobacco Rattle Virus 1, Tobacco Rattle Virus 2
TUA5	Tubulin Alpha 5
TUB4	Tubulin Beta 4
VIGS	Virus Induced Gene Silencing
WGD	Whole Genome Duplication
YEB	Yeast Extract and Beef Extract medium
ZYP1	Zipper 1

Publications and presentations

Publications

The major part of the work presented in this monographic dissertation has been submitted in the format of an article at the journal eLife, and it is currently under revision. A first version of the manuscript can be found at bioRxiv (www.biorxiv.org) under the title “*Live cell imaging of meiosis in Arabidopsis thaliana - a landmark system*”.

Oral presentations

- *The students and postdocs Meiosis Workshop*, 19-20/09/2016, Montpellier, France
- *MeioNet*, 14-16/06/2017, Miraflores de la Sierra, Madrid, Spain

Poster presentations

- *Gordon Research Seminar: Meiosis* 25-26/06/2016, New London, USA
- *Gordon Research Conference: Meiosis* 26/06-01/07/2016, New London, USA
- *EMBO Conference on Meiosis 2017* 27/08-1/09/2017, Hvar, Croatia
- *EMBL Conference: from Images to Knowledge with ImageJ and Friends* 06-08/12/2018, Heidelberg, Germany

Eidesstattliche Versicherung /Declaration On Oath

Hiermit erkläre ich an Eides statt, dass ich die vorliegende Dissertationsschrift selbst verfasst und keine anderen als die angegebenen Quellen und Hilfsmittel benutzt habe.

I hereby declare, on oath, that I have written the present dissertation by my own and have not used other than the acknowledged resources and aids.

Hamburg, den

Unterschrift

Confirmation of correct English

OXFORD
BROOKES
UNIVERSITY

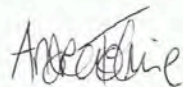
Dr Frances Tolmie
Visiting Researcher
Department of Biological and Medical Sciences
Oxford Brookes University
01865 488404
p0076589@brookes.ac.uk

Oxford, 13th December 2018

To whom it may concern,

I am writing to confirm that the thesis submitted by Maria Ada Prusicki has been written in correct English throughout its entire text.

Yours,



Dr Andrea Frances Tolmie

Visiting Researcher,

Department of Biological and Medical Sciences,

Oxford Brookes University

Acknowledgments

My first acknowledgements are for Prof. Arp Schnittger, who welcomed me in his newly born Hamburger group, and engaged me in a very challenging, yet rewarding project. Many thanks for his support and the continuous enthusiasm over all these years, for trusting my work (sometimes even more than me) and for giving me the opportunity to freely experiment and use the last microscopy technologies.

I would like to thank Prof. Wim Walter, to kindly agree to be my second supervisor, and to examine the final dissertation.

Thanks to Prof. Olivier Hamant, who shared his microscopy knowledge without reserve, and thanks to Emma Keizer, Rik van Rosmalen and Prof. Christian Fleck for coming in aid there, where my knowledge was the weakest: in the mathematical analysis of my data. Thanks to Prof. Stefan Hoth, and Prof. Christian Voigt, for offering their microscopes when we still did not have one.

I would like to thank to the COMREC ITN, which introduced me to the world of meiosis, giving me the opportunity to meet and discuss with some of the main researchers in the field. The “COMREC” was not only a very good scientific and economical support, but its main value has been the great network of people that it created: thanks to all of you Vanesa, Amy, Jihed, Marina, Gunjita, Divya, Mikel, Jason, Adrian, Mateusz, Sevgin and Pablo for these nice years.

An important acknowledgment to Stephanie Leyk who, during her internship as a student developed part of the material I have been working on in the following years.

The work presented here has been possible only because of the constant discussion and advices of the present and past Schnittger group members, a special thank to Shini, Erik, Maren Heese, Gaëtan, Vane, Chao, Kostı, Yuki, Marti, Joke, Steph, Poyu, Reinhold, Katja, Dagmar, Ika, XinAi and Viola. Thanks to all other lab members, that became too many to be listed all at once. Thanks to Felix, who, besides designing the landmark duration calculator, was always ready to have a chat and a beer. Many thanks for Maren Roeper, without her support I would be still stuck in German bureaucracy.

Special thanks to Frances Tolmie, who, even long after her duty as supervisor terminated, kept on being present in my scientific life, ending up with the proof reading of this dissertation during her birthday celebrations.

Thanks to Vanesa, Gaëtan, Eugen and Pablo to the everyday life support and for all the laughs and crepes we had together. You are the best thing that happened during my life in Hamburg. Thanks to Joke for all the chocolate and happy songs provided during the years, thanks to Marti for being always ready to help, even when her days are very full and busy. Thanks to Francesca, Andrea and Tobia to give me the chance to escape biology from time to time.

A final and very special thank is for my family, who supported me during my whole career as a student, always encouraging me to go further in my achievements.